



UNIVERSITÀ DELLA
CALABRIA

UNIVERSITÀ DELLA CALABRIA

Dipartimento di Ingegneria Informatica, Modellistica, Elettronica e Sistemistica

Dottorato di Ricerca in

Information and Communication Technology

CICLO

XXXIII

**Innovative Techniques to Support the Surveying and the Exploration
of Underwater Sites by Scientific and Recreational Divers**

Settore Scientifico Disciplinare: ING-INF/04

Coordinatore:

Prof. Felice Crupi

Firma  Firma oscurata in base alle linee guida del Garante della privacy

Supervisore:

Prof. Alessandro Casavola

Firma  Firma oscurata in base alle linee guida del Garante della privacy

Correlatori:

Prof. Fausto...

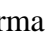
Firma  Firma oscurata in base alle linee guida del Garante della privacy

Prof. Francesco Pupo

Firma  Firma oscurata in base alle linee guida del Garante della privacy

Dottorando:

Marino Mangeruga

Firma  Firma oscurata in base alle linee guida del Garante della privacy

List of Publications

The work conducted during the Ph.D. period led to the following publications:

1. **Mangeruga, M.**, Casavola, A., Pupo, F., & Bruno, F. (2020). An Underwater Pathfinding Algorithm for Optimised Planning of Survey Dives. *Remote Sensing*, 12(23), 3974.
2. Čejka, J., **Mangeruga, M.**, Casavola, A., Bruno, F., Skarlatos, D., & Liarokapis, F. (2020). Evaluating the Potential of Augmented Reality Interfaces for Exploring Underwater Historical Sites. *IEEE Access*.
3. Bruno, F., Barbieri, L., Lagudi, A., **Mangeruga, M.**, Pupo, F., & Casavola, A. (2019, September). A Cooperative Monitoring System for Diver Global Localization and Operation Support. In *International Conference on Design, Simulation, Manufacturing: The Innovation Exchange* (pp. 410-421). Springer, Cham.
4. Bruno, F., Barbieri, L., **Mangeruga, M.**, Cozza, M., Lagudi, A., Čejka, J., ... & Skarlatos, D. (2019). Underwater augmented reality for improving the diving experience in submerged archaeological sites. *Ocean Engineering*, 190, 106487.
5. **Mangeruga, M.**, Cozza, M., & Bruno, F. (2018). Evaluation of underwater image enhancement algorithms under different environmental conditions. *Journal of Marine Science and Engineering*, 6(1), 10.
6. **Mangeruga, M.**, Bruno, F., Cozza, M., Agrafiotis, P., & Skarlatos, D. (2018). Guidelines for underwater image enhancement based on benchmarking of different methods. *Remote Sensing*, 10(10), 1652.
7. Bruno, F., Petriaggi, B. D., **Mangeruga, M.**, & Cozza, M. (2018). Un tablet subacqueo per la documentazione e la fruizione dei siti archeologici sommersi. *Archeomatica*, 9(3).
8. Bruno, F., Lagudi, A., Barbieri, L., Muzzupappa, M., **Mangeruga, M.**, Cozza, M., ... & Peluso, R. (2018). Virtual Reality Technologies for the Exploitation of Underwater Cultural Heritage. *Latest Developments in Reality-Based 3D Surveying and Modelling*; Remondino, F., Georgopoulos, A., González-Aguilera, D., Agrafiotis, P., Eds, 220-236.

List of Figures

Figure 1. Software architecture.....	14
Figure 2. GUI at first start.....	15
Figure 3. Setting the parameter of an algorithm.	15
Figure 4. Error: the user has selected no algorithms.	16
Figure 5. Error: the user has not selected an input folder.....	16
Figure 6. GUI during the processing of the selected images.....	16
Figure 7. Example of Log panel messages.	17
Figure 8. Web interface with sample images.....	18
Figure 9. Algorithm selection.	18
Figure 10. Sample output image enhanced with ACE.	19
Figure 11. Log panel after processing with ACE algorithm.	19
Figure 12. Underwater images dataset. (a–c) Images acquired at Underwater Archaeological Park of Baiae, named respectively Baia1, Baia2, Baia3. Credits: MiBACT-ISCR; (d–f) Images acquired at Cala Cicala shipwreck, named respectively CalaCicala1, CalaCicala2, CalaCicala3. Credits: University of Calabria; (g–i) Images acquired at Cala Minnola, named respectively CalaMinnola1, CalaMinnola2, CalaMinnola3. Credits: University of Calabria; (l–n) Images acquired at Mazotos, named respectively Mazotos1, Mazotos2, Mazotos3. Credits: MARELab, University of Cyprus.....	23
Figure 13. The image “Baia1” enhanced with all five algorithms. (a) Original image; (b) Enhanced with ACE; (c) Enhanced with CLAHE; (d) Enhanced with LAB; (e) Enhanced with NLD; (f) Enhanced with SP.....	25
Figure 14. Artefacts in the sample image “CalaMinnola1” enhanced with SP algorithm.....	28
Figure 15. Sample of SP algorithm enhancement for visual evaluation. (a,b) “Baia2” original and enhanced images; (c,d) “CalaCicala3” original and enhanced images; (e,f) “CalaMinnola1” original and enhanced images; (g,h) “Mazotos1” original and enhanced images.....	29
Figure 16. Underwater images dataset. (a–c) Images acquired at Underwater Archaeological Park of Baiae, named respectively Baia1, Baia2, Baia3. Credits: MiBACT-ISCR; (d–f) Images acquired at Cala Cicala shipwreck, named respectively CalaCicala1, CalaCicala2, CalaCicala3. Credits: Soprintendenza Belle Arti e Paesaggio per le province di CS, CZ, KR and University of Calabria; (g–i) Images acquired at Cala Minnola, named CalaMinnola1, CalaMinnola2, CalaMinnola3, respectively. Credits: Soprintendenza del Mare and University of Calabria; (j–l) Images acquired at Mazotos with artificial light, named respectively MazotosA1, MazotosA2, MazotosA3. Credits: MARELab, University of Cyprus; (m–o) Images acquired at	

Mazotos with natural light, named respectively MazotosN4, MazotosN5, MazotosN6. Credits: MARELab, University of Cyprus.	32
Figure 17. The image “MazotosN4” enhanced with all five algorithms. (a) Original image; (b) Enhanced with ACE; (c) Enhanced with CLAHE; (d) Enhanced with LAB; (e) Enhanced with NLD; (f) Enhanced with SP.	34
Figure 18. Artefacts in the sample images “CalaMinnola1” (a) and “CalaMinnola2” (b) enhanced with SP algorithm.....	36
Figure 19. A sample section of the survey submitted to the expert panel.	38
Figure 20. Examples of original and corrected images of the 5 different datasets. Credits: MiBACT-ISCR (Baiae images); Soprintendenza Belle Arti e Paesaggio per le province di CS, CZ, KR and University of Calabria (Cala Cicala images); Soprintendenza del Mare and University of Calabria (Cala Minnola images); MARELab, University of Cyprus (MazotosA images); Department of Fisheries and Marine Research of Cyprus (MazotosN images).....	43
Figure 21. The dense point clouds for all the datasets and for all the available imagery.....	45
Figure 22. The results of the computed parameters for the five different datasets.	48
Figure 23. The Combined 3D metric (<i>C3Dm</i>), representing an overall evaluation of 3D reconstruction performance of the five tested image enhancing methods on the five datasets.	50
Figure 24. Textured 3D models based on MazotosA dataset and created with two different strategies. (a) 3D model created by means of only LAB enhanced imagery both for the 3D reconstruction and texture. (b) 3D model created following the methodology suggested above: the 3D reconstruction was performed using the LAB enhanced imagery and the texturing using the more faithful to the reality ACE imagery.....	53
Figure 25. The prototype of the Underwater Tablet developed in the Visas project.	55
Figure 26. The LBL configuration.....	56
Figure 27. The new underwater case with the Bluetooth keyboard.....	58
Figure 28. Example of deployment of an SBL/USBL system.....	59
Figure 29. The two new acoustic localization systems coupled with the underwater tablet. (a) The USBL system; (b) the SBL system.	59
Figure 30. The Bluetooth keyboard integrated in the case (a) and the related Five Buttons UI (b).	61
Figure 31. Five Buttons UI menu hierarchy.	61
Figure 32. Actual app navigation flow.	62
Figure 33. Underwater site and Dive Plan selection.....	63
Figure 34. The user can decide to skip the connection to the computer board.....	64
Figure 35. Two different setups of the Navigation Screen as an example of the UI modularity.	64
Figure 36. Customizable Computer Board UI.	65

Figure 37. Example of Navigation UI with the colour pairs reported in Table 17.	66
Figure 38. Main navigation screen.	67
Figure 39. Visualization of additional information regarding the active POI.....	68
Figure 40. An active POI is highlighted in yellow (a). A visited POI is highlighted in red (b).	68
Figure 41. Different POIs are visualized according to the zoom level. Less zooming (a); more zooming (b).	68
Figure 42. Acquisition of geo-localized photos (a) and textual notes (b) through the underwater tablet.	69
Figure 43. Messaging feature. Sending a new message (a) and visualize the messaging history (b).	69
Figure 44. Underwater itinerary in the submerged archaeological site of Punta Scifo. (Images courtesy of the Marine Protected Area of “Capo Rizzuto”).....	72
Figure 45. Planimetric archaeological map of “Villa con ingresso a protiro”. (Image courtesy of ISCR).	75
Figure 46. Different portions of the 3D hypothetical reconstruction of the Villa: atrium with impluvium (a), room with pelte mosaic (b).	76
Figure 47. The button to switch the AR status.	77
Figure 48. Top View of the hypothetical reconstruction.....	78
Figure 49. First Person View of the hypothetical reconstruction.	78
Figure 50. Hybrid tracking system’s architecture.	80
Figure 51. Deepening on the architecture of the hybrid tracking system.	80
Figure 52. Acoustic data acquired moving along the ground-truth (a), and comparison of acoustic and data tracked according to hybrid approach (b).	82
Figure 53. Divers testing the UWAR feature through the underwater tablet.	84
Figure 54. Two graphics about the results of the questionnaires. (a) Tcha-Tokey questionnaire; (b) NASA TLX questionnaire, lower is better.	86
Figure 55. The stages of the pathfinding algorithm and communication with DecoAPI.....	92
Figure 56. A representation of the three different types of movements allowed in a 3D grid with the related distance costs.....	94
Figure 57. The search tree in the sample case of three points of interest (POIs).....	98
Figure 58. A modern shipwreck.	100
Figure 59. A sample of a seamount.	100
Figure 60. A sample of a landslide.	101
Figure 61. The 3D grids of each underwater site: (a) the shipwreck, (b) the seamount, and (c) the landslide.	101
Figure 62. The path suggested by the algorithm changes over time.	103
Figure 63. The evolution of the air consumption cost (a) and the decompression cost (b) with the increasing of the depth.....	106

Acronyms

ACE	Automatic Colour Enhancement
AHE	Adaptive Histogram Equalization
ANOVA	ANalysis Of VAriance
API	Application Programming Interface
AR	Augmented Reality
ASV	Autonomous Surface Vehicle
AUV	Autonomous Underwater Vehicle
CLAHE	Contrast Limited Adaptive Histogram Equalization
DCP	Dark Channel Prior
DVL	Doppler Velocity Log
GNSS	Global Navigation Satellite System
GPS	Global Positioning System
GUI	Graphical User Interface
HMD	Head Mounted Display
IMU	Inertial Measurement Unity
LBL	Long BaseLine
MVS	Multi View Stereo
NLD	Non-Local Dehazing
POI	Point Of Interest
QR	Quick Response
RMV	Respiratory Minute Volume
SBL	Short BaseLine
SfM	Structure from Motion
SP	Screened Poisson
TTS	Time To Surface
UCH	Underwater Cultural Heritage
UI	User Interface
USBL	Ultra-Short BaseLine
UUV	Unmanned Underwater Vehicle
UW	UnderWater
UWAR	UnderWater Augmented Reality
VIO	Visual Inertial Odometry
VR	Virtual Reality

Contents

ABSTRACT	1
1 INTRODUCTION	3
1.1 MOTIVATIONS.....	3
1.2 GOALS.....	3
1.3 THESIS OVERVIEW.....	4
1.3.1 <i>Thesis Outline</i>	4
1.3.2 <i>Contributions</i>	5
2 UNDERWATER IMAGE ENHANCEMENT	6
2.1 INTRODUCTION.....	6
2.2 STATE OF THE ART.....	7
2.3 A SOFTWARE TOOL FOR ENHANCING UNDERWATER IMAGES.....	10
2.3.1 <i>Selected Algorithms and Their Implementation</i>	11
2.3.2 <i>Software Architecture</i>	13
2.4 EVALUATION OF UNDERWATER IMAGE ENHANCEMENT ALGORITHMS UNDER DIFFERENT ENVIRONMENTAL CONDITIONS ...	20
2.4.1 <i>Case studies</i>	20
2.4.2 <i>Evaluation Methods</i>	23
2.4.3 <i>Results</i>	25
2.4.4 <i>Conclusions</i>	28
2.5 GUIDELINES FOR UNDERWATER IMAGE ENHANCEMENT BASED ON BENCHMARKING OF DIFFERENT METHODS.....	30
2.5.1 <i>Case studies</i>	30
2.5.2 <i>Benchmarking Based on Objective Metrics</i>	32
2.5.3 <i>Benchmarking Based on Expert Panel</i>	37
2.5.4 <i>Benchmarking Based on the Results of 3D Reconstruction</i>	42
2.5.5 <i>Comparison of the Three Benchmarks Results</i>	50
2.5.6 <i>Conclusions</i>	52
3 UNDERWATER ASSISTED NAVIGATION	54
3.1 INTRODUCTION.....	54
3.2 STATE OF THE ART.....	56
3.3 HARDWARE SETUP	57
3.3.1 <i>Waterproof case</i>	57
3.3.2 <i>Acoustic localization system</i>	58
3.4 DIVY: THE UNDERWATER NAVIGATION APP	60
3.4.1 <i>Five Buttons UI</i>	60
3.4.2 <i>App navigation flow</i>	62
3.4.3 <i>Modular UI components</i>	64

3.4.4	<i>Configurable Themes</i>	66
3.4.5	<i>Main navigation screen</i>	67
3.4.6	<i>POI information</i>	67
3.4.7	<i>Acquisition of geo-localized data</i>	69
3.4.8	<i>Messaging</i>	69
3.5	CONCLUSIONS	70
4	UNDERWATER AUGMENTED REALITY (UWAR)	71
4.1	INTRODUCTION.....	71
4.2	STATE OF THE ART	73
4.3	THE CASE-STUDY: THE UNDERWATER ARCHAEOLOGICAL PARK OF BAIAE	74
4.4	UWAR IMPLEMENTATION.....	76
4.5	HYBRID TRACKING.....	79
4.5.1	<i>Field test</i>	81
4.6	USERS EVALUATION	83
4.7	CONCLUSIONS	87
5	UNDERWATER PATH PLANNING	88
5.1	INTRODUCTION.....	88
5.2	MATERIALS AND METHODS	91
5.2.1	<i>Space Partitioning</i>	92
5.2.2	<i>Phase 1 (Links Generation): Calculating Optimal Links between Pairs of POIs</i>	93
5.2.3	<i>Phase 2 (Path Optimisation): Calculating Optimal Path to Visit all POIs</i>	97
5.3	RESULTS.....	99
5.3.1	<i>Case Studies</i>	99
5.3.2	<i>Space Partitioning: 3D Grids</i>	101
5.3.3	<i>Generated Paths</i>	102
5.4	DISCUSSION	104
5.5	CONCLUSIONS	106
6	CONCLUSIONS AND FUTURE WORK.....	108
6.1	CONCLUSIONS	108
6.2	FUTURE WORK.....	111
	REFERENCES	113

Abstract

In the submerged environment divers often suffer from low visibility conditions that make difficult the orientation within an underwater site. At present, there is a lack of technologies and tools supporting the divers to better orientate themselves in the underwater environment and to simplify their comprehension of the context. The research aims to design and develop innovative solutions to support divers, both recreative and technical/scientific ones, through a novel system for underwater navigation and exploration, providing them with underwater geo-localization, contextualized information, augmented reality (AR) contents and recommendation about the optimal path to follow during the dive.

A first aspect on which the research work focused is the Underwater Image Enhancement. This study has led to the development of a software tool to enhance underwater images with well-known methods at the SoA. A benchmark of these well-known methods has been produced and some guidelines to evaluate the underwater image enhancement methods have been formulated. The effort of this part of the research has been to guide the community towards the definition of a more effective and objective methodology for the evaluation of underwater image enhancement methods. Another aspect of the research concerned the Underwater Navigation and Underwater AR (UWAR). A software for underwater tablets, namely Divy, has been designed and developed to support divers' navigation and exploration. It enables the divers to access different features such as the visualization of a map of the underwater site that allows them to know their position within the submerged site, the possibility to acquire geo-localized data, the visualization of additional information about specific points of interest and the communication with the surface operators through an underwater messaging system.

On this basis, the UWAR concept applied in Underwater Cultural Heritage sites has been designed and developed as well, consisting of an augmented visualization representing a hypothetical 3D reconstruction of the archaeological remains as they appeared in the past. The geo-localization is provided by an acoustic localization system, but this kind of technology suffers from a low update rate, and cannot be employed alone for the AR purpose. To improve the performance of the UWAR and provide the users with a smooth AR visualization, a hybrid technique that merges data from an acoustic localization system with data coming from a visual inertial-odometry framework has been conceived and developed to deliver positioning information with a higher update rate with respect to the acoustic system alone. In particular, given the low update rate of the acoustic system, a strategy has been implemented aimed to fill the gaps between two consecutive acoustic positioning data. User testing has been conducted to assess the effectiveness and potential of the developed UWAR technologies.

Finally, an innovative approach to dive planning based on an original underwater pathfinding algorithm has been conceived. It computes the best 3D path to follow during the dive in order to maximise the number of Points of Interest (POIs) visited, while taking into account the safety limitations strictly related to scuba diving. This approach considers the morphology of the 3D space in which the dive takes place to compute the best path, taking into account the diving decompression limits and avoiding the obstacles through the analysis of a 3D map of the site.

1 Introduction

1.1 Motivations

Due to water turbidity and biological colonization, in the submerged environment the divers often suffer from low visibility conditions and this leads to a less understanding of the underwater environment and a higher probability for them to miss the sense of direction. Unfortunately, GNSS sensors (GPS, GLONASS, and Galileo) are inadequate to this end since their signals are absorbed in water after a few centimetres below the sea level. Guided or accompanied diving tours in recreative or archaeological sites, are carried out with experienced divers, but it is not possible to perform a fluid and direct communication unless they use full-face diving masks or analogous dedicated equipment. At the moment, there are few attempts to support the divers by facilitating their comprehension of the context and by supporting them to orientate in the underwater environment. There is a lack of technologies and tools to support the divers engaged both in recreational and scientific/technical underwater activities. A system that could assist the divers in the underwater navigation and exploration, providing them with underwater geo-localization, contextualized information and recommendation about the path follow, would be extremely useful in this context.

1.2 Goals

The aim of the research is to design and develop innovative solutions to support the diver through a novel system for the underwater navigation and exploration. A key capability consists of a 3D navigation feature, provided by means of an underwater tablet, that allows the diver to know her/his position within the underwater environment, access contextualised information (including 3D models displayed in Augmented Reality), acquire geo-localized environmental data, and receive assistance about the shortest path through which it is possible to safely reach the desired targets. The system is designed to assist both recreational and scientific/technical divers.

The research work focuses on three main aspects:

- **Underwater Image enhancement:** a study about the techniques for enhancing the underwater imagery has been conducted since underwater photography is the documentation method most used by divers. A benchmark has been conducted in order to evaluate the most performing algorithms able to improve the quality of the images as well as the 3D photogrammetric models of the underwater sites.
- **Underwater Navigation and Underwater AR (UWAR):** the aim is to provide the diver with a map of the underwater scene that allows him to know his position within the submerged site; archaeological, historical, biological and scientific information about the specific context;

and an enhanced diving experience through an on-site augmented visualization representing a 3D hypothetical reconstruction of the ancient ruins present in the underwater site.

- **Underwater Path planning:** the aim is to provide the divers (mainly scientific/technical ones) with an innovative approach to dive planning based on an original underwater pathfinding algorithm that computes the best 3D path to follow during the dive in order to maximise the number of Points of Interest (POIs) visited, while taking into account the safety limitations strictly related to scuba diving.

1.3 Thesis Overview

1.3.1 Thesis Outline

This thesis is organized in the following chapters:

- **Chapter 2:** this chapter describes the research conducted in the field of the underwater image enhancement. In particular, well-known methods from the state of the art were selected and used to enhance a dataset of images produced in various underwater sites with different conditions of depth, turbidity, and lighting. These enhanced images were evaluated by means of three different approaches: objective metrics often adopted in the related literature, a panel of experts in the underwater field, and an evaluation based on the results of 3D reconstructions. The aim was to pave the way towards the definition of an effective methodology for the performance evaluation of the underwater image enhancement techniques. Furthermore, a software has been developed, useful for automatically processing a dataset of underwater images with a set of image enhancement algorithms. Employing this tool for the enhancement of the underwater images ensures to minimize the pre-processing effort and enables the underwater community to quickly verify the performance of the different methods on their own datasets.
- **Chapter 3:** this chapter describes the design and the development of underwater navigation system by the means of an underwater tablet that support the diver providing him/her with geo-localization, contextualized information, and other several features, such as geo-localized data acquisition, underwater messaging, underwater augmented reality and underwater pathfinding.
- **Chapter 4:** this chapter investigates the feasibility and potentials offered by the AR technologies for improving the diving experience in the underwater archaeological sites, and provides an overview of the UnderWater Augmented Reality (UWAR) feature. A hybrid tracking technique has been designed, that integrates acoustic localization and visual-inertial odometry, in order to perform an augmented visualization representing

the actual conditions of the ancient ruins in the underwater site and a hypothetical 3D reconstruction of the archaeological remains as they appeared in the past of the Roman era by means of the underwater tablet described in the previous chapter.

- **Chapter 5:** this chapter presents a novel approach to dive planning based on an original underwater pathfinding algorithm that computes the best 3D path to follow during the dive in order to be able to maximise the number of Points of Interest (POI) visited, while taking into account the safety limitations. The proposed solution considers the morphology of the 3D space in which the dive takes place to compute the best path, taking into account the decompression limits and avoiding the obstacles through the analysis of a 3D map of the site.
- **Chapter 6:** Finally, the last chapter presents the conclusions and some guidelines for future work.

1.3.2 Contributions

The main contribution of the research described in this Ph.D thesis are the following:

- Design and development of a software tool to enhance the underwater images with five well-known methods at the SoA;
- Benchmarking of well-known methods for underwater image enhancement;
- Formulation of guidelines to evaluate the underwater image enhancement methods;
- Design and development of a software for underwater tablets to support divers' navigation and exploration;
- Design and development of a hybrid technique that merges data from an acoustic localization system with data coming from a visual inertial-odometry framework;
- Design, development and user testing of the Underwater Augmented Reality concept applied in Underwater Cultural Heritage sites;
- Design and development of a novel underwater pathfinding algorithm.

2 Underwater Image Enhancement

2.1 Introduction

The degradation of underwater images quality is mainly attributed to light scattering and absorption. The light is attenuated as it propagates through water and the attenuation varies according to the wavelength of light within the water column depth and depends also on the distance of the objects from the point of view. The suspended particles in the water are also responsible for light scattering and absorption. In many cases, the image taken underwater seems to be hazy, in a similar way as it happens in landscape photos degraded by haze, fog or smoke, which also cause absorption and scattering. Moreover, as the water column increases, the various components of sunlight are differently absorbed by the medium, depending on their wavelengths. This leads to a dominance of blue/green colour in the underwater imagery that is known as colour cast. The visibility can be increased and the colour can be recovered by using artificial light sources in an underwater imaging system. But artificial light does not illuminate the scene uniformly and it can produce bright spots in the images due to the backscattering of light in the water medium.

In literature, there are many algorithms aimed to enhance the quality of underwater images through different approaches. A first research has been conducted and presented in [1] with the main purpose to identify an algorithm that performs well in different environmental conditions. As described in detail in Section 2.4, some algorithms have been selected from the state of the art and have been employed to enhance a dataset of images produced in various underwater sites, representing different environmental and illumination conditions. These enhanced images have been evaluated through some quantitative metrics. By analysing the results of these metrics, we tried to understand which of the selected algorithms performed better than the others. Another purpose of this research was to establish if a quantitative metric was enough to judge the behaviour of an underwater image enhancement algorithm. The aim was to demonstrate that, even if the metrics can provide an indicative estimation of image quality, they could lead to inconsistent or erroneous evaluations.

Later, a more in-depth study has been conducted and presented in [2]. As described in detail in Section 2.5, the same five well-known methods selected from the state of the art have been employed to enhance a slightly different dataset of images produced in various underwater sites with different conditions of depth, turbidity, and lighting. These enhanced images were evaluated by means of three different approaches: objective metrics often adopted in the related literature, a panel of experts in the underwater field, and an evaluation based on the results of 3D reconstructions. As stated before, in the literature there are many enhancement algorithms that improve different aspects of the

underwater imagery. Each paper, when presenting a new algorithm or method, usually compares the proposed technique with some alternatives present in the current state of the art. There are no studies on the reliability of benchmarking methods, as the comparisons are based on various subjective and objective metrics. This second work aimed to pave the way towards the definition of an effective methodology for the performance evaluation of the underwater image enhancement techniques. Moreover, this work could orientate the underwater community towards choosing which method can lead to the best results for a given task in different underwater conditions.

Furthermore, a software has been developed, useful for automatically processing a dataset of underwater images with a set of image enhancement algorithms. It is described in detail in Section 2.3 and it has been employed in both the research works previously introduced to simplify the benchmarking of these algorithms.

2.2 State of the Art

The problem of underwater image enhancement is closely related to single image dehazing, in which images are degraded by weather conditions such as haze or fog. A variety of approaches have been proposed to solve image dehazing, and in the present section their most effective examples have been reported. Furthermore, this section also describes methods that address the problem of non-uniform illumination in the images and those that focus on colour correction.

Single image dehazing methods assume that only one input image is available and rely on image priors to recover a dehazed scene. One of the most cited works on single image dehazing is the dark channel prior (DCP) [3]. It assumes that, within small image patches, there will be at least one pixel with a dark colour channel. It then uses this assumption to estimate the transmission and to recover the image. However, this prior was not designed to work underwater, and it does not take into account the different absorption rates of the three colour channels. In [4], an extension of DCP to deal with underwater image restoration is presented. Given that the red channel is often nearly dark in underwater images, this new prior called Underwater Dark Channel Prior (UDCP) considers just the green and the blue colour channels in order to estimate the transmission. An author mentioned many times in the field is Fattal, R and his two works [5,6]. In the first work [5], Fattal et al., taking into account surface shading and the transmission function, tried to resolve ambiguities in data by searching for a solution in which the resulting shading and transmission functions are statistically uncorrelated.

The second work [6] describes a new method based on a generic regularity in natural images, which is referred to as colour-lines. On this basis, Fattal et al. derived a local formation model that explains the colour-lines in the context of hazy scenes and used it to recover the image. Another work focused on lines of colour is presented in [7,8]. The authors describe a new prior for single image

dehazing that is defined as a Non-Local prior, to underline that the pixels forming the lines of colour are spread across the entire image, thus capturing a global characteristic that is not limited to small image patches.

Some other works focus on the problem of non-uniform illumination that, in the case of underwater imagery, is often produced by an artificial light in deep water. The work proposed in [9] assumes that natural underwater images are Rayleigh distributed and uses maximum likelihood estimation of scale parameters to map distribution of image to Rayleigh distribution. Next, Morel et al. [10] present a simple gradient domain method that acts as a high-pass filter, trying to correct the illumination without affecting the image details. A simple prior which estimates the depth map of the scene considering the difference in attenuation among the different colour channels is proposed in [11]. The scene radiance is recovered from a hazy image through an estimated depth map by modelling the true scene radiance as a Markov Random Field.

Bianco et al. presented, in [12], the first proposal for the colour correction of underwater images by using $\alpha\beta$ colour space. White balancing is performed by moving the distributions of the chromatic components (α , β) around the white point and the image contrast is improved through a histogram cut-off and stretching of the luminance (l) component. More recently, in [13], a fast enhancement method for non-uniformly illuminated underwater images is presented. The method is based on a grey-world assumption applied in the Ruderman-lab opponent colour space. The colour correction is performed according to locally changing luminance and chrominance by using the summed-area table technique. Due to the low complexity cost, this method is suitable for real-time applications, ensuring realistic colours of the objects, more visible details and enhanced visual quality. Works [14,15] present a method of unsupervised colour correction for general purpose images. It employs a computational model that is inspired by some adaptation mechanisms of the human vision to realize a local filtering effect by taking into account the colour spatial distribution in the image.

Additionally, a method for contrast enhancement has also been addressed, since underwater images are often lacking in contrast. This is the Contrast Limited Adaptive Histogram Equalization (CLAHE) proposed in [16] and summarized in [17], which was originally developed for medical imaging and has proven to be successful for enhancing low-contrast images.

In [18], a fusion-based underwater image enhancement technique using contrast stretching and Auto White Balance is presented. In [19], a dehazing approach that builds on an original colour transfer strategy to align the colour statistics of a hazy input to the ones of a reference image, also captured underwater, but with neglectable water attenuation, is delivered. There, the colour-transferred input is restored by inverting a simplified version of the McGlamery underwater image formation model, using the conventional Dark Channel Prior (DCP) to estimate the transmission map and the backscattered light parameter involved in the model.

Work [20] proposes a Red Channel method in order to restore the colours of underwater images. The colours associated with short wavelengths are recovered, leading to a recovery of the lost contrast. According to the authors, this Red Channel method can be interpreted as a variant of the DCP method used for images degraded by the atmosphere when exposed to haze. Experimental results show that the proposed technique handles artificially illuminated areas gracefully, and achieves a natural colour correction and superior or equivalent visibility improvement when compared to other state-of-the-art methods. However, it is suitable either for shallow waters, where the red colour still exists, or for images with artificial illumination. The authors in [21] propose a modification to the well-known DCP method. Experiments on real-life data show that this method outperforms competing solutions based on the DCP. Another method that relies in part on the DCP method is presented in [22], where an underwater image restoration method is presented based on transferring an underwater style image into a recovered style using Multi-Scale Cycle Generative Adversarial Network System. There, a Structural Similarity Index Measure loss is used to improve underwater image quality. Then, the transmission map is fed into the network for multi-scale calculation on the images, which combine the DCP method and Cycle-Consistent Adversarial Networks. The work presented in [23] describes a restoration method that compensates for the colour loss due to the scene-to-camera distance of non-water regions without altering the colour of pixels representing water. This restoration is achieved without prior knowledge of the scene depth.

In [24], a deep learning approach is adopted; a Convolutional Neural Network-based image enhancement model is trained efficiently using a synthetic underwater image database. The model directly reconstructs the clear latent underwater image by leveraging on an automatic end-to-end and data-driven training mechanism. Experiments performed on synthetic and real-world images indicate a robust and effective performance of the proposed method.

In [25], exposure bracketing imaging is used to enhance the underwater image by fusing an image that includes sufficient spectral information of underwater scenes. The fused image allows authors to extract reliable grey information from scenes. Even though this method gives realistic results, it seems to be limited in no real-time applications due to the exposure bracketing process.

In the literature, very few attempts at underwater image enhancement methods evaluation through feature matching have been reported, while even fewer of them focus on evaluating the results of 3D reconstruction using the initial and enhanced imagery. Recently, a single underwater image restoration framework based on the depth estimation and the transmission compensation was presented [26]. The proposed scheme consists of five major phases: background light estimation, submerged dark channel prior, transmission refinement and radiance recovery, point spread function deconvolution and transmission and colour compensation. The authors used a wide variety of underwater images with various scenarios in order to assess the restoration performance of the

proposed method. In addition, potential applications regarding autopilot and three-dimensional visualization were demonstrated. In another recent work, Akkaynak and Treibitz [27] proposed a novel image formation model for underwater images, stating that it outperforms the methods that use an atmospheric model.

Ancuti et al., in [28], as well as in [29], where an updated version of the method is presented, delivered a novel strategy to enhance underwater videos and images built on the fusion principles. There, the utility of the proposed enhancing technique is evaluated through matching by employing the SIFT [30] operator for an initial pair of underwater images, and also for the restored versions of the images. In [31,32], the authors investigated the problem of enhancing the radiometric quality of underwater images, especially in cases where this imagery is going to be used for automated photogrammetric and computer vision algorithms later. There, the initial and the enhanced imagery were used to produce point clouds, meshes and orthoimages, which in turn were compared and evaluated, revealing valuable results regarding the tested image enhancement methods. Finally, in [33], the major challenge of caustics is addressed by a new approach for caustics removal [34]. There, in order to investigate its performance and its effect on the SfM-MVS (Structure from Motion—Multi View Stereo) and 3D reconstruction results, a commercial software performing SfM-MVS was used, the Agisoft’s Photoscan [35] as well as other key point descriptors such as SIFT [30] and SURF [36]. In the tests performed using the Agisoft’s Photoscan, an image pair of the five different datasets was inserted and the alignment step was performed. Regarding the key point detection and matching, using the in-house implementations, a standard detection and matching procedure was followed, using the same image pairs and filtering the initial matches using the RANSAC [37] algorithm and the fundamental matrix. Subsequently, all datasets were used in order to create 3D point clouds. The resulting point clouds were evaluated in terms of the total number of points and roughness, a metric that also indicates the noise on the point cloud.

2.3 A Software Tool for Enhancing Underwater Images

A software has been developed, useful for automatically processing a dataset of underwater images with a set of image enhancement algorithms, and it has been employed in the present work to simplify the benchmarking of these algorithms. This software implements five algorithms (ACE, CLAHE, LAB, NLD and SP) that perform well and employ different approaches for the resolution of the underwater image enhancement problem, such as image dehazing, non-uniform illumination correction and colour correction.

The decision to select certain algorithms among all the others is based on a brief preliminary evaluation of their enhancement performance. There are numerous methods of underwater image enhancement, and the vast majority of them has been considered. Unfortunately, many authors do

not release the implementation of their algorithms. An implementation that relies only on what authors described in their papers does not guarantee the accuracy of the enhancement process and can mislead the evaluation of an algorithm. Consequently, we selected those algorithms for which we could find a trustworthy implementation performed by the authors of the papers or by a reliable author. Within these algorithms, a preliminary evaluation has been conducted, in order to select the ones that seemed to perform better in different underwater conditions.

The source codes of the five selected algorithms were adapted and merged in the software tool. The OpenCV [38] library has been employed for tool development in order to exploit its functions for image managing and processing.

2.3.1 Selected Algorithms and Their Implementation

2.3.1.1 Automatic Colour Enhancement (ACE)

The ACE algorithm is a quite complex technique, due to its direct computation on an $N \times N$ image costs $O(N^4)$ operations. For this reason, the approach proposed in [15] has been followed that describes two fast approximations of ACE. First, an algorithm that uses a polynomial approximation of the slope function to decompose the main computation into convolutions, reducing the cost to $O(N^2 \log N)$. Second, an algorithm based on interpolating intensity levels that reduces the main computation to convolutions too. In our test, ACE was processed using the level interpolation algorithm with 8 levels. Two parameters that can be adjusted to tune the algorithm behaviour are α and the weighting function $\omega(x, y)$. The α parameter specifies the strength of the enhancement: the larger this parameter, the stronger the enhancement. In our test, the standard values have been used for this parameter, e.g. $\alpha = 5$ and $\omega(x, y) = 1/\|x - y\|$. For the implementation, the ANSI C source code referred in [15] has been adapted in the enhancement tool.

2.3.1.2 Contrast Limited Adaptive Histogram Equalization (CLAHE)

The CLAHE [16,17] algorithm is an improved version of AHE, or Adaptive Histogram Equalization. Both are aimed to improve the standard histogram equalization. CLAHE was designed to prevent the over amplification of noise that can be generated using the adaptive histogram equalization. CLAHE partitions the image into contextual regions and applies the histogram equalization to each of them. Doing so, it balances the distribution of used grey values in order to make hidden features of the image more evident. This algorithm has been implemented in the enhancement tool employing the CLAHE function provided by the OpenCV library. The input images are converted in $\alpha\beta$ colour space and then the CLAHE algorithm is applied only on the luminance (l) channel. OpenCV provides two parameters in order to control the output of this algorithm: the tile size and the contrast limit. The first parameter is the size of each tile in which the

original image is partitioned and the second one is a parameter useful to limit the contrast enhancement in each tile. If noise is present, it will be amplified as well. So, in noisy images, such as underwater images, it should be better to limit the contrast enhancement to a low value, in order to avoid the amplification of noise. In our test, we set tile size at 8x8 pixels and contrast limit to 2.

2.3.1.3 Colour Correction Method on $\alpha\beta$ Space (LAB)

This method [12] is based on the assumptions of grey world and uniform illumination of the scene. The idea behind this method is to convert the input image from RGB to LAB space, correct colour casts of an image by adjusting the α and β components, increasing contrast by performing histogram cut-off and stretching and then convert the image back to the RGB space. The author provided us with a MATLAB implementation of this algorithm but, due to the intermediate transformations of colour space, needed to convert the input image from RGB to LAB and due to the lack of optimization of the MATLAB code, this implementation was very time-consuming. Therefore, we managed to port this code in C++ by employing OpenCV among other libraries. This enabled us to include this algorithm in our enhancement tool and to decrease the computing time by an order of magnitude.

2.3.1.4 Non-Local Image Dehazing (NLD)

The basic assumption of this algorithm is that colours of a haze-free image can be well approximated by a few hundred distinct colours. These few colours can be grouped in tight colour clusters in RGB space. The pixels that compose a cluster are often located at different positions across the image plane and at different distances from the camera. So, each colour cluster in the clear image becomes a line in RGB space of a hazy image, at which the authors refer to as a hazy-line. By means of these haze-lines, this algorithm recovers both the distance map and the dehazed image. The algorithm is linear in the size of the image and the authors have published an official MATLAB implementation [7]. In order to include this algorithm in our enhancement tool, a porting in C++ has been conducted, employing different library as OpenCV, Eigen [39] for the operation on sparse matrix not supported by OpenCV and FLANN [40] (Fast Library for Approximate Nearest Neighbours) to compute the colour cluster.

2.3.1.5 Screened Poisson Equation for Image Contrast Enhancement (SP)

The output of the algorithm is an image which is the result of applying the Screened Poisson equation [10] to each colour channel separately, together with simplest colour balance [41] with a variable percentage of saturation as parameter (s). The Screened Poisson equation can be solved by using the discrete Fourier transform. Once found the solution in Fourier domain, the application of

the discrete inverse Fourier transform yields the result image. The simplest colour balance is applied both before and after the Screened Poisson equation solving. The complexity of this algorithm is $O(n \log n)$. The ANSI C source code is provided by the authors in [10] and it has been adapted in the enhancement tool. For the Fourier transform, this code relies on the library FFTw [42]. The algorithm output can be controlled with the trade-off parameter α and the level of saturation of the simplest colour balance s . In our evaluation, we used as parameters $\alpha = 0.0001$ and $s = 0.2$.

2.3.1.6 Running time

Table 1 shows the running times of these different algorithms on a sample image of 4000×3000 pixels. These times were estimated by the means of the software tool on a machine with an i7-920 @ 2.67 GHz processor.

Table 1. Running times (seconds) of different algorithms on a sample image of 4000×3000 pixels.

ACE	SP	NLD	LAB	CLAHE
30.6	21.2	283	9.8	1.7

2.3.2 Software Architecture

The software was developed in C++ taking advantage of the features provided by OpenCV for reading, writing, managing and elaborating the images. The project is designed so that the inclusion of a new algorithm would be painless. Figure 1 shows some details about the software architecture. The concept of algorithm has been abstracted through an interface named `IEnhancementAlgorithm` that defines a virtual function named `enhanceImage`. This function should be implemented by each class that represents an algorithm. The core of the application, implemented by the class `ImageEnhancement`, does not require any information about the details of implementation of each algorithm. This class can instance and use each algorithm without having to specify the exact class of the object that will be created. In fact, the creation of the algorithm object is demanded to the `AlgorithmFactory` class.

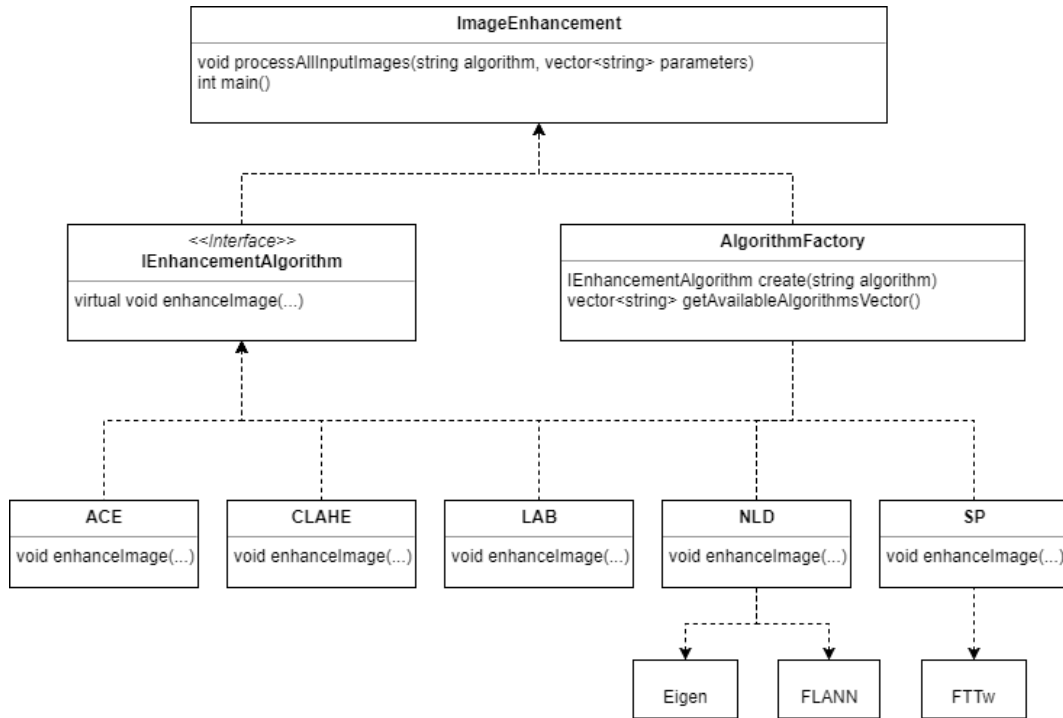


Figure 1. Software architecture

As can be noticed in Figure 1, some algorithms use additional libraries for their computation. This is the case of NLD that employs the Eigen and FLANN library, and SP that uses the FTTw library.

The software is compiled as a standalone executable that can be run from the command line. The syntax to run the software in such a way is *"ImageEnhancement.exe [algorithm_name] [input_path output_path] [parameter1 parameter2 ... parameterN]"*.

Where:

- [algorithm_name] is the string code that identifies the algorithm chosen for image processing; the algorithm string accepted are "ace", "clah", "lab", "nld", "sp" o "all". The latter is intended to process all input images with all the five algorithms.
- [input_path output_path] are the folder path for input images and the folder path for output images respectively; the default folders are "\in" and "\out".
- [parameter1 parameter2 ... parameterN] are parameters to be passed to the chosen algorithm in order to adjust its behaviour.

The command line syntax has been reported for the sake of completeness, but it is not intended to be used by the final user. For this purpose, a Graphical User Interface has been developed that is more user-friendly for a normal usage.

2.3.2.1 Graphical User Interface

A Graphical User Interface (GUI) has been designed and developed that is intuitive and easy to use for a standard user. The GUI is written in Java whereas the application core with the algorithms' implementation is written in C++ for a better performance, as described in the previous section.

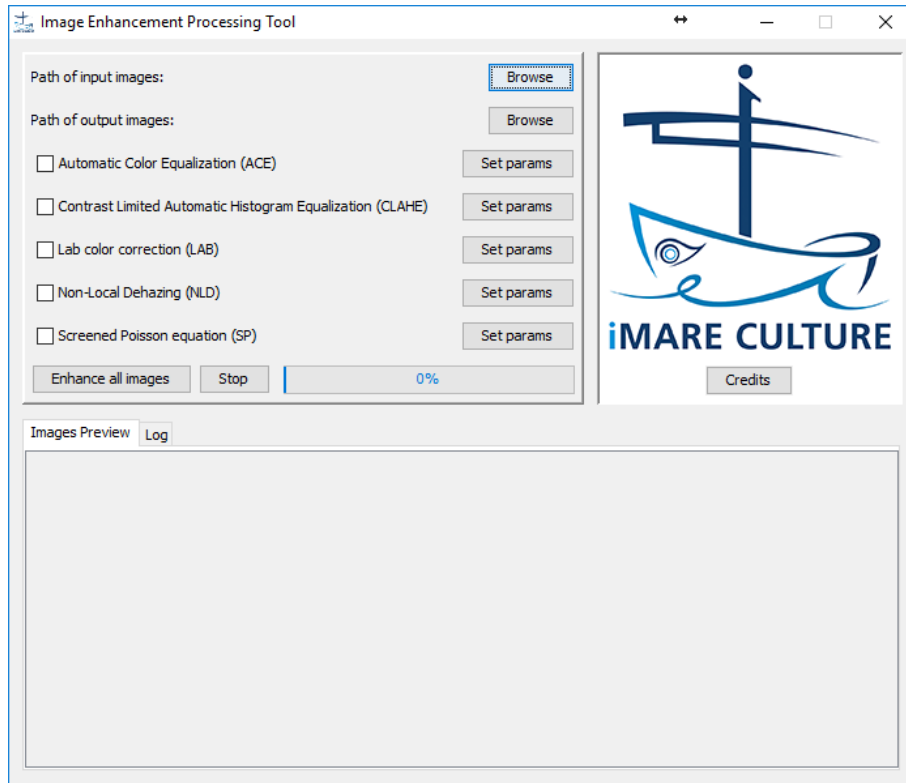


Figure 2. GUI at first start.

Figure 2 shows as the GUI appears right after the application is started. The top-right panel is composed of various fields and buttons that enable the user to configure and control the processing of the images. The first two fields from the top are the paths of input and output folders respectively and they can be chosen through the related *Browse* button. The check buttons just below permit to choose the algorithms to use for the enhancement of the input images. The parameters of each algorithm can be tuned through the related *Set Params* button (Figure 3).

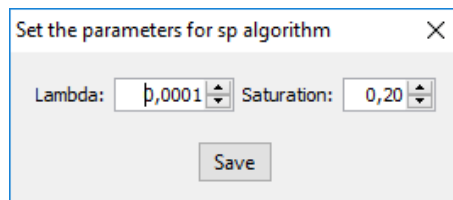


Figure 3. Setting the parameter of an algorithm.

Once selected all the desired options, it is possible to start the processing by pushing the button *Enhance all images*. Doing so, all the images in the input folder will be processed with all the selected algorithms and the chosen parameters. The output images will be saved in the output folder picked

by the user and organized in different subfolders for each algorithm. If there is some missing information in the chosen configuration, it is noticed to the user with proper messages before starting the processing, as showed in Figure 4 and Figure 5.

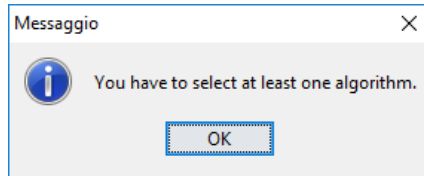


Figure 4. Error: the user has selected no algorithms.

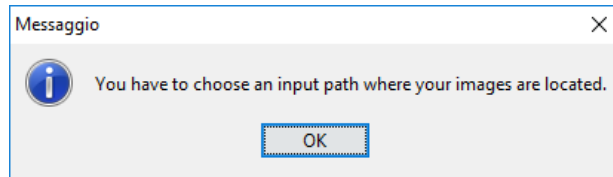


Figure 5. Error: the user has not selected an input folder.

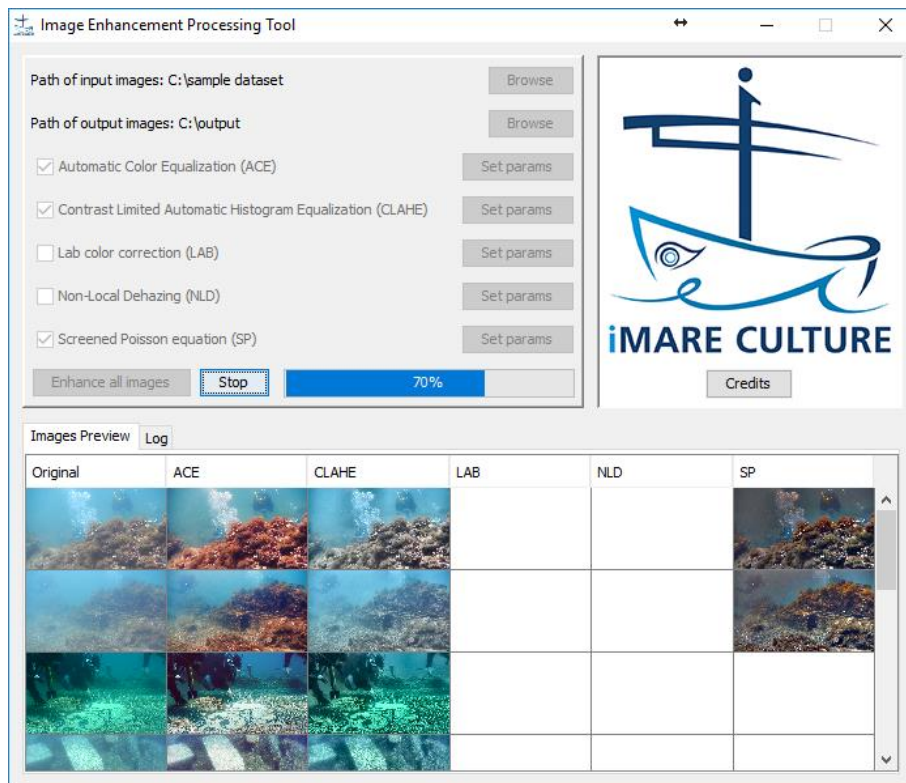


Figure 6. GUI during the processing of the selected images.

Figure 6 shows the GUI during the processing of the images. The progress of the process is reported by the progress bar near the stop button. As soon as an image is processed, it is showed in the *Image Preview* panel in a grid with all the original and enhanced images. The grid is composed of different rows for each input image; the first column shows the original images and the other columns show the same image enhanced with the algorithm associated with the column. This panel shows only a preview of ten images, so the grid is limited to ten rows. The complete output can be found in

the output folder chosen by the user. The Stop button enables the user to early stop the processing; all the images already processed remain stored in the output folder in any case.

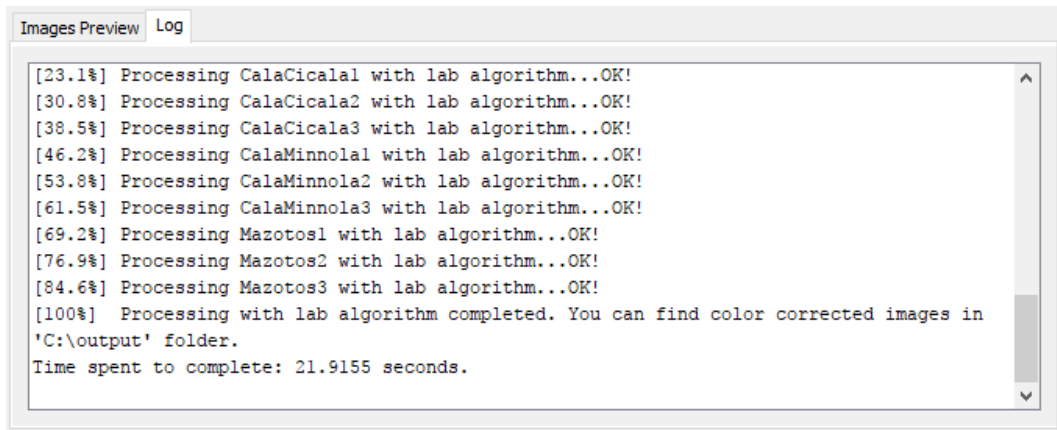


Figure 7. Example of Log panel messages.

The Log panel reports some detailed information about processing status and eventual errors, as shown in Figure 7.

2.3.2.2 Web Interface

In addition, a web interface has been developed that provides an example of the functionalities of the image enhancement tool. It is developed in PHP and enables a user to upload on a remote server a set of images and process them with one or all available algorithms. The web interface is intended for supporting remote control of an image processing server, then, it can be used by a single user at a time. It has been developed only for internal use in the i-MareCulture consortium.

Figure 8 shows the web interface, that interacts with the core application running on the server and displays the output images. The C++ core application is the same just described in the previous sections. The top-left panel permits to choose some local images by pushing *Browse* and to upload them on the remote server by pushing *Upload Images*. Doing so, the images will be sent to the server and reported in the list just below the upload button, as showed in Figure 8.

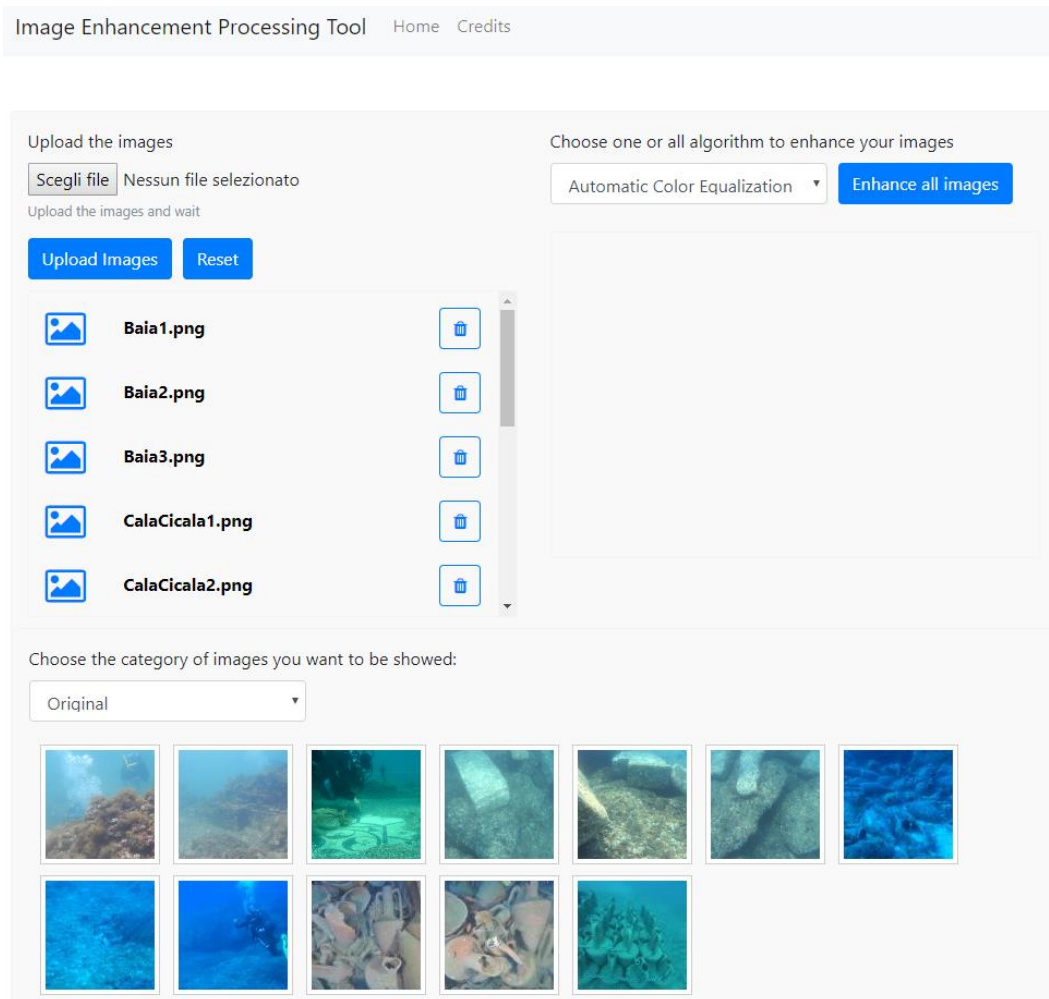


Figure 8. Web interface with sample images.

The top-right panel enables the user to select the algorithm by which all the input images will be processed. This selection can be done with the dropdown menu showed in Figure 9. By selecting *All algorithms* in place of a specific algorithm name, the image will be automatically processed with all five algorithms.

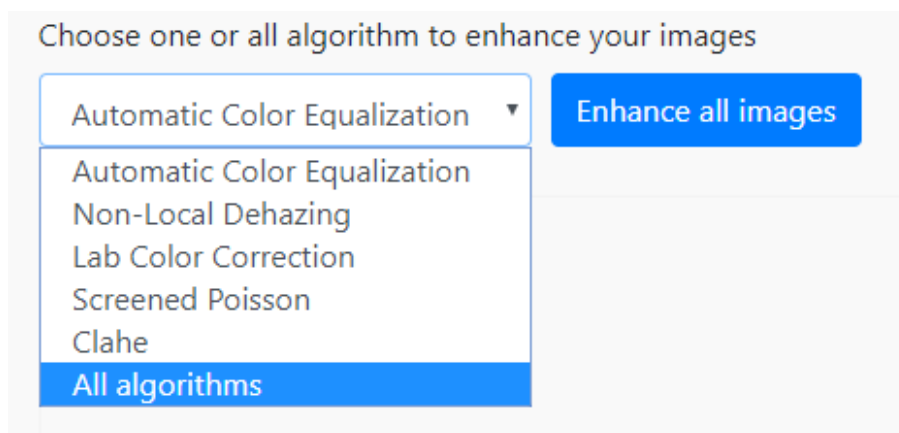


Figure 9. Algorithm selection.

The output images will be reported in the bottom panel. A dropdown menu permits to switch between the original images and the ones enhanced with each algorithm (Figure 10).

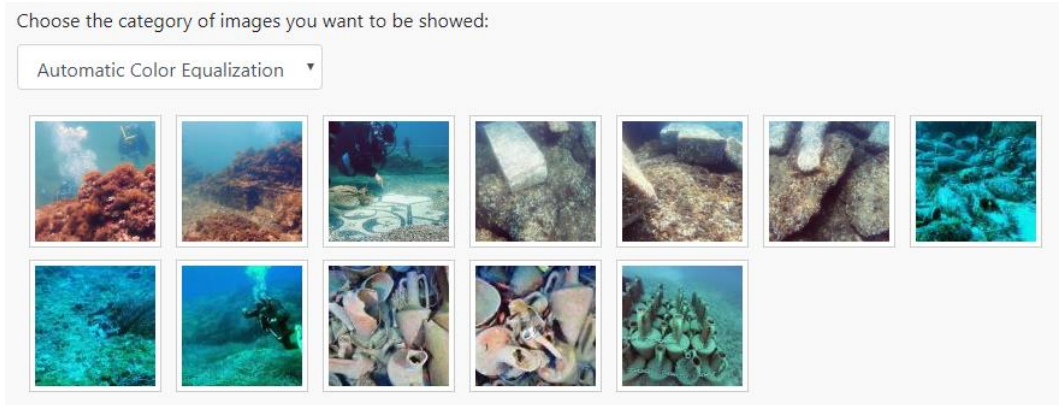


Figure 10. Sample output image enhanced with ACE.

The Log Panel reports some detailed information about the processing of the images, as shown in Figure 11.

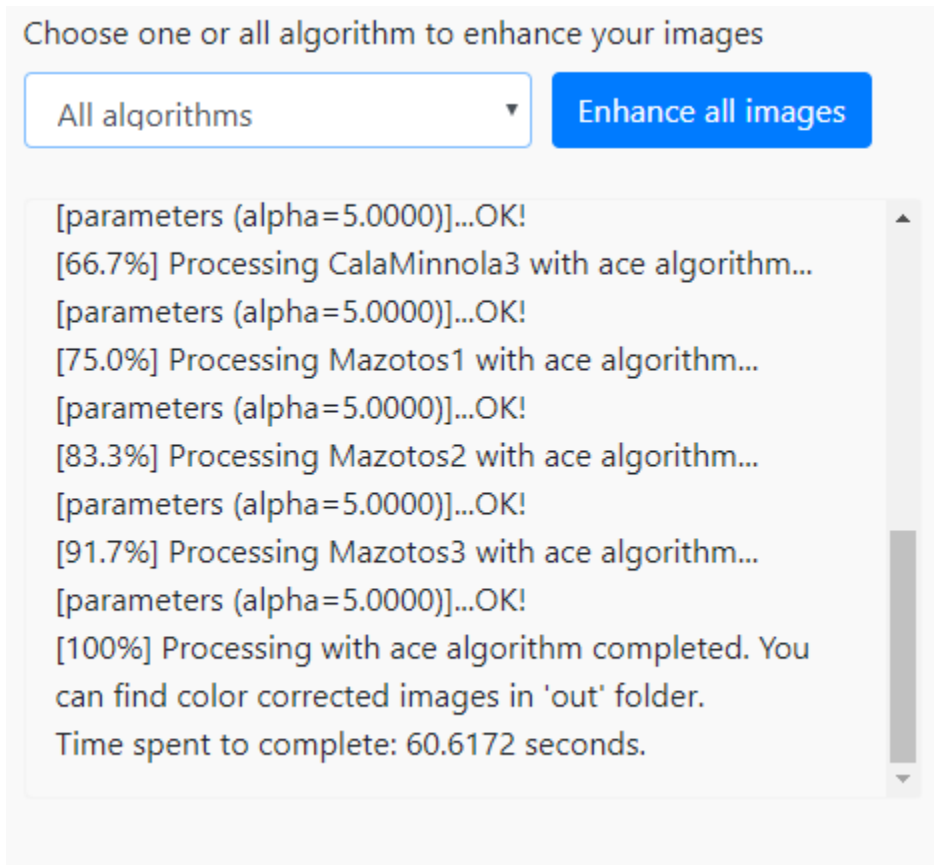


Figure 11. Log panel after processing with ACE algorithm.

Finally, the button Reset enables the user to delete the input and output images from the server, and to start over again with image processing.

2.4 Evaluation of Underwater Image Enhancement Algorithms under Different Environmental Conditions

The work presented in this section is part of the i-MARECULTURE project [43–45] that aims to develop new tools and technologies for improving the public awareness about underwater cultural heritage. In particular, it includes the development of a Virtual Reality environment that reproduces faithfully the appearance of underwater sites, giving the possibility to visualize the archaeological remains as they would appear in air. This goal requires a comparison of the different image enhancement algorithms to figure out which one performs better in different environmental and illumination conditions. Five algorithms have been selected from the state of the art and used to enhance a dataset of images produced in various underwater sites at heterogeneous conditions of depth, turbidity and lighting. These enhanced images have been evaluated by means of some quantitative metrics. There are several different metrics known in scientific literature employed to evaluate underwater enhancement algorithms, so only three of them have been chosen to complete this evaluation.

2.4.1 Case studies

We tried to produce a dataset of images that was as heterogeneous as possible, in order to better represent the variability of environmental and illumination conditions that characterizes underwater imagery. Furthermore, we choose images taken with different cameras and with different resolutions, because in the real application cases the underwater image enhancement algorithms have to deal with images produced by unspecific sources. This section describes the underwater sites, the dataset of images and the motivations that lead us to choose them.

2.4.1.1 Underwater Sites

Four different sites have been selected on which the images for the evaluation of the underwater image enhancement algorithms were taken. The selected sites are representative of different states of environmental and geomorphologic conditions (i.e. water depth, water turbidity etc.).

Two of them are pilot sites of the i-MARECULTURE project, the Underwater Archaeological Park of Baiae and the Mazotos shipwreck. The other two are the Cala Cicala and Cala Minnola shipwrecks.

2.4.1.1.1 *Underwater Archaeological Park of Baiae*

The Underwater Archaeological Park of Baiae is located off the north-western coasts of the bay of Puteoli (Naples). This site has been characterized by a periodic volcanic and hydrothermal activity and it has been subjected to gradual changes in the levels of the coast with respect to the sea level.

The Park safeguards the archaeological remains of the Roman city that are submerged at a depth ranging between 1 and 14–15m below sea level. This underwater site is usually characterized by a very poor visibility because of the water turbidity, which in turn is mainly due to the organic particles suspended in the medium. So, the underwater images produced here are strongly affected by the haze effect [46].

2.4.1.1.2 *Mazotos Shipwreck*

The second site is the Mazotos shipwreck that lies at a depth of 44 m, ca.14 nautical miles (NM) southwest of Larnaca, Cyprus, off the coast of Mazotos village. The wreck lies on a sandy, almost flat seabed and consists of an oblong concentration of at least 800 amphorae, partly or totally visible before any excavation took place. The investigation of the shipwreck is conducted jointly by the Maritime Research Laboratory (MARE Lab) of the University of Cyprus and the Department of Antiquities, under the direction of Dr Stella Demesticha. Some 3D models of the site have been created by using photogrammetric techniques [47]. The visibility in this site is very good but the red absorption at this depth is nearly total, so the images were taken using an artificial light for recovering the colour.

2.4.1.1.3 *Cala Cicala*

In 1950, near Cala Cicala, within the Marine Protected Area of Capo Rizzuto (Province of Crotone, Italy), the archaeological remains of a large Roman Empire ship were discovered at a depth of 5 m. The so-called Cala Cicala shipwreck, still set for sailing, carried a load of raw or semi-finished marble products of considerable size. In previous work, the site has been reconstructed with 3D photogrammetry and it can be enjoyed in Virtual Reality [48]. The visibility in this site is good.

2.4.1.1.4 *Cala Minnola*

The underwater archaeological site of Cala Minnola is located on the East coast of the island of Levanzo, in the archipelago of the Aegadian Islands, few miles from the west coast of Sicily. The site preserves the wreck of a Roman cargo ship at a depth from the sea level ranged from 25 m to 30 m [49]. The roman ship was carrying hundreds of amphorae which should have been filled with wine. During the sinking, many amphorae were scattered across the seabed. Furthermore, the area is covered by large seagrass beds of *Posidonia*. In this site, the visibility is good but, due to the water depth, the images taken here suffer from serious colour cast because of the red channel absorption and, therefore, they appear bluish.

2.4.1.2 Image Dataset

For each underwater site described in the previous section, we selected three representative images for a total of twelve images. These images constitute the underwater dataset that we employed to complete our evaluation of image enhancement algorithms.

Each row of Figure 12 represents an underwater site. The properties and modality of acquisition of the images vary depending on the underwater site. In the first row (a–c) we can see the images selected for the Underwater Archaeological Park of Baiae that, due to the low water depth, are naturally illuminated. The first two (a,b) were acquired with a Nikon Coolpix, a non-SLR (Single-Lens Reflex) camera, at a resolution of 1920×1080 pixels. The third image (c) was taken with a Nikon D7000 DSLR (Digital Single-Lens Reflex) camera with a 20 mm f/2.8 lens and have the same resolution of 1920×1080 pixels. The second row (d–f) shows three images of some semi-finished marble from the Cala Cicala shipwreck. They were acquired with natural illumination using a Sony X1000V, a 4 K action camera, with a resolution of 3840×2160 pixels. In the third row (g–i) we can see the amphorae of a Roman cargo ship and a panoramic picture, all taken at the underwater site of Cala Minnola. These images were acquired with an iPad Air and have a resolution of 1920×1080 pixels. Despite of the depth of this underwater site, these pictures were taken without artificial illumination and so they look bluish. Therefore, these images are a challenge for understanding how the selected underwater algorithms can deal with such a situation to recover the colour cast. In the last row we can find the pictures of the amphorae at the Mazotos shipwreck. Due to the considerable water depth, these images were acquired with an artificial light, using a Canon PowerShot A620, a non-SLR camera, with a resolution of 3072×2304 pixels that implicates an image ratio of 4:3, different from the 16:9 ratio of the images taken at the other underwater sites. The use of artificial light to acquire these images had produced a bright spot due to the backward scattering.

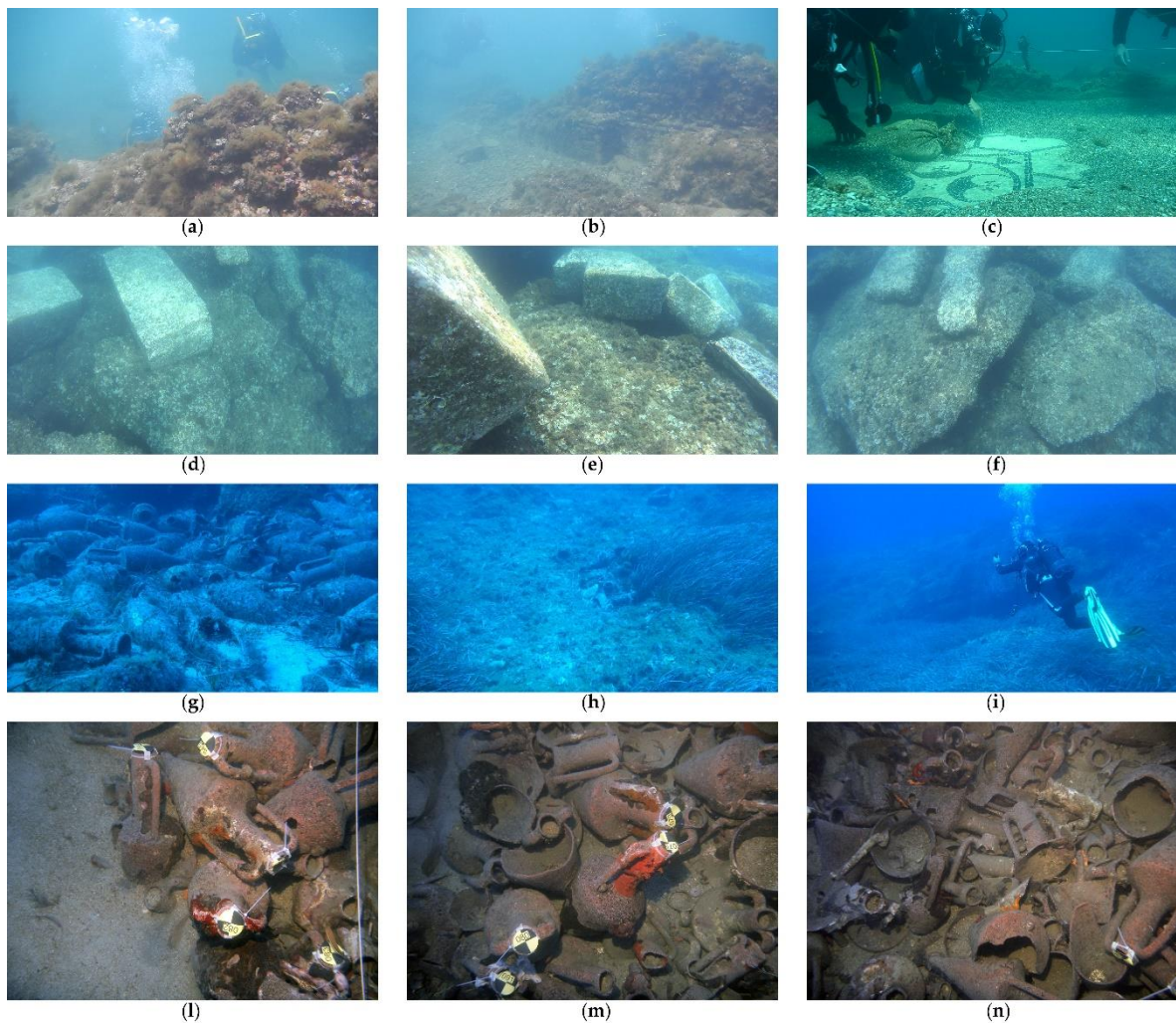


Figure 12. Underwater images dataset. (a–c) Images acquired at Underwater Archaeological Park of Baiae, named respectively Baia1, Baia2, Baia3. Credits: MiBACT-ISCR; (d–f) Images acquired at Cala Cicala shipwreck, named respectively CalaCicala1, CalaCicala2, CalaCicala3. Credits: University of Calabria; (g–i) Images acquired at Cala Minnola, named respectively CalaMinnola1, CalaMinnola2, CalaMinnola3. Credits: University of Calabria; (l–n) Images acquired at Mazotos, named respectively Mazotos1, Mazotos2, Mazotos3. Credits: MARELab, University of Cyprus.

The described dataset is composed by very heterogeneous images that address a wide range of potential underwater environmental conditions and problems, as the turbidity in the water that make the underwater images hazy, the water depth that causes colour casting and the use of artificial light that can lead to bright spots. It makes sense to expect that each of the selected image enhancement algorithms should perform better on the images that represent the environmental conditions against which it was designed.

2.4.2 Evaluation Methods

Each image included in the dataset described in the previous section was processed with each of the image enhancement algorithm introduced in the Section 2.3.1, taking advantage of the enhancement processing tool that has been developed including all the selected algorithms in order to speed up the processing task, as described in Section 2.3. The authors suggested some standard

parameters for their algorithms in order to obtain good enhancing results. Some of these parameters could be tuned differently in the various underwater conditions in order to improve the result. We decided to let all the parameters with the standard values in order not to influence our evaluation with a tuning of the parameters that could have been more effective for an algorithm than for another.

Some quantitative metrics have been employed, representative of a wide range of metrics used in the field of underwater image enhancement, to evaluate all the enhanced images. In particular, these metrics are employed in the evaluation of hazy images in [50]. Similar metrics are defined in [51] and employed in [9]. So, the objective performance of the selected algorithms is evaluated in terms of the following metrics. The first one is obtained by calculating the mean value of image brightness. Formally, it is defined as

$$M_c = \frac{1}{R * L} \sum_{i=1}^R \sum_{j=1}^L I_c(i, j),$$

where $c \in \{r, g, b\}$, $I_c(i, j)$ is the intensity value of the pixel (i, j) in the colour channel c , (i, j) denotes i -th row and j -th column, R and L denotes the total number of rows and columns respectively. When M_c is smaller, the efficiency of image dehazing is better. The mean value on the three colour channels is a simple arithmetic mean $\bar{M} = \frac{M_r + M_g + M_b}{3}$.

Another metric is the information entropy, that represents the amount of information contained in the image. It is expressed as

$$E_c = - \sum_{i=0}^{255} p(i) \log_2 p(i),$$

where $p(i)$ denotes the distribution probability of the pixels at intensity level i . An image with the ideal equalization histogram possesses the maximal information entropy of 8 bit. So, the bigger the entropy, the better the enhanced image. The mean value on the three colour channels is defined as

$$\bar{E} = \sqrt{\frac{E_r^2 + E_g^2 + E_b^2}{3}}$$

The third metric is the average gradient of the image which represents the local variance among the pixels of the image, so bigger its value better the resolution of the image. It is defined as:

$$G_c = \frac{1}{(R-1)(L-1)} \sum_{i=1}^{R-1} \sum_{j=1}^{L-1} \sqrt{\frac{(I_c(i, j) - I_c(i+1, j))^2 + (I_c(i, j) - I_c(i, j+1))^2}{2}},$$

where $I_c(i, j)$ is the intensity value of the pixel (i, j) in the colour channel c , (i, j) denotes i -th row and j -th column, R and L denote the total number of rows and columns, respectively. The mean value on the three colour channels is a simple arithmetic mean $\bar{G} = \frac{G_r + G_g + G_b}{3}$.

2.4.3 Results

This section reports the results of the quantitative evaluation performed on all the images in the dataset, both for the original ones and for the ones enhanced with each of the previously described algorithms. The dataset is composed of twelve images. So, enhancing them with the five algorithms, the total of the images to be evaluated with the quantitative metrics is 72 (12 originals and 60 enhanced). For practical reasons, only a sample of the results are reported here, that consists of the original image named as “Baia1” and its five enhanced versions (Figure 13).

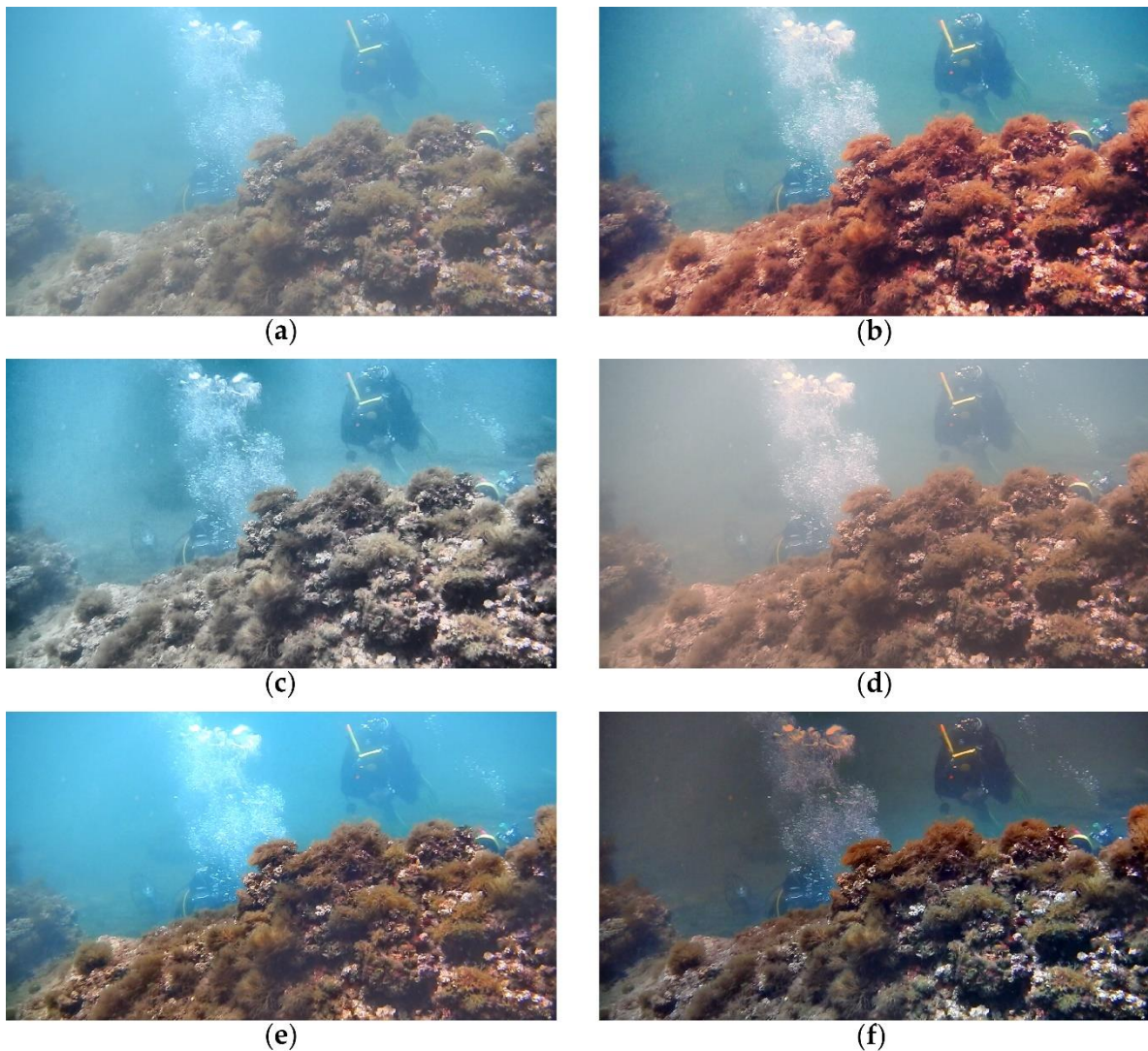


Figure 13. The image “Baia1” enhanced with all five algorithms. (a) Original image; (b) Enhanced with ACE; (c) Enhanced with CLAHE; (d) Enhanced with LAB; (e) Enhanced with NLD; (f) Enhanced with SP.

Table 2 contains the results of quantitative evaluation performed on the images showed in Figure 13. The first column reports the metric values for the original images and the following columns report the correspondent values for the images enhanced with the concerning algorithms. Each row, instead, reports the value of each metric calculated for each colour channel and its mean

value, as defined in Section 2.4.2. The values marked in bold correspond to the best value for the metric defined by the corresponding row. Focusing on the mean values of the three metrics (\bar{M} , \bar{E} , \bar{G}), it can be deduced that the SP algorithm performed better on the mean brightness, the ACE algorithm performed better on enhancing the information entropy and the CLAHE algorithm improved more than the others the average gradient. So, according to these values, these three algorithms in this case of the “Baia1” sample image gave qualitatively equal outcomes. Perhaps it is possible to deduce another consideration by analysing the value of the metrics for the single colour channels. In fact, looking at all the values marked in bold, the SP algorithm reached better results more times than the other two. So, the SP algorithms should have performed slightly better in this case.

Table 2. Results of evaluation performed on “Baia1” image with the metrics described in Section 2.4.2.

Metric	Original	ACE	CLAHE	LAB	NLD	SP
M_r	118,8779	121,3866	107,9892	147,7181	98,3905	78,6978
M_g	156,2414	123,5079	145,7983	136,7457	138,6915	78,2849
M_b	171,1170	131,6431	160,3155	134,6618	154,4564	82,7051
\bar{M}	148,7454	125,5125	138,0343	139,7085	130,5128	79,8959
E_r	6,5921	7,5117	7,2489	7,0265	6,8572	6,9347
E_g	7,0803	7,5441	7,2724	7,2481	7,5670	6,8022
E_b	7,2470	7,4635	7,4429	7,2316	7,3182	6,8077
\bar{E}	6,9787	7,5065	7,3219	7,1694	7,2534	6,8485
G_r	1,1796	2,2861	2,3747	1,4686	1,9560	2,1638
G_g	1,0852	1,9536	2,2623	1,1895	1,7800	2,2108
G_b	1,0885	1,7300	2,2184	1,1100	1,6897	2,3788
\bar{G}	1,1177	1,9899	2,2851	1,2560	1,8086	2,2511

For each image in the dataset, a table such as Table 2 has been produced. Since it is neither practical nor useful to report here all these tables, they have been summarized in a single table (Table 3).

Table 3. Summary table of the average metrics calculated for each site.

Site	Metric	ACE	CLAHE	LAB	NLD	SP
Baia	\bar{M}_s	115,8122	123,2329	126,8077	121,1528	91,3817
	\bar{E}_s	7,4660	7,0356	7,1174	6,8857	6,9379
	\bar{G}_s	3,1745	3,3090	1,9550	2,2086	3,4887
Cala Cicala	\bar{M}_s	124,1400	114,0906	121,3140	106,5964	82,5998
	\bar{E}_s	7,5672	7,3381	7,0156	6,9552	7,1274
	\bar{G}_s	4,1485	4,5598	2,4708	3,4608	5,5009
Cala Minnola	\bar{M}_s	89,7644	113,3513	112,0117	117,3263	78,1474
	\bar{E}_s	6,8249	6,4641	6,5882	5,6996	6,6617
	\bar{G}_s	3,4027	2,9892	1,6508	1,3137	4,4859
Mazotos	\bar{M}_s	123,5133	109,6471	71,1168	37,6775	87,2824
	\bar{E}_s	7,7147	7,5857	7,0223	6,4598	6,9556
	\bar{G}_s	3,7880	4,2094	2,1968	2,9404	3,1438

Table 3 has four sections, one for each underwater site. Each of these sections reports the average values of the metrics calculated for the related site and defined as

$$\bar{M}_s = \frac{\bar{M}_1 + \bar{M}_2 + \bar{M}_3}{3}, \bar{E}_s = \frac{\bar{E}_1 + \bar{E}_2 + \bar{E}_3}{3}, \bar{G}_s = \frac{\bar{G}_1 + \bar{G}_2 + \bar{G}_3}{3},$$

where $(\bar{M}_1, \bar{E}_1, \bar{G}_1)$, $(\bar{M}_2, \bar{E}_2, \bar{G}_2)$, $(\bar{M}_3, \bar{E}_3, \bar{G}_3)$ are the metrics calculated for the first, the second and the third sample image of the related site, respectively. Obviously, the calculation of these metrics was carried out on the three images enhanced by each algorithm. In fact, each column reports the metrics related to a given algorithm.

This table enables us to deduce some more global considerations about the performances of the selected algorithms on our images dataset. Focusing on the values in bold, we can deduce that the SP algorithm has performed better in the sites of Baiae, Cala Cicala and Cala Minnola, having totalized the higher values in two out of three metrics (\bar{M}_s, \bar{G}_s) . Moreover, looking at the entropy (\bar{E}_s) , i.e. the metric on which SP has lost, we can recognize that the values calculated for this algorithm are not so far from the values calculated for the other algorithms. As regards the underwater site of Mazotos, the quantitative evaluation conducted with these metrics seems not to converge on any of the algorithms. Moreover, the ACE algorithm seems to be the one that performs better in enhancing the information entropy of the images.

For the sake of completeness, we want to report a particular case that is worth mentioning. Looking at Table 4, it is possible to conclude that the SP algorithm performed better than all the others according to all the three metrics in the case of "CalaMinnola2."

Table 4. Average metrics for the sample image "CalaMinnola2" enhanced with all algorithms.

Metric	Original	ACE	CLAHE	LAB	NLD	SP
\bar{M}	115,8251	92,5778	117,1927	127,1310	126,4759	84,1991
\bar{E}	5,5796	6,8707	6,3996	6,6333	5,7615	7,0316
\bar{G}	1,4500	4,0349	3,4717	1,9238	1,4994	6,1327

In Figure 14 we can see the CalaMinnola2 image enhanced with the SP algorithm. It is quite clear, looking at this image, that the SP algorithm in this case has generated some 'artefacts,' likely due to the oversaturation of some image details. This issue could be probably solved or attenuated by tuning the saturation parameter of the SP algorithm, which has been fixed to a standard value, as for the parameters of the other algorithms too. Anyway, the question is that the metrics were misled by this 'artefacts,' assigning a high value to the enhancement made by this algorithm.

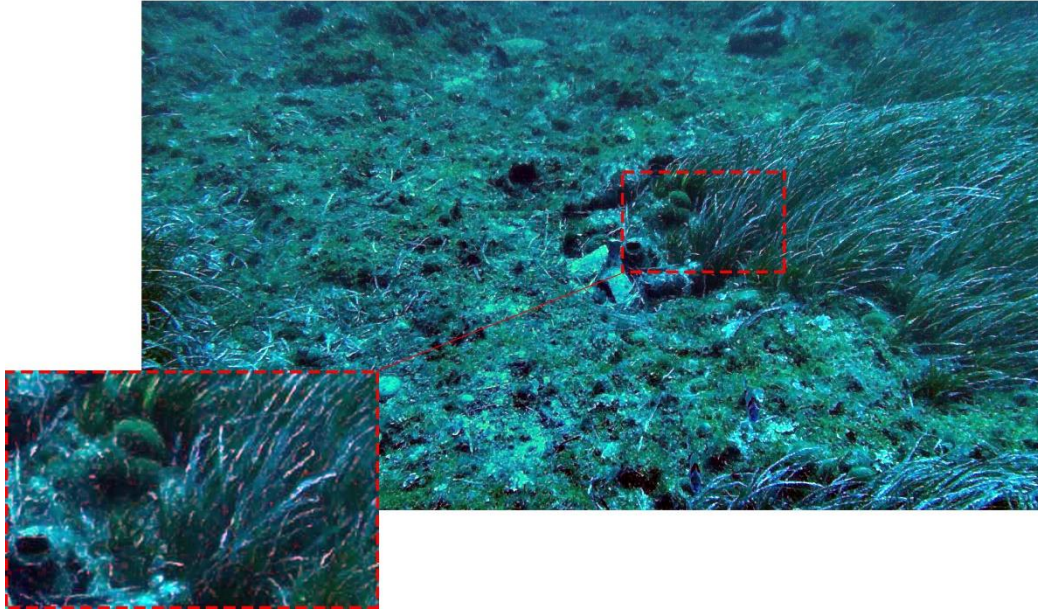


Figure 14. Artefacts in the sample image “CalaMinnola1” enhanced with SP algorithm.

2.4.4 Conclusions

In this work, five state-of-the-art algorithms have been selected for the enhancement of images taken on four underwater sites with different environmental and illumination conditions. These algorithms have been evaluated by means of three quantitative metrics selected among those already adopted in the field of underwater image enhancement. Our purpose was to establish which algorithm performs better than the others and whether or not the selected metrics were good enough to compare two or more image enhancement algorithms.

According to the quantitative metrics, the SP algorithm seemed to perform better than the other in all the underwater sites, except for Mazotos. For this site, each metric assigned a higher value to a different algorithm, preventing us to decide which algorithm performed better on the Mazotos images. Such an undefined result is the first drawback to evaluate the underwater images relying only on quantitative metrics. Moreover, these quantitative metrics, implementing only a blind evaluation of a specific intrinsic characteristic of the image, are unable to identify ‘problems’ in the enhanced images, as the ‘artefacts’ generated by the SP algorithms in the case documented in Figure 14 and Table 4.

Anyway, looking at Figure 15 and performing a qualitative analysis from the point of view of the human perception, the result suggested by the quantitative metrics seems to be confirmed, as the SP algorithm performed well in most of the cases. The only case on which the SP algorithm failed was in the Cala Minnola underwater site, probably due to an oversaturation of some image details that probably could be fixed by tuning its saturation parameter.

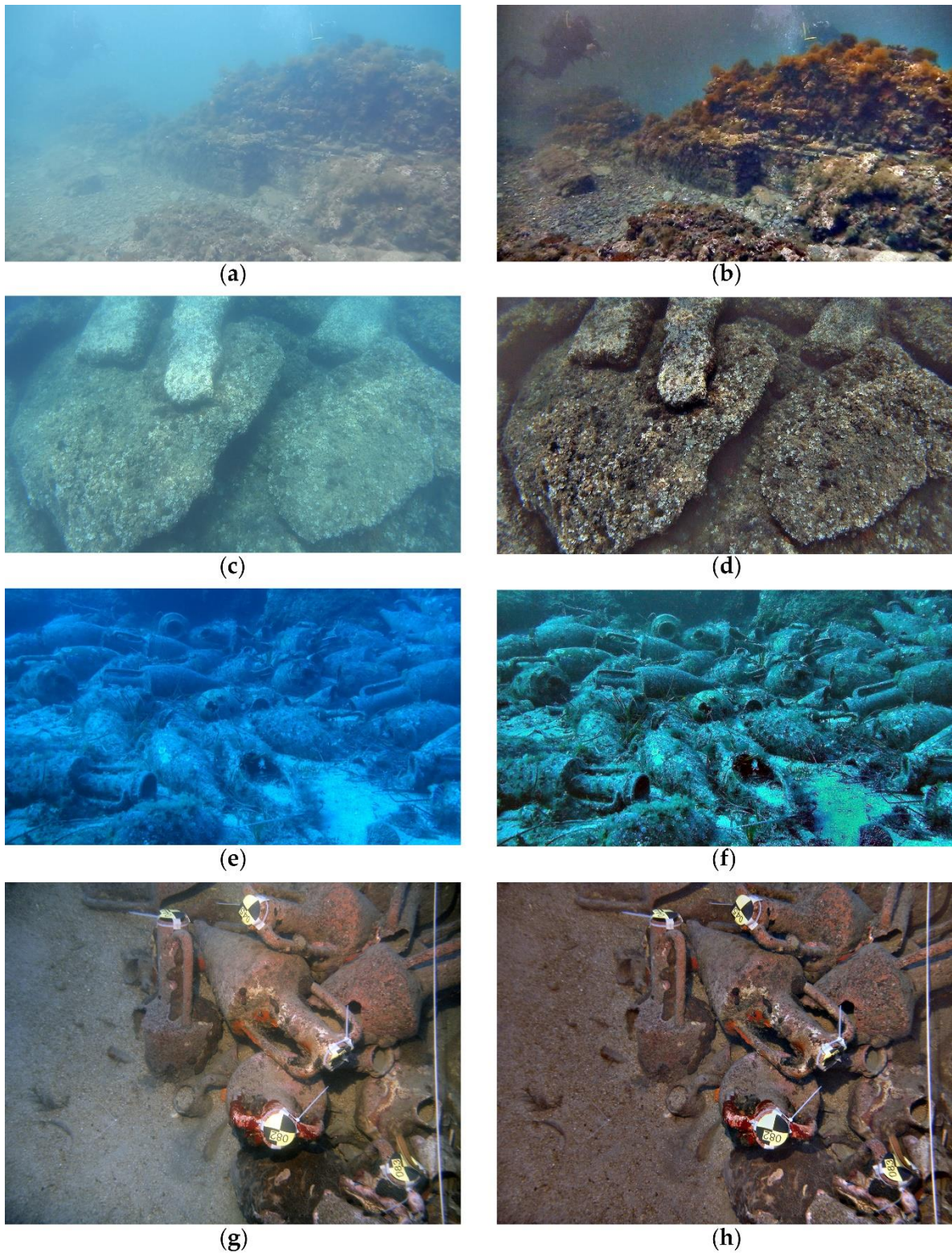


Figure 15. Sample of SP algorithm enhancement for visual evaluation. (a,b) “Baia2” original and enhanced images; (c,d) “CalaCicala3” original and enhanced images; (e,f) “CalaMinnola1” original and enhanced images; (g,h) “Mazotos1” original and enhanced images.

In conclusion, even if the quantitative metrics can provide a useful indication about image quality, they do not seem reliable enough to be blindly employed for an objective evaluation of the

performances of an underwater image enhancement algorithm. Hence, the following section describes an alternative methodology to evaluate the underwater image enhancement algorithms.

2.5 Guidelines for Underwater Image Enhancement Based on Benchmarking of Different Methods

The benchmark presented in this section is a part of the iMARECULTURE project [43–45], which aims to develop new tools and technologies to improve the public awareness of underwater cultural heritage. In particular, it includes the development of a Virtual Reality environment that reproduces faithfully the appearance of underwater sites, thus offering the possibility to visualize the archaeological remains as they would appear in air. This goal requires the benchmarking of different image enhancement methods to figure out which one performs better in different environmental and illumination conditions. In Section 2.4, a previous work is described in which five methods were selected from the state of the art and used to enhance a dataset of images produced in various underwater sites at heterogeneous conditions of depth, turbidity and lighting. These enhanced images were evaluated by means of some quantitative metrics. In this section, two more approaches will be introduced, meant for a more comprehensive benchmarking of the underwater image enhancement methods. The first of these additional approaches was conducted with a panel of experts in the field of underwater imagery, members of iMARECULTURE project, and the other one is based on the results of 3D reconstructions. Furthermore, since we modified some images in our dataset by adding some new ones, the results of the quantitative metrics have been also reported, as done in the previous section.

In highly detailed underwater surveys, the availability of radiometric information, along with 3D data regarding the surveyed objects, becomes crucial for many diagnostics and interpretation tasks [52]. To this end, different image enhancement and colour correction methods have been proposed and tested for their effectiveness in both clear and turbid waters [53]. Our purpose was to supply the researchers in the underwater community with more detailed information about the employment of a specific enhancement method in different underwater conditions. Moreover, we were interested in verifying whether different benchmarking approaches have produced consistent results.

2.5.1 Case studies

A heterogeneous dataset of images has been assembled that can represent the variability of environmental and illumination conditions that characterizes underwater imagery. Images taken with different cameras and with different resolutions have been selected, considering that—when applied in the real world—the underwater image enhancement methods have to deal with images

produced by unspecified sources. This section briefly describes the underwater sites and the dataset of images.

2.5.1.1 Underwater Sites

Four different sites were selected on which the images for the benchmarking of the underwater image enhancement algorithms were taken. The selected sites are representative of different states of environmental and geomorphologic conditions (i.e., water depth, water turbidity, etc.) and they were the same as the ones described in Section 2.4.1.1. The second site is the Mazotos shipwreck, which lies at a depth of 44 m. The visibility in this site is very good, but the red absorption at this depth is nearly total. In the previous work, the images for this site were taken only with artificial light. Now, images taken both with natural light and with an artificial light for recovery of the colour have been considered.

2.5.1.2 Image Dataset

Three representative images have been selected for each underwater site described in the previous section, except for Mazotos for which we selected three images with natural light and three with artificial light, for a total of fifteen images. These images constitute the underwater dataset that has been employed to complete our benchmarking of image enhancement methods.

Each row of Figure 16 represents an underwater site. The properties and modality of acquisition of the images vary depending on the underwater site. The first three rows (a–i) show, respectively, the images acquired in the Underwater Archaeological Park of Baiae, within the Cala Cicala shipwreck, and among the underwater site of Cala Minnola. These are the same as the ones presented in the Section 2.4.1.2.

In the last two rows (j–o), we find the pictures of the amphorae at the Mazotos shipwreck. These images are different from those we employed in the previous work presented in Section 2.4. Due to the considerable water depth, the first three images (j–l) were acquired with an artificial light, which produced a bright spot due to the backward scattering. The last three images were taken with natural light; therefore, they are affected by colour cast. Images (j,k) were acquired using a Nikon D90 with a resolution of 4288×2848 pixels, (l,n,o) were taken using a Canon EOS 7D with a resolution of 5184×3456 pixels, and image (m) was acquired with a Garmin VIRBXE, an action camera, with a resolution of 4000×3000 pixels.



Figure 16. Underwater images dataset. (a–c) Images acquired at Underwater Archaeological Park of Baiae, named respectively Baia1, Baia2, Baia3. Credits: MiBACT-ISCR; (d–f) Images acquired at Cala Cicala shipwreck, named respectively CalaCicala1, CalaCicala2, CalaCicala3. Credits: Soprintendenza Belle Arti e Paesaggio per le province di CS, CZ, KR and University of Calabria; (g–i) Images acquired at Cala Minnola, named CalaMinnola1, CalaMinnola2, CalaMinnola3, respectively. Credits: Soprintendenza del Mare and University of Calabria; (j–l) Images acquired at Mazotos with artificial light, named respectively MazotosA1, MazotosA2, MazotosA3. Credits: MARELab, University of Cyprus; (m–o) Images acquired at Mazotos with natural light, named respectively MazotosN4, MazotosN5, MazotosN6. Credits: MARELab, University of Cyprus.

2.5.2 Benchmarking Based on Objective Metrics

2.5.2.1 Evaluation Methods

Each image included in the dataset described in the previous section was processed with each of the image enhancement algorithms previously introduced, taking advantage of the enhancement processing tool described in section 2.3. The authors suggested some standard parameters for their

algorithms in order to obtain good enhancing results. Some of these parameters could be tuned differently in various underwater conditions in order to improve the result. As in the previous work, all the parameters have been set to standard values in order not to influence the evaluation with the tuning of the parameters. The quantitative metrics employed to evaluate all the enhanced images are the same described in the previous section. To recap, the first one is obtained by calculating the mean value of image brightness (M_c). When M_c is smaller, the efficiency of image dehazing is better. The mean value on the three colour channels (\bar{M}) is a simple arithmetic mean. The second metric is the information entropy (E_c) that represent the amount of information contained in the image. The bigger the entropy, the better the enhanced image. The mean value (\bar{E}) on the three colour channels is defined as a root mean square. The third metric is the average gradient of the image (G_c), which represents a local variance among the pixels of the image; therefore, a larger value indicates a better resolution of the image. The mean value on the three colour channels is a simple arithmetic mean. A more detailed description of these metrics can be found in Section 2.4.2.

2.5.2.2 Results

This section reports the results of the objective evaluation performed on all the images in the dataset, both for the original ones and for the ones enhanced with each of the previously described algorithms. The dataset consists of 15 images. Each image has been enhanced by means of the five algorithms; therefore, the total amount of images to be evaluated with the quantitative metrics is 90 (15 originals and 75 enhanced). For practical reasons, only a sample of our results has been reported here, i.e., a mosaic composed of the original image named as “MazotosN4” and its five enhanced versions (Figure 17).



(a)



(b)



(c)



(d)



(e)



(f)

Figure 17. The image “MazotosN4” enhanced with all five algorithms. (a) Original image; (b) Enhanced with ACE; (c) Enhanced with CLAHE; (d) Enhanced with LAB; (e) Enhanced with NLD; (f) Enhanced with SP.

Table 5 presents the results of the benchmarking performed through the selected metrics on the images showed in Figure 17. The first column reports the metric values for the original images, and the following columns report the correspondent values for the images enhanced with the concerning algorithms. Each row, on the other hand, reports the value of each metric calculated for each colour channel and its mean value, as previously defined. The values marked in bold correspond to the best value for the metric defined by the corresponding row. By analysing the mean values of the metrics

(\bar{E}, \bar{G}) , it can be deduced that the ACE algorithm performed better on enhancing the information entropy and the SP algorithm performed better on the average gradient.

Focusing on the value of the metric (\bar{M}), we can notice that all the algorithms failed to improve the mean brightness parameter. Looking further into the results and analysing the mean brightness of the single colour channels, we can recognise that its values are very low on the red channel. The validity of the mean brightness metric is based on the assumption that an underwater image is a hazy image and, consequently, a good dehazing leads to a reduced mean brightness. However, this assumption cannot hold in deep water, where the imagery is often non-hazy, but with a heavy red channel absorption. Therefore, further brightness reducing of this channel in such a situation cannot be considered a valuable result. This is exactly the case of the ‘‘MazotosN4’’ image where the \bar{M} metric was misled, considering that the original image is better than the others. This case has been reported in order to underline the inadequacy of the mean brightness metric for evaluating images taken in deep water with natural illumination.

Table 5. Results of benchmarking performed on ‘‘MazotosN4’’ image with the objective metrics.

Metric	Original	ACE	SP	NLD	LAB	CLAHE	
1	M_r	13.6907	61.6437	102.6797	10.9816	83.6466	39.8337
	M_g	105.3915	119.5308	118.5068	110.1816	98.1805	119.2274
	M_b	170.9673	126.7339	115.2361	181.4046	109.9632	185.5852
	\bar{M}	96.6832	102.6361	112.1409	100.8559	97.2635	114.8821
2	E_r	4.6703	6.3567	6.7489	3.7595	6.6936	6.4829
	E_g	6.6719	7.4500	7.1769	6.6726	6.8375	7.2753
	E_b	7.1811	7.5279	7.1045	7.2187	6.9055	7.3364
	\bar{E}	6.2688	7.1316	7.0126	6.0764	6.8128	7.0423
3	G_r	0.9600	2.6480	6.1200	1.0462	1.0752	2.4432
	G_g	1.0069	2.4210	3.9631	1.0958	1.0870	2.4754
	G_b	1.1018	2.4332	4.2334	1.1566	1.1235	2.4776
	\bar{G}	1.0229	2.5007	4.7722	1.0995	1.0952	2.4654

¹ Mean brightness (less is better). ² Information entropy (more is better). ³ Average gradient (more is better).

Along the same lines, we would like to report with greater detail another particular case that has just been mentioned in section 2.4.3. Looking at Table 6 and Table 7, it is possible to conclude that the SP algorithm performed better than all the others according to all the three metrics in both cases of ‘‘CalaMincola1’’ and ‘‘CalaMincola2’’ (Figure 18).

Table 6. Average metrics for the sample image ‘‘CalaMincola1’’ enhanced with all algorithms.

Metric	Original	ACE	SP	NLD	LAB	CLAHE
\bar{M} 1	96.0213	87.4779	86.9252	106.3991	98.8248	107.8050
\bar{E} 2	5.8980	6.9930	7.1923	6.0930	6.9573	6.7880
\bar{G} 3	1.5630	3.8668	5.6263	1.6227	2.0122	3.2843

¹ Mean brightness (less is better). ² Information entropy (more is better). ³ Average gradient (more is better).

Table 7. Average metrics for the sample image “CalaMinnola2” enhanced with all algorithms.

Metric	Original	ACE	SP	NLD	LAB	CLAHE
\bar{M} 1	115.8251	92.5778	84.1991	126.4759	127.1310	117.1927
\bar{E} 2	5.5796	6.8707	7.0316	5.7615	6.6333	6.3996
\bar{G} 3	1.4500	4.0349	6.1327	1.4994	1.9238	3.4717

¹ Mean brightness (less is better). ² Information entropy (more is better). ³ Average gradient (more is better).

In Figure 18 we can see a detail of “CalaMinnola1” and “CalaMinnola2” images enhanced with the SP algorithm. Looking at these images, it becomes quite clear that the SP algorithm in these cases have generated some ‘artefacts’, likely due to the oversaturation of some image details. As stated before, this issue could probably be solved or attenuated by tuning the saturation parameter of the SP algorithm which we have fixed to a standard value, as we did for the parameters of the other algorithms, too. Anyway, the issue is that the metrics were misled by these ‘artefacts’, assigning a high value to the enhancement made by this algorithm.

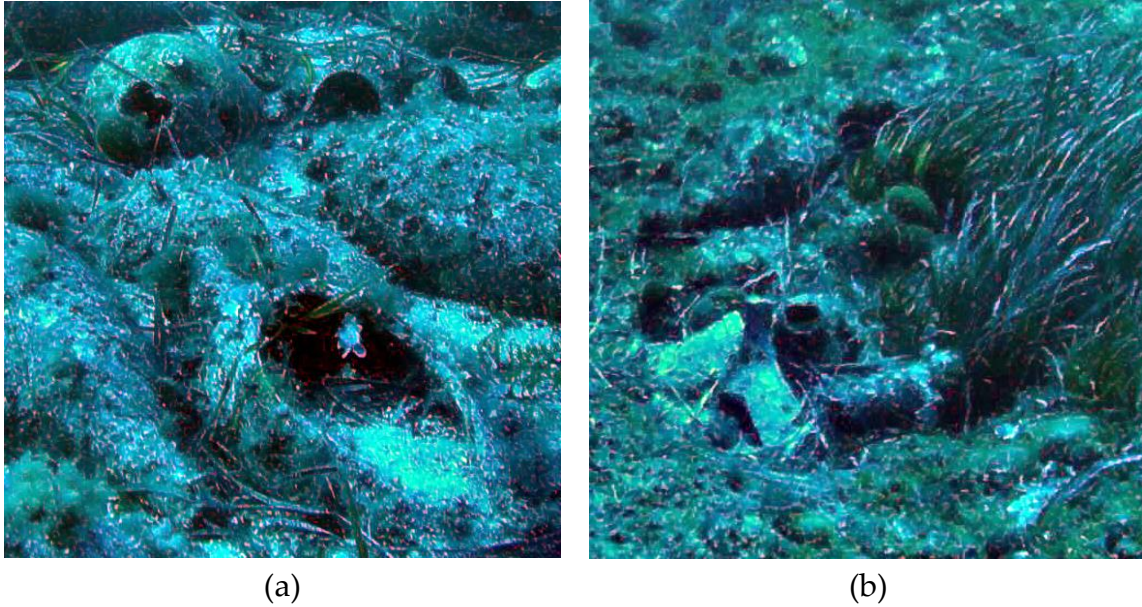


Figure 18. Artefacts in the sample images “CalaMinnola1” (a) and “CalaMinnola2” (b) enhanced with SP algorithm.

Nonetheless, for each image in the dataset we have elaborated a table such as Table 5. Since it is neither practical nor useful to report all these tables here, we summarized them in a single one (Table 8).

Table 8. Summary table of the average metrics calculated for each site.

Site	Metric	ACE	SP	NLD	LAB	CLAHE
Baiae	\bar{M}_s	115.8122	91.3817	121.1528	126.8077	123.2329
	\bar{E}_s	7.4660	6.9379	6.8857	7.1174	7.0356
	\bar{G}_s	3.1745	3.4887	2.2086	1.9550	3.3090
Cala Cicala	\bar{M}_s	124.1400	82.5998	106.5964	121.3140	114.0906
	\bar{E}_s	7.5672	7.1274	6.9552	7.0156	7.3381
	\bar{G}_s	4.1485	5.5009	3.4608	2.4708	4.5598
Cala Minnola	\bar{M}_s	89.7644	78.1474	117.3263	112.0117	113.3513
	\bar{E}_s	6.8249	6.6617	5.6996	6.5882	6.4641

	\bar{G}_s	3.4027	4.4859	1.3137	1.6508	2.9892
MazotosA	\bar{M}_s	122.0792	110.1639	68.7037	93.5767	118.1187
	\bar{E}_s	7.6048	7.1057	6.6954	6.8260	7.4534
	\bar{G}_s	2.5653	2.8744	2.3156	1.4604	2.7938
MazotosN	\bar{M}_s	90.0566	79.5346	94.3764	85.4173	103.1706
	\bar{E}_s	6.5203	6.3511	5.9011	6.6790	6.8990
	\bar{G}_s	1.8498	3.3325	0.8368	1.1378	2.3457

Table 8 consists of five sections, one for each underwater site. Each of these sections reports the average values of the three metrics calculated for the related site. These average values are defined, within each site, as the arithmetic mean of the metrics calculated for the first, the second and the third sample image. Obviously, the calculation of these metrics was carried out for each algorithm on the three images enhanced using them. In fact, each column reports the metrics related to a given algorithm.

This table enables us to deduce more generalized considerations about the performances of the selected algorithms on our dataset of images. Focusing on the values in bold, we can deduce that the SP algorithm performed better at the sites of Baiae, Cala Cicala, Cala Minnola, and MazotosN, having the best total values in two out of three metrics (\bar{M}_s, \bar{G}_s). Moreover, looking at the entropy (\bar{E}_s), i.e., the metric on which SP lost, we can recognize that the values calculated for this algorithm are not so far from the values calculated for the other algorithms. However, the ACE algorithm seems to be the one that performs best at enhancing the information entropy of the images. As regards the images taken on the underwater site of Mazotos with artificial light (MazotosA), the objective evaluation conducted with these metrics seems not to converge on any of the algorithms. Such an undefined result, along with the issues previously reported, are drawbacks caused by evaluating the underwater images relying only on quantitative metrics.

As concluded also in the section 2.4, even if the quantitative metrics can provide a useful indication about image quality, they do not seem reliable enough to be blindly employed for evaluating the performances of an underwater image enhancement algorithm. Hence, the next subsection describes an alternative methodology to evaluate the underwater image enhancement algorithms, based on a qualitative evaluation conducted with a panel of experts in the field of underwater imagery being members of iMARECULTURE project.

2.5.3 Benchmarking Based on Expert Panel

An alternative methodology has been designed to evaluate the underwater image enhancement algorithms. A panel of experts in the field of underwater imagery (members of iMARECULTURE project) was assembled. This panel is composed of several professional figures from five different countries, such as underwater archaeologists, photogrammetry experts and computer graphics

scientists with experience in underwater imagery. This panel expressed an evaluation on the quality of the enhancement conducted on the underwater images dataset through some selected algorithms.

2.5.3.1 Evaluation Methods

The dataset of images and the selected algorithms are the same ones that were employed and described in the previous section. A survey with all the original and enhanced images was created in order to be submitted to the expert panel. A questionnaire was set up for this purpose, a section of which is shown in Figure 19.

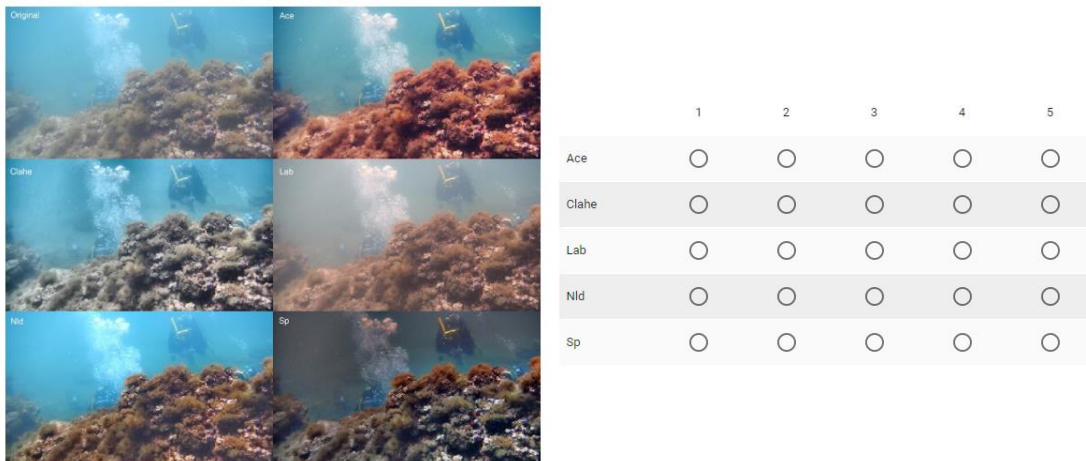


Figure 19. A sample section of the survey submitted to the expert panel.

The questionnaire is composed of fifteen sections like the one shown in the picture; one for each of the fifteen images in the dataset. Each mosaic is composed of an original image and the same image enhanced with five different algorithms. Each of these underwater images is labelled with the acronym of the algorithm that produced them. Under the mosaic there is a multiple-choice table. Each row is labelled with the algorithm's name and represents the image enhanced with the algorithm. For each of these images, the expert had to provide an evaluation expressed as a number from one to five, where "one" represents a very poor enhancement and "five" a very good one, considering both the effects of colour correction and contrast/sharpness enhancement. The hi-res images were provided separately to the experts in order to fulfil a better evaluation.

2.5.3.2 Results

All these evaluations, expressed by each expert on each enhanced image of our dataset, provide a lot of data that needs to be interpreted. A feasible way to aggregate all these data in order to extract some useful information is to calculate an average vote expressed by the experts on the images of a single site divided by algorithm. This average is calculated as a mean vote of the three images of the site.

The values in Table 9 show that ACE reached the higher average vote for the sites of Baiae, Cala Cicala and Cala Minnola and CLAHE has the higher average vote for Mazotos in both cases of artificial and natural light. It is worth noting that ACE gained a second place on Mazotos (both cases).

Table 9. Average vote divided by site and algorithm.

Site	ACE	SP	NLD	LAB	CLAHE
Baiae	3.64	3.55	2.58	2.48	2.97
Cala Cicala	3.64	2.94	2.21	2.70	3.06
Cala Minnola	3.48	2.91	1.91	2.61	2.55
Mazotos (artificial light)	3.55	2.45	2.33	3.24	3.97
Mazotos (natural light)	2.88	2.21	2.15	2.39	3.30

However, a simple comparison of these average values could be unsuitable from a statistical point of view. Consequently, we performed the ANOVA (ANalysis Of VAriance) on these data. The ANOVA is a statistical technique that compares different sources of variance within a dataset. The purpose of the comparison is to determine whether significant differences exist between two or more groups. In our specific case, the purpose is to determine whether the difference between the average vote of the algorithms is significant. Therefore, the groups for our ANOVA analysis are represented by each algorithm and the analysis is repeated for each site.

Table 10 shows the results of ANOVA test. A significance value below 0.05 entails that there is a significant difference between the means of our group. For the sake of completeness, we reported in the table also the degrees of freedom (df) and the F-values (F).

Table 10. ANOVA test results.

Underwater Site		Sum of Squares	df	Mean Square	F	Sig.
Baiae	Between Groups	37.612	4	9.403	6.995	0.000
	Within Groups	215.091	160	1.344		
	Total	252.703	164			
Cala Cicala	Between Groups	35.758	4	8.939	7.085	0.000
	Within Groups	201.879	160	1.262		
	Total	237.636	164			
Cala Minnola	Between Groups	43.479	4	10.870	7.704	0.000
	Within Groups	225.758	160	1.411		
	Total	269.236	164			
MazotosA	Between Groups	65.309	4	16.327	14.142	0.000
	Within Groups	184.727	160	1.155		
	Total	250.036	164			
MazotosN	Between Groups	31.855	4	7.964	5.135	0.001
	Within Groups	248.121	160	1.551		
	Total	279.976	164			

The significance values for each site are reported in the last column and are all below the 0.05 threshold. This indicates that, for each site, there is a significant difference between the average value gained by each algorithm. However, this result is not enough, because it does not show which algorithms are effectively better than the others. Thus, we conducted a “post hoc” analysis, named

Tukey’s HSD (Honest Significant Difference), which is a test that determines specifically which groups are significantly different. This test assumes that the variance within each group is similar; therefore, a test of homogeneity of variances is needed to establish whether this assumption can hold for our data.

Table 11 shows the results of the homogeneity test. The significance is reported in the last column and a value above 0.05 indicates that the variance between the algorithms is similar with regard to the related site. Cala Cicala and MazotosA have a significance value below 0.05, so for these two sites, the assumption of homogeneity of variances does not hold. We employed a different “post hoc” analysis for these two sites, i.e., Games-Howell, that does not require the assumption of equal variances.

Table 11. Test of homogeneity of variances.

Underwater Site	Levene Statistic	df1	df2	Significance
Baiae	1.748	4	160	0.142
Cala Cicala	3.418	4	160	0.010
Cala Minnola	1.689	4	160	0.155
MazotosA	2.762	4	160	0.030
MazotosN	1.980	4	160	0.100

The differences between the mean values, totalled for each algorithm at an underwater site, is significant at the level 0.05. Analysing the results reported in Table 9 and in Table 12, we produced this interpretation of the expert panel evaluation:

- **Baiae:** ACE and SP are better than LAB and NLD, whereas CLAHE does not show results significantly better or worse than the other algorithms.
- **Cala Cicala:** ACE is better than LAB and NLD. CLAHE is better than NLD.
- **Cala Minnola:** ACE is better than CLAHE, LAB and NLD. SP is significantly better than NLD but does not show significant differences with the other algorithms.
- **MazotosA:** ACE is better than NLD and SP. CLAHE is better than LAB, NLD and SP. There are no significant differences between ACE and CLAHE.
- **MazotosN:** CLAHE is better than LAB, NLD e SP. There are no significant differences between ACE and CLAHE.

Table 12. “Post hoc” analysis performed on all sites. In parentheses, the “post hoc” test employed on each site is specified.

Algorithm Name	Algorithm Name	Significance				
		Baiae (Tukey)	Cala Cicala (Games-Howell)	Cala Minnola (Tukey)	MazotosA (Games-Howell)	MazotosN (Tukey)
Ace	Clahe	0.139	0.112	0.014	0.421	0.639
	Lab	0.001	0.005	0.025	0.735	0.511
	Nld	0.003	0.000	0.000	0.002	0.128
	Sp	0.998	0.185	0.286	0.001	0.195

Sp	Ace	0.998	0.185	0.286	0.001	0.195
	Clahe	0.263	0.994	0.726	0.000	0.004
	Lab	0.003	0.936	0.838	0.016	0.976
	Nld	0.008	0.172	0.007	0.994	1.000
Nld	Ace	0.003	0.000	0.000	0.002	0.128
	Clahe	0.641	0.009	0.194	0.000	0.002
	Lab	0.998	0.382	0.125	0.019	0.933
	Sp	0.008	0.172	0.007	0.994	1.000
Lab	Ace	0.001	0.005	0.025	0.735	0.511
	Clahe	0.438	0.524	1.000	0.013	0.028
	Nld	0.998	0.382	0.125	0.019	0.933
	Sp	0.003	0.936	0.838	0.016	0.976
Clahe	Ace	0.139	0.112	0.014	0.421	0.639
	Lab	0.438	0.524	1.000	0.013	0.028
	Nld	0.641	0.009	0.194	0.000	0.002
	Sp	0.263	0.994	0.726	0.000	0.004

In a nutshell, ACE works fine at all sites. CLAHE works as well as ACE at all sites except Cala Minnola. SP works fine too at the sites of Baiaie, Cala Cicala and Cala Minnola.

Table 13 shows a simplified version of the analysis performed on the expert evaluation through ANOVA. The “Mean Vote” column reports the average vote expressed by all the experts on the three images related to the site and to the algorithm represented by the row. The rows are ordered by descending “Mean Vote” order within each site. The “Significance” column indicates if the related “Mean Vote” is significantly different from the higher “Mean Vote” at the related site. Consequently, the bold values indicate the algorithm with the higher “Mean Vote” for each site. The values highlighted in orange represent the algorithms with a “Mean Vote” not significantly different from the first one within the related site.

Table 13. Summary table of ANOVA analysis.

Site	Algorithm	Mean Vote	Significance
Baiaie	Ace	3.64	-
	Sp	3.55	0.998
	Clahe	2.97	0.139
	Nld	2.58	0.003
	Lab	2.48	0.001
Cala Cicala	Ace	3.64	-
	Clahe	3.06	0.112
	Sp	2.94	0.185
	Lab	2.7	0.005
	Nld	2.21	0
Cala Minnola	Ace	3.48	-
	Sp	2.91	0.286
	Lab	2.61	0.025
	Clahe	2.55	0.014
	Nld	1.91	0
MazotosA	Clahe	3.97	-

	Ace	3.55	0.639
	Lab	3.24	0.028
	Sp	2.45	0.004
	Nld	2.33	0.002
	Clahc	3.3	-
MazotosN	Ace	2.88	0.421
	Lab	2.39	0.013
	Sp	2.21	0
	Nld	2.15	0

2.5.4 Benchmarking Based on the Results of 3D Reconstruction

The tool has been employed by the researchers of the Cyprus University of Technology for analysing the impact of the image enhancement in the case of underwater 3D photogrammetric reconstructions. Their analysis and results are reported in this section.

Computer vision applications in underwater settings are particularly affected by the optical properties of the surrounding medium [54]. In the 3D underwater reconstruction process, the image enhancement is a necessary pre-processing step that is usually tackled with two different approaches. The first one focuses on the enhancement of the original underwater imagery before the 3D reconstruction in order to restore the underwater images and potentially improve the quality of the generated 3D point cloud. This approach in some cases of non-turbid water [31,32] proved to be unnecessary and time-consuming, while in high-turbidity water it seems to have been effective enough [46,55]. The second approach suggests that, in good visibility conditions, the colour correction of the produced textures or orthoimages is sufficient and time efficient [31,32]. This section presents the investigation as to whether and how the pre-processing of the underwater imagery using the five implemented image enhancement algorithms affects the 3D reconstruction using automated SfM-MVS software. Specifically, each one of the presented algorithms is evaluated according to its performance in improving the results of the 3D reconstruction using specific metrics over the reconstructed scenes of the five different datasets.

2.5.4.1 Evaluation Methods

To address the above research issues, five different datasets were selected to capture underwater imagery ensuring different environmental conditions (i.e., turbidity etc.), depth, and complexity. The five image enhancement methods already described were applied to these datasets. Subsequently, dense 3D point clouds (3Dpc) were generated for each dataset using a robust and reliable commercial SfM-MVS software. The produced 3D point clouds were then compared using Cloud Compare [56] open-source software and statistics were computed. The followed process is quite similar to the one presented in [31,32].

2.5.4.2 Test Datasets

The dataset used for the evaluations of the 3D reconstruction results was almost the same as the ones presented in the subsection 2.5.1.2. The only exception is that the MazotosN images used in this section were captured on an artificial reef constructed using 1-m-long amphorae, replicas from the Mazotos shipwreck [57]. Although the images of MazotosN were acquired in two different locations, all the images were captured by exactly the same camera under the same turbidity and illumination conditions. Moreover, both locations were at the same depth, thus resulting in the same loss of red colour in all of the images from both locations due to a strong absorption and scarce illumination typical of these depths. The images from the artificial reef present abrupt changes on the imaged object depth, thus causing a more challenging task for the 3D reconstruction

For evaluating the 3D reconstruction results, a large number of images of the datasets described above was used, having the required overlap as they were acquired for photogrammetric processing. Each row of Figure 20 represents a dataset, while in each column, the results of the five image enhancement algorithms, as well as the original image, are presented.

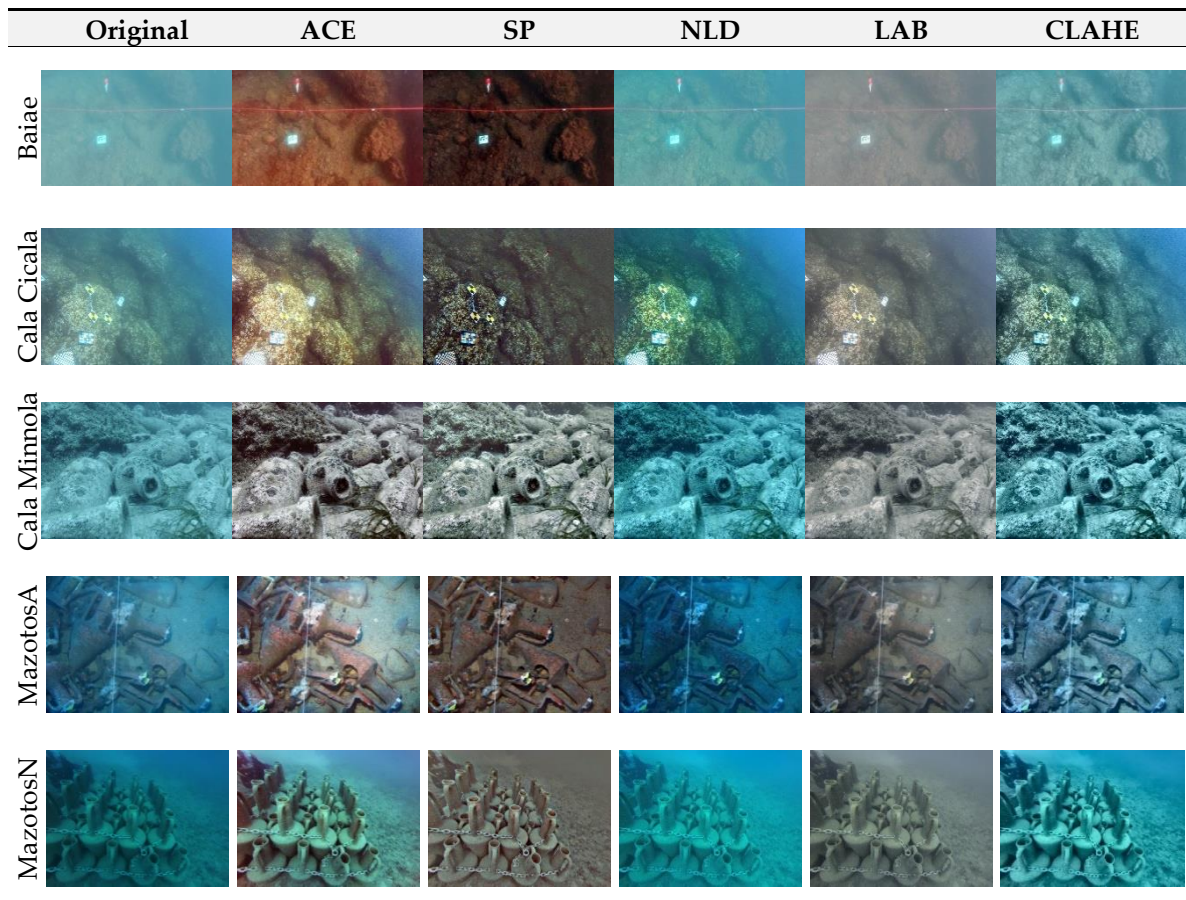


Figure 20. Examples of original and corrected images of the 5 different datasets. Credits: MiBACT-ISCR (Baiae images); Soprintendenza Belle Arti e Paesaggio per le province di CS, CZ, KR and University of Calabria (Cala Cicala images); Soprintendenza del Mare and University of Calabria (Cala Minnola images); MARELab, University of Cyprus (MazotosA images); Department of Fisheries and Marine Research of Cyprus (MazotosN images).

2.5.4.3 SfM-MVS Processing

Subsequently, enhanced imagery was processed using SfM-MVS with Agisoft's Photoscan commercial software [35]. The main reason for using this specific software for the performed tests, instead of other commercial SfM-MVS software or SIFT [30] and SURF [36] detection and matching schemes, is that according to our experience in underwater archaeological 3D mapping projects, it proves to be one of the most robust and maybe the most commonly used among the underwater archaeological 3D mapping community [52]. For each site, six different 3Dpcs were created, one with each colour-corrected dataset (Figure 21): (i) One with the original uncorrected imagery, which is considered the initial solution, (ii) a second one using ACE, (iii) a third one using the imagery that resulted implementing SP the colour correction algorithm, (iv) a fourth one using NLD enhanced imagery, (v) a fifth one using LAB enhanced imagery, and (vi) a sixth one using CLAHE enhanced imagery. All three RGB channels of the images were used for these processes.

For the processing of each test site, the alignment and calibration parameters of the original (uncorrected) dataset were adopted. This ensured that the alignment parameters will not affect the dense image matching step and the comparisons between the generated point clouds can be realized. To scale the 3D dense point clouds, predefined Ground Control Points (GCPs) were used for calculating the alignment parameters of the original imagery to be also used for the enhanced imagery. The above procedure was adopted in order to ensure a common ground for the comparison of the 3D point clouds, since the data were of real-life applications and targeting control points for each dataset would introduce additional errors to the process (targeting errors, etc.). Subsequently, 3D dense point clouds of medium quality and density were created for each dataset. No filtering during this process was performed in order to obtain the total number of dense point clouds, as well as to evaluate the resulting noise. It should be noted that medium-quality dense point clouds mean that the initial images' resolutions were reduced by a factor of 4 (2 times by each side) in order to be processed by the SfM-MVS software [35].

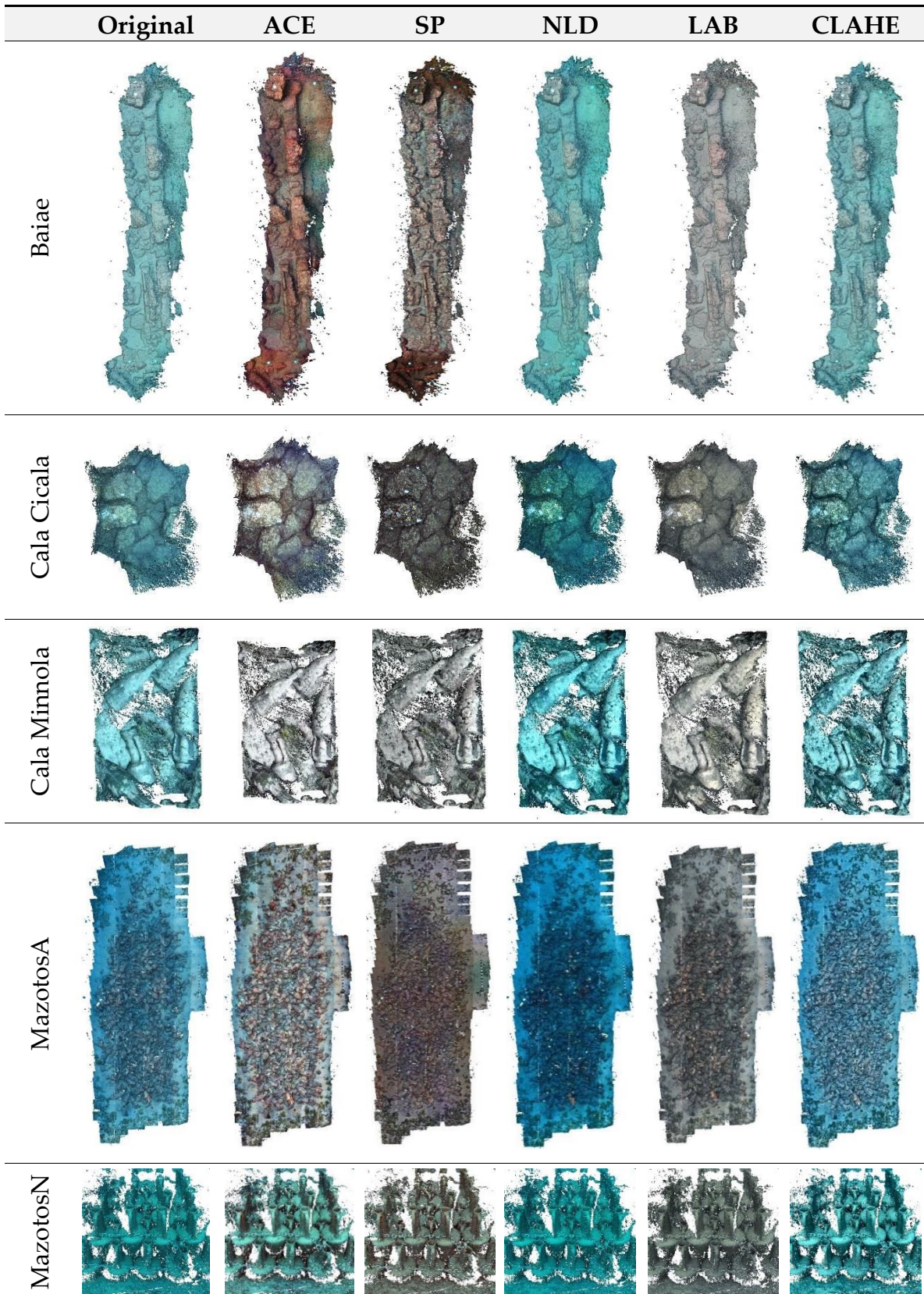


Figure 21. The dense point clouds for all the datasets and for all the available imagery.

2.5.4.4 Metrics for Evaluating the Results of the 3D Reconstructions

All the dense point clouds presented above (Figure 21) were imported into Cloud Compare freeware [56] for further investigation. In particular, the following parameters and statistics, used also in [58,59], were computed for each point cloud:

1. **Total number of points.** All the 3D points of the point cloud were considered for this metric, including any outliers and noise [56]. For our purposes, the total number of 3D points reveal the effect of an algorithm on the matchable pixels between the images. The more corresponding pixels are found in the Dense Image Matching (DIM) step on the images, the more points are generated. Higher values of total number of points are considered better in these cases; however, this should be crosschecked with the point density metric, since it might be an indication of noise on the point cloud.
2. **Cloud to cloud distances.** Cloud to cloud distances are computed by selecting two-point clouds. The default way to compute this kind of distance is the ‘nearest neighbour distance’: for each point of the compared cloud, Cloud Compare searches the nearest point in the reference cloud and computes the Euclidean distance between them [56]. This search was performed within a maximum distance of 0.03 m, since this is a reasonable accuracy for real-world underwater photogrammetric networks [60]. All points farther than this distance will not have their true distance computed—the threshold value will be used instead. For the performed tests, this metric is used to investigate the deviation of the “enhanced” point cloud, generated using the enhanced imagery, from the original one. However, since there are no reference point clouds for these real-world datasets, this metric is not used for the final evaluation. Nevertheless, this metric can be used as an indication of how much an algorithm affects the final 3D reconstruction. Small RMSE (Root Mean Square Error) means small changes; hence the algorithm is not that intrusive, nor effective.
3. **Surface Density.** The density is estimated by counting the number of neighbours N (inside a sphere of radius R) for each point [56]. The surface density used for this evaluation is defined as $\frac{N}{\pi \times R^2}$, i.e., the number of neighbours divided by the neighbourhood surface. Cloud Compare estimates the surface density for all the points of the cloud and then it calculates the average value for an area of 1 m² in a proportional way. Surface density is considered to be a positive metric, since it defines the number of the points on a potential generated surface, excluding the noise being present as points out of this surface. This is also the reason of using the surface density metric instead of the volume density metric.
4. **Roughness.** For each point, the ‘roughness’ value is equal to the distance between this point and the best fitting plane computed on its nearest neighbours [56], which are the points within a

sphere centred on the point. The radius of that sphere was set to 0.025 m for all datasets. This value was chosen as the maximum distance between two points in the less dense point cloud. Roughness is considered to be a negative metric since it is an indication of noise on the point cloud, assuming an overall smooth surface.

2.5.4.5 Results

The values of the computed metrics for the five different datasets and the five different image enhancement algorithms are presented in Figure 22. The following considerations can be deduced regarding each metric:

1. **Total number of points.** SP algorithm produced the less 3D points in the 60% of the test cases while LAB produced more points than all the others, including the original datasets in the 80% of the test cases. In fact, only for the Cala Minnola dataset, the LAB points were noticeably less than the original points. Additionally, NLD images produced more points than the CLAHE-corrected imagery in 80% of the tests, and more points than the ACE-corrected imagery in 80% of the cases. ACE-corrected imagery always produced fewer points than the original imagery, except in the case of the Cala Minnola dataset.
2. **Cloud to cloud distances.** The SP- and CLAHE-corrected imagery presented the greatest distances in 100% of the cases, while the NLD- and LAB-corrected imagery presented the smallest cloud to cloud distances in 100% of the cases. However, these deviations were less than 0.001 m in all the cases.
3. **Surface Density.** In most of the cases, surface density was linear to the total number of points. However, this was not observed in the Baiae dataset test, where LAB- and NLD-corrected imagery produced more points in the dense point cloud, although their surface density was less than the density of the point cloud of the original imagery. This is an indication of outlier points and noise in the dense point cloud. Volume density of the point clouds was also computed; however, it is not presented here, since it is linear to the surface density.
4. **Roughness.** SP-corrected imagery produced the roughest point cloud in the 60% of the cases, while for MazotosA dataset the roughest was the original point cloud. LAB and NLD corrected imagery seemed to produce almost equal or less noise than the original imagery in most of the cases.

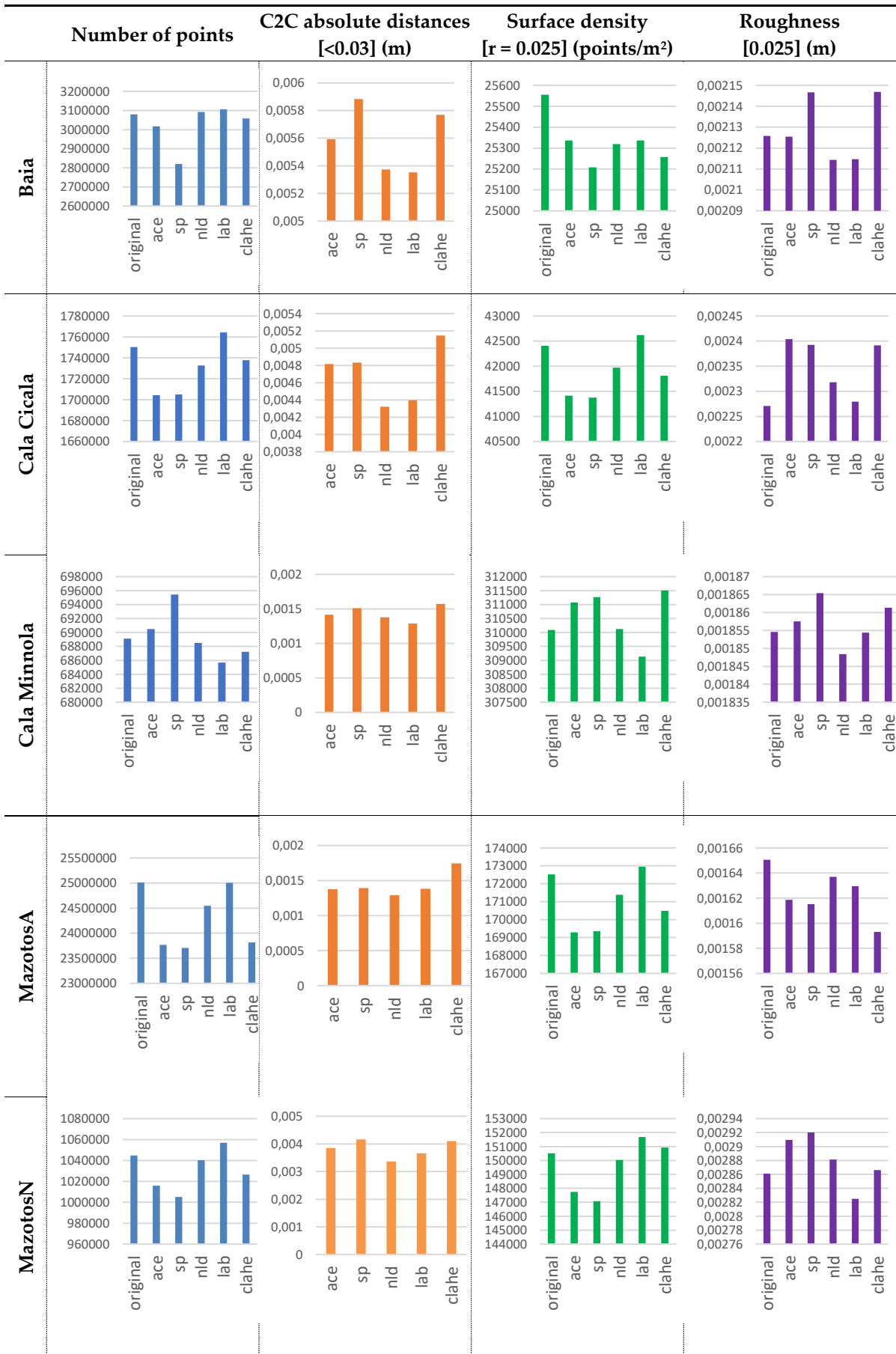


Figure 22. The results of the computed parameters for the five different datasets.

To facilitate an overall comparison of the tested algorithms in terms of 3D reconstruction performance and evaluate the numerous results presented above, the surface density D and roughness R metrics were normalized and combined into one overall metric, named as the Combined 3D metric ($C3Dm$). To achieve that, the score of every image enhancement algorithm on D and R was normalized to the score of the 3D reconstruction computed using the original images. Hence, the 100% score is referred to the original 3D reconstruction. If an image enhancement algorithm has a negative impact on the 3D reconstruction, then the score should be less than 100% and if it has a positive impact, the score should be more than 100%. For both surface density D and roughness R , the same weight was used.

The score totalled for each algorithm was computed independently for each dataset as the average value ($[Av_{original}]_{dataset}$) of the normalized metrics $\widehat{D}_{algorithm}, \widehat{R}_{algorithm}$ (Equation (2)). The same computation was performed to calculate the score ($[Av_{original}]_{dataset}$) of each original reconstruction for each original dataset (Equation (1)). The $C3Dm$ was computed for each algorithm summing up the scores totalized by the algorithm on each dataset and normalizing it to the score totalized by the original images (Equation (3)).

$$[Av_{original}]_{dataset} = \frac{[\widehat{D}_{original} + \widehat{R}_{original}]_{dataset}}{2} \quad (1)$$

$$[Av_{algorithm}]_{dataset} = \frac{[\widehat{D}_{algorithm} + \widehat{R}_{algorithm}]_{dataset}}{2} \quad (2)$$

$$C3Dm_{algorithm} = \frac{\sum [Av_{algorithm}]_{dataset}}{\sum [Av_{original}]_{dataset}} \quad (3)$$

The *total number of points* and the *Cloud to cloud distances* metrics were not used for the computation of the $C3Dm$. The reason for this is that the first one is highly correlated with the surface density metric, while the second one is not based on reference data that could have been used as ground truth. However, these two metrics were used individually to deduce some valuable considerations in the performance of the tested algorithms.

Figure 23 shows the $[Av_{algorithm}]_{dataset}$ for each algorithm and each dataset, and the $C3Dm_{algorithm}$ for each dataset. The results, that are also presented in Table 14, suggest that the LAB algorithm improves the 3D reconstruction in most of the cases, while the other tested algorithms do not, and they do have a negative effect on it. However, the final $C3Dm_{lab}$ is not significantly different from the one of the other algorithms. Consequently, LAB performs better than the others, while CLAHE follows up with almost 1.4% difference.

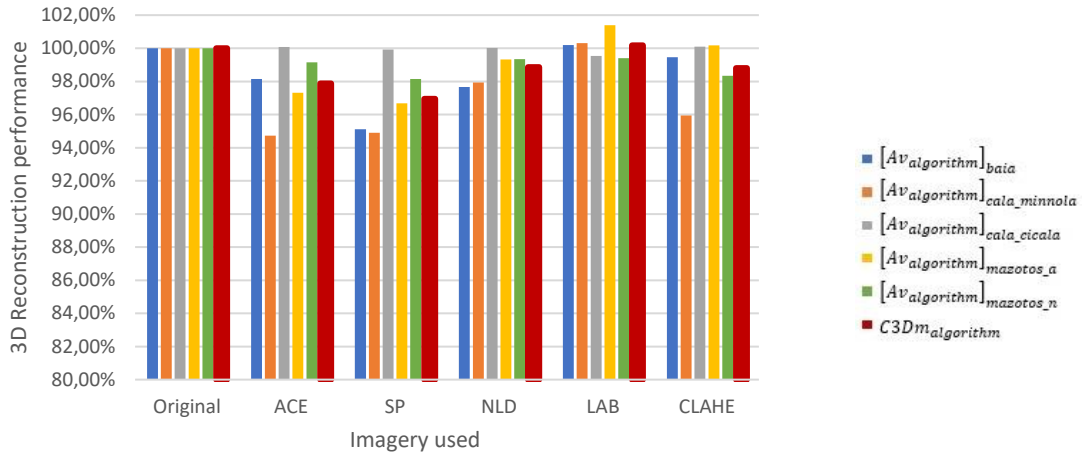


Figure 23. The Combined 3D metric ($C3Dm$), representing an overall evaluation of 3D reconstruction performance of the five tested image enhancing methods on the five datasets.

ACE and SP seem to produce the least valuable results, in terms of 3D reconstruction, and this was expected, since the enhanced imagery resulted by these algorithms in some cases has generated some ‘artefacts,’ likely due to the oversaturation of some image details. However, the differences on the performance are less than 4%.

In conclusion, the most remarkable consideration that arises from Table 14 is that four out of five algorithms worsen the results of the 3D reconstruction process and only the LAB slightly improves the results.

Table 14. Average metrics and average expert vote calculated for each site.

Site	Metric	Original	ACE	SP	NLD	LAB	CLAHE
All	Combined 3D metric ($C3Dm$)	100%	97.9%	97.0%	98.9%	100.2%	98.8%

2.5.5 Comparison of the Three Benchmarks Results

According to the objective metrics results reported in Section 2.5.2, the SP algorithm seemed to perform better than the others in all the underwater sites, except for the case MazotosA. For these images, taken on Mazotos with artificial light, each metric assigned a higher value to a different algorithm, preventing us from deciding which algorithm performed better on this dataset. It is also worth to remember that the ACE algorithm seems to be the one that performs better in enhancing the information entropy of the images. However, objective metrics do not seem consistent nor significantly different enough to allow the best algorithm nomination. On the other hand, the opinion of experts seems to be that the ACE algorithm is the one that performs better on all sites, and CLAHE and SP perform as fine as ACE at some sites. Additionally, the 3D reconstruction quality seems to be decreased by all the algorithms, except LAB that slightly improves it.

Table 15 shows a comparison between average objective metrics, average vote of experts and $C3Dm$ divided by site. The best score for each evaluation is marked in bold. Let us recall that the values highlighted in orange in the expert evaluation rows (Exp) are not significantly different from each other within the related site. It is worth noting that the objective metric that seems to get closest to the expert opinion is \bar{E} , i.e., information entropy. Indeed, \bar{E} is consistent with the expert opinion, regarding the nomination of the best algorithm within the related site, in all the five sites. \bar{M} and \bar{G} are consistent with each other on 4/5 sites and with the expert opinion on 3/5 sites.

Table 15. Average metrics and average expert votes calculated for each site.

Site	Metric	ACE	SP	NLD	LAB	CLAHE
Baiae	\bar{M}_s	115.8122	91.3817	121.1528	126.8077	123.2329
	\bar{E}_s	7.4660	6.9379	6.8857	7.1174	7.0356
	\bar{G}_s	3.1745	3.4887	2.2086	1.9550	3.3090
	Exp	3.64	3.55	2.58	2.48	2.97
	$C3Dm$	0.9814	0.9511	0.9767	1.0019	0.9947
Cala Cicala	\bar{M}_s	124.1400	82.5998	106.5964	121.3140	114.0906
	\bar{E}_s	7.5672	7.1274	6.9552	7.0156	7.3381
	\bar{G}_s	4.1485	5.5009	3.4608	2.4708	4.5598
	Exp	3.64	2.94	2.21	2.70	3.06
	$C3Dm$	0.9473	0.9490	0.9793	1.0032	0.9594
Cala Minnola	\bar{M}_s	89.7644	78.1474	117.3263	112.0117	113.3513
	\bar{E}_s	6.8249	6.6617	5.6996	6.5882	6.4641
	\bar{G}_s	3.4027	4.4859	1.3137	1.6508	2.9892
	Exp	3.48	2.91	1.91	2.61	2.55
	$C3Dm$	1.0007	0.9992	1.0001	0.9953	1.0011
MazotosA	\bar{M}_s	122.0792	110.1639	68.7037	93.5767	118.1187
	\bar{E}_s	7.6048	7.1057	6.6954	6.8260	7.4534
	\bar{G}_s	2.5653	2.8744	2.3156	1.4604	2.7938
	Exp	3.55	2.45	2.33	3.24	3.97
	$C3Dm$	0.9731	0.9668	0.9932	1.0140	1.0018
MazotosN	\bar{M}_s	90.0566	79.5346	94.3764	85.4173	103.1706
	\bar{E}_s	6.5203	6.3511	5.9011	6.6790	6.8990
	\bar{G}_s	1.8498	3.3325	0.8368	1.1378	2.3457
	Exp	2.88	2.21	2.15	2.39	3.30
	$C3Dm$	0.9915	0.9815	0.9935	0.9940	0.9834

To recap, the concise result of the objective and expert evaluation seems to be that LAB and NLD do not perform as well as the other algorithms. ACE could be employed in different environmental condition with good results. CLAHE and SP can produce a good enhancement in some environmental conditions.

On the other hand, according to the evaluation based on the results of 3D reconstruction, the LAB algorithm seems to have the best performance, producing more 3D points, insignificant cloud to cloud distances, high surface density and low roughness 3D point clouds.

2.5.6 Conclusions

Five well-known state-of-the-art methods have been selected for the enhancement of images taken on various underwater sites with five different environmental and illumination conditions. A benchmark for these methods has been produced based on three different evaluation techniques:

- an objective evaluation based on metrics selected among those already adopted in the field of underwater image enhancement;
- a subjective evaluation based on a survey conducted with a panel of experts in the field of underwater imagery;
- an evaluation based on the improvement that these methods may bring to 3D reconstructions.

The purpose was twofold. First of all, it has been tried to establish which methods perform better than the others and whether or not there existed an image enhancement method, among the selected ones, that could be employed seamlessly in different environmental conditions in order to accomplish different tasks such as visual enhancement, colour correction and 3D reconstruction improvement.

The second aspect was the comparison of the three above mentioned evaluation techniques in order to understand if they provide consistent results. Starting from the second aspect, it can be stated that the 3D reconstructions are not significantly improved by discussed methods, probably the minor improvement obtainable with the LAB could not justify the effort to pre-process hundreds or thousands of images required for larger models. On the other hand, the subjective metrics and the expert panel appear to be quietly consistent and, in particular, the \bar{E} identifies the same best methods of the expert panel on all the datasets. Consequently, an important conclusion that can be drawn from this analysis is that \bar{E} should be adopted in order to have an objective evaluation that provides results consistent with the judgement of qualitative evaluations performed by experts in image enhancement. This is an interesting point, because it is not so easy to organize an expert panel for such kind of benchmark.

On the basis of these considerations, the five selected methods can be compared by means of the objective metrics (in particular \bar{E}) and the expert panel. It is quite apparent from Table 15 that ACE, in almost all the environmental conditions, is the one that improves the underwater images more than the others. In some cases, SP and CLAHE can lead to similar good results.

Moreover, thanks to the tool described in Section 2.3, the community working in underwater imaging would be able to quickly generate a dataset of enhanced images processed with five state of the art methods and use them in their works or to compare new methods. For instance, in case of an underwater 3D reconstruction, the tool can be employed to try different combinations of methods and quickly verify if the reconstruction process can be improved somehow. A possible strategy could be to pre-process the images with the LAB method trying to produce a more accurate 3D model and,

afterwards, to enhance the original images with another method such as ACE to achieve a textured model more faithful to the reality (Figure 24). Employing the tool for the enhancement of the underwater images ensures to minimize the pre-processing effort and enables the underwater community to quickly verify the performance of the different methods on their own datasets.

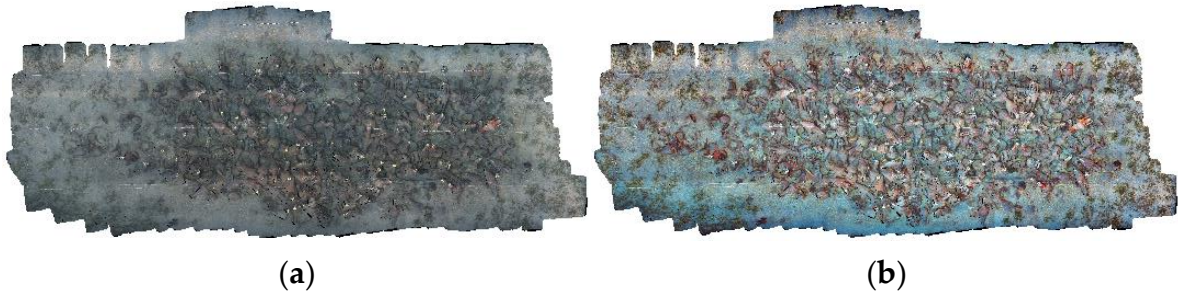


Figure 24. Textured 3D models based on MazotosA dataset and created with two different strategies. (a) 3D model created by means of only LAB enhanced imagery both for the 3D reconstruction and texture. (b) 3D model created following the methodology suggested above: the 3D reconstruction was performed using the LAB enhanced imagery and the texturing using the more faithful to the reality ACE imagery.

Finally, Table 16 summarizes our conclusions and provides the community with some more categorical guidelines regarding which method should be used according to different underwater conditions and tasks. In this table, the visual enhancement row refers to the improvement of the sharpness, contrast and colour of the images. The 3D Reconstruction row refers to the improvement of the 3D model, apart from the texture. As previously described, the texture of the model should be enhanced with a different method, according to the environmental conditions and, therefore, to the previous “visual enhancement” guidelines. Furthermore, as far as the evaluation of other methods that have not debated here is concerned, our guideline is to evaluate them with the \bar{E} metric, as pursuant to our results, it is the metric that is closest to the expert panel evaluation.

Table 16. Suggested methods according to different underwater conditions and tasks.

Task	Underwater Conditions	Suggested Methods
Visual enhancement	Shallow water	ACE, SP
	Deep water (natural illumination)	ACE, CLAHE, SP
	Deep water (artificial illumination)	ACE, CLAHE
3D Reconstruction (model)	Every condition	LAB

In the end, let us underline, though, that we are fully aware of the fact that there are several other methods for underwater image enhancement and manifold metrics for the evaluation of these methods. It was not possible to debate them all in a single study. Our effort has been to guide the community towards the definition of a more effective and objective methodology for the evaluation of the underwater image enhancement methods.

3 Underwater Assisted Navigation

3.1 Introduction

The activities carried out in the marine environment, specifically in archaeological and biological underwater sites, present many problems and limitations compared to those performed in dry conditions.

Over the past few years, these activities have benefited from the advent of unmanned marine vehicles, both for the surface (ASV, Autonomous Surface Vehicle) and the submerged (UUV, Unmanned Underwater Vehicle) environment, that support and facilitate the exploration and survey of the marine ecosystem thanks to their reduced overall dimensions and reduced costs, when compared to research vessels, and the overcoming of all those limitations due to the presence of human operators [61–66]. Although these technologies have given a substantial boost to the marine scientific research, there are still many scenarios in which the human presence cannot be replaced by autonomous and robotic systems. In particular, where the depths allow it, human intervention is often preferred. However, this preference is made critical by the lack of technological tools on the market that can support divers in their work. In fact, the gap between operational needs and the support provided by the technological devices on the market is still very large.

For example, in the archaeology field, great efforts have been focused on the documentation, monitoring and conservation of the underwater cultural heritage. These activities could greatly benefit from the introduction of new devices and technological tools capable of supporting divers in the gathering of data related to the archaeological remains and to the marine environment in which they are located. Such data would be then of great help for a correct and efficient planning of the restoration and conservation activities to perform on site by the underwater archaeologists. The cooperation between man and technology can therefore represent an efficient solution to overcome the difficulties in working in a challenging and unpredictable context like the marine environment.

Another example that could benefit from the development of appropriate technological tools is represented by the inspection and recovery activities undertaken in the submerged environment by the enforcement authorities. In fact, due to the lack of a precise and reliable positioning system for the underwater environment, these activities are usually carried out by exploring the search area through systematic movements, e.g., starting from the centre of the area and moving in a spiral direction, or starting from one end and moving along parallel and equidistant lines. The search and exploration activities carried out in this manner could be subject to many difficulties and problems with orientation due to the water turbidity. Therefore, a navigation and geolocation system would be of great support to efficiently and safely perform this kind of activities.

Furthermore, it is very difficult for a diver to manually calculate the safest and shortest route, that passes through predefined targets, taking into account all the different variables of the case: travel distance, the amount of air remaining in the tank, decompression stops, etc.. At present, the dive computers that are on the market allow to measure time and depth of a dive and calculate a safe ascent profile, but they are not able to provide information neither reliable estimates of the route ahead.

The idea to develop an underwater tablet to support the diver providing him/her with geo-localization and contextualized information has been conceptualized with the project Visas in 2015 [67–69]. In this context, a prototype of the underwater tablet (Figure 25) has been developed by employing an acoustic localization system in LBL (Long BaseLine) configuration (Figure 26). This system was mainly intended to support recreational divers and it has been deployed and tested in two pilot sites. Later, this system has been extended during the Lab4Dive project [70] in order to be employed in scientific applications for conducting surveys allowing the user to acquire geo-localized data, e.g. textual notes and pictures.

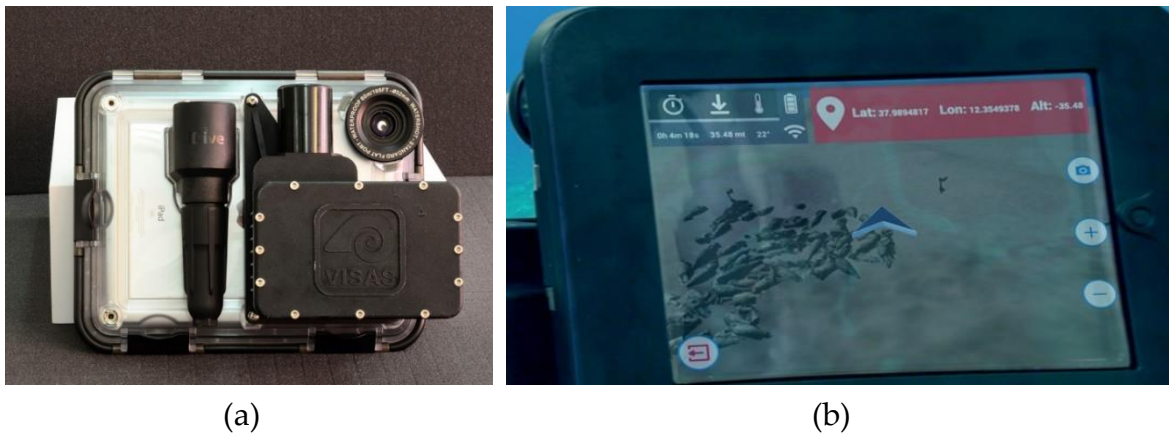


Figure 25. The prototype of the Underwater Tablet developed in the Visas project.

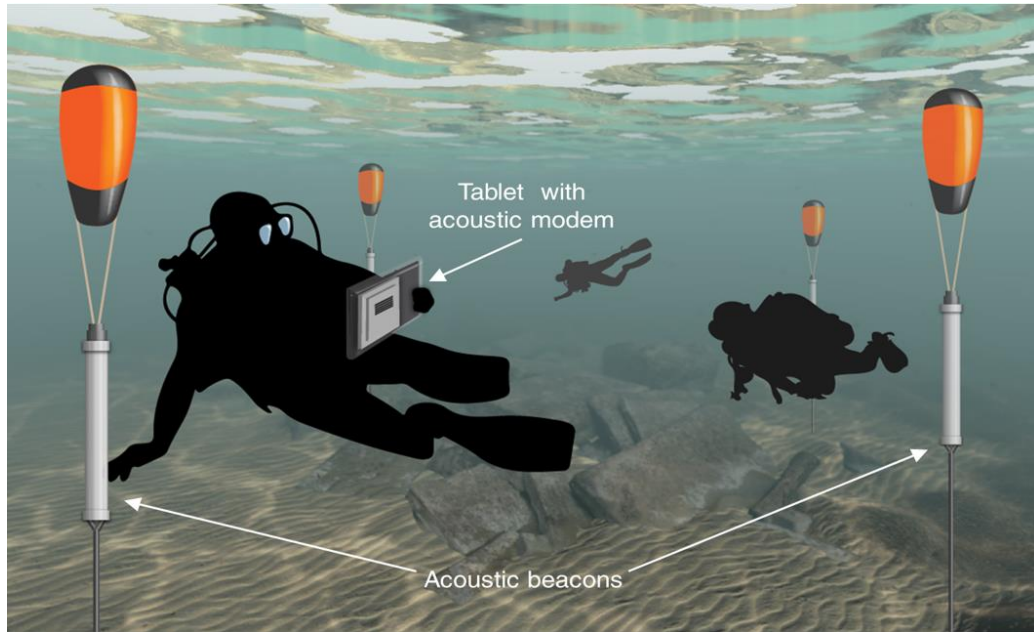


Figure 26. The LBL configuration.

Starting from these results, the present research has contributed to the development of the underwater tablet by implementing relevant features for the i-MareCulture [45] and MOLUX [71] projects. The present chapter describes the hardware/software improvements and contributions that this research work has provided to the prototype of the underwater tablet in order to develop an underwater navigation system with several relevant features. Furthermore, on the basis of this system, two main advanced techniques have been developed: the Underwater Augmented Reality and the Underwater Path Planning. The next chapter describes the Underwater Augmented Reality feature developed in the context of the i-MareCulture project. Likewise, the last chapter describes the Underwater Path Planning developed for the MOLUX project.

3.2 State of the Art

Most of the existing underwater navigation systems have been specifically developed for the military field in order to perform operations in an unknown underwater environment without the presence of a support vessel. These are mainly commercial solutions that cannot be efficiently adapted to other fields, in fact, in the archaeological and scientific fields the activities are usually undertaken with the adoption of the bathymetric map of the seafloor and the supervision of the operations from the shore or from a support vessel. Based on this premise, a first example of underwater navigation system is DiNIS (Diver Navigation and Imaging System) [72], developed by Kenautics, that has been designed primarily to meet the needs of the military special forces. It consists of a display and a series of commercial sensors integrated into a single housing without other external components. The main features of this system are the navigation between waypoints and the acquisition of sonar images and video. The navigation is performed by means of underwater sensors,

such as Doppler Velocity Log (DVL), Inertial Motion Unit and Attitude, Heading, and Roll Sensor (IMU/AHRS), pressure sensor, and GPS which can provide only data about the positioning on the sea surface and not underwater. Moreover, the system adopts a proprietary algorithm based on Kalman filter to provide the diver with accurate information about position and velocity. Other commercial solutions come from the product line offered by Mistral, among which the EDGE [73] system is the one with more functionalities that have been designed specifically to perform secret military operations in the underwater environment. This system creates a connection network between different nodes, with or without the visual horizon, to assure a long-range data transfer through acoustic techniques. The system consists of an EDGE Commander, placed on the support vessel, and an EDGE Nav, used by the divers, for the underwater navigation and communication. In particular, the EDGE Nav consists of a display and a number of sensors integrated into a single compact package, and the navigation system adopts GPS, IMU and DVL sensors to calculate the position of the diver.

The Blueprint Subsea company also produces underwater navigation systems. In particular, this company has developed an underwater laptop, Artemisis [74] that integrated a sonar for the identification of a target, DVL, GPS, and S57/S63 electronic navigation maps. This system has been designed for military purposes and for supporting the divers in the navigation and localization of objects placed on the seabed. The system is equipped with a display and five buttons that allows the diver to interact with it. Before the dive, it is possible to upload on the device files related to the mission, which contain the targets that the diver can decide to visit. With regards to non-commercial solutions, the CADDY (Cognitive Autonomous Diving Buddy) [75] project proposes an autonomous surface vehicle to improve the monitoring, the assistance and the safety of the diver. It features cognitive functions to interpret, with a camera, the diver's actions and his/her health conditions. Nevertheless, the system does not support the diver for the exploration activities and for collecting geolocated data.

3.3 Hardware Setup

This section describes the hardware setup of the Underwater Navigation system proposed in this research work that is composed of the tablet, the waterproof case and the acoustic localization system.

3.3.1 Waterproof case

In the Visas prototype, the tablet was enclosed in a waterproof case that should preserve all the touchscreen functionalities thanks to a pressure management system that ensures the presence of an air gap between the tablet display and the housing membrane. However, this case proved to be ineffective in real use due to the different issues from which it suffers. Therefore, a new underwater

case produced by EasyDive [76] that is more affordable and easier to use has been adopted (Figure 27). The housing is made from a solid block of anodized aluminium for maximum resistance overtime against wear and saltiness. The tablet can be controlled using a Bluetooth keyboard composed of five buttons equipped with optical sensors and placed on the right side of the case, under the housing glass.

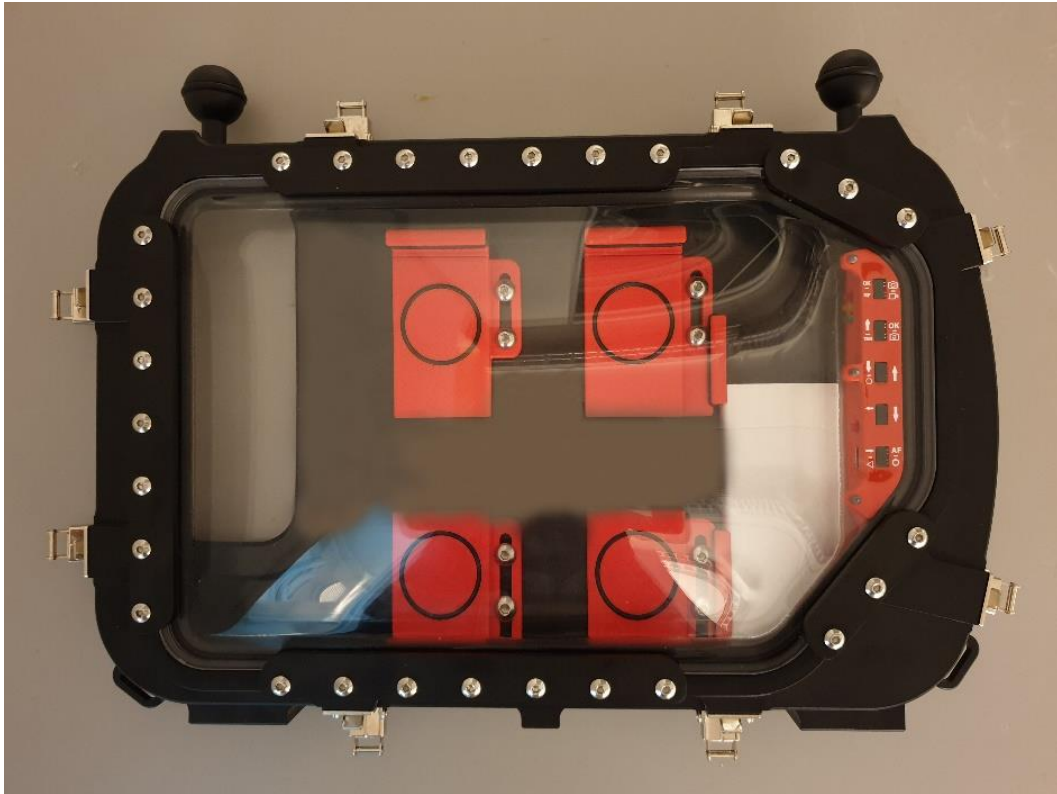


Figure 27. The new underwater case with the Bluetooth keyboard.

3.3.2 Acoustic localization system

In the Visas project, the employed acoustic localization system was in LBL configuration. This involved the fixed installation of four transponders within the underwater site that must be deployed before the diving. During the present research work, the LBL configuration has been dismissed and two new acoustic localization systems (Figure 29) have been integrated with the underwater navigation system: a USBL system developed by Blueprint and an SBL system developed by Applicon, an Unical Spinoff. In contrast to the LBL system, these two new systems do not require a fixed installation of acoustic transponders within the site. In fact, the transponders of these systems can be placed on a buoy or on a boat (Figure 28).

In particular, the Short Base-Line (SBL) positioning system provided by AppliCon Srl and described by Cario et al. [77], consists of a base with four transmitters and one or more underwater receivers. The underwater receiver is intended to be coupled with the tablet; therefore, it was also conformed to the new underwater case and designed to be compact (Figure 29b). Through this

localization system, the tablet can know its position relative to the base and, if the latter is geo-localized, it can know its absolute geographical position. During a test in the archaeological site of Baiae, it has been evaluated that the tablet, coupled with this localization system, could operate within a maximum range from the base around 70 meters and can receive localization data at an update rate of 1 Hz.

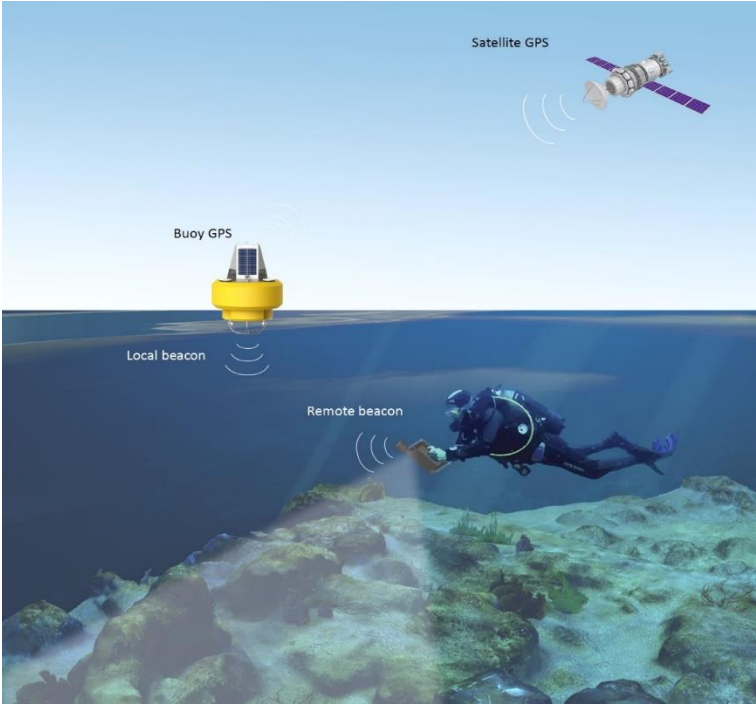


Figure 28. Example of deployment of an SBL/USBL system.



Figure 29. The two new acoustic localization systems coupled with the underwater tablet. (a) The USBL system; (b) the SBL system.

3.4 DIVY: the Underwater Navigation App

The underwater tablet has been provided with a dedicated software, namely Divy, that has been completely redesigned against the prototype of the Visas project, and that enables the diver to access different features such as the visualization of a map of the underwater site that allows the diver to know his position within the submerged site, the possibility to acquire geo-localized data, the visualization of additional information about specific points of interest and a functionality for the communication with the surface operators.

Furthermore, the software provides the user with an enhanced diving experience through an on-site augmented visualization of a 3D hypothetical reconstruction that shows to the diver as the actual ruins should appear in the past. This feature is described in detail in the next section.

3.4.1 Five Buttons UI

The UI has been mostly redesigned in order to group all the interaction buttons on the right side of the screen. This allows a diver to access all the features of the app with just one hand. Furthermore, the new UI has been designed to fit the layout of the new underwater case (Figure 27).

As described in Section 3.3.1, this case is provided with a Bluetooth keyboard (Figure 30a) composed of five buttons and placed on the right side of the case. Hence, the UI has been redesigned so that the features can be accessed completely by means of only five buttons placed on the right side of the UI (Figure 30b). These buttons can be triggered both through the touchscreen and through the Bluetooth keyboard integrated into the underwater case.

Each of the five buttons is composed by an icon and a label representing the actual function of the button. Indeed, the buttons are dynamic and can represent different functions in the app lifecycle (Figure 31).

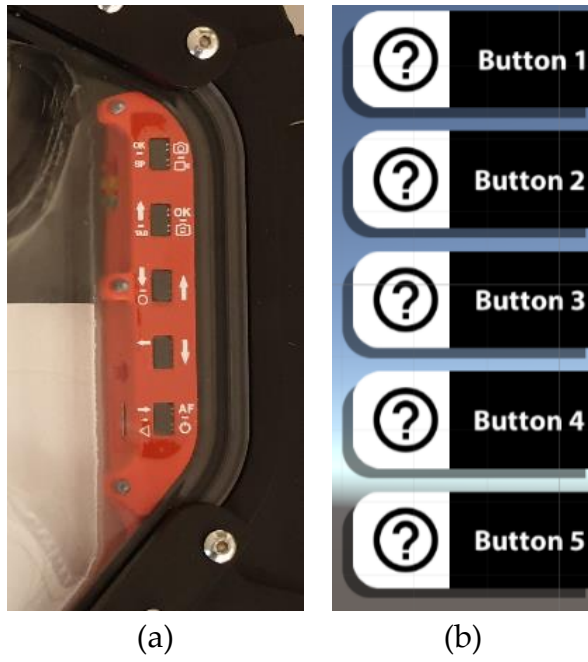


Figure 30. The Bluetooth keyboard integrated in the case (a) and the related Five Buttons UI (b).

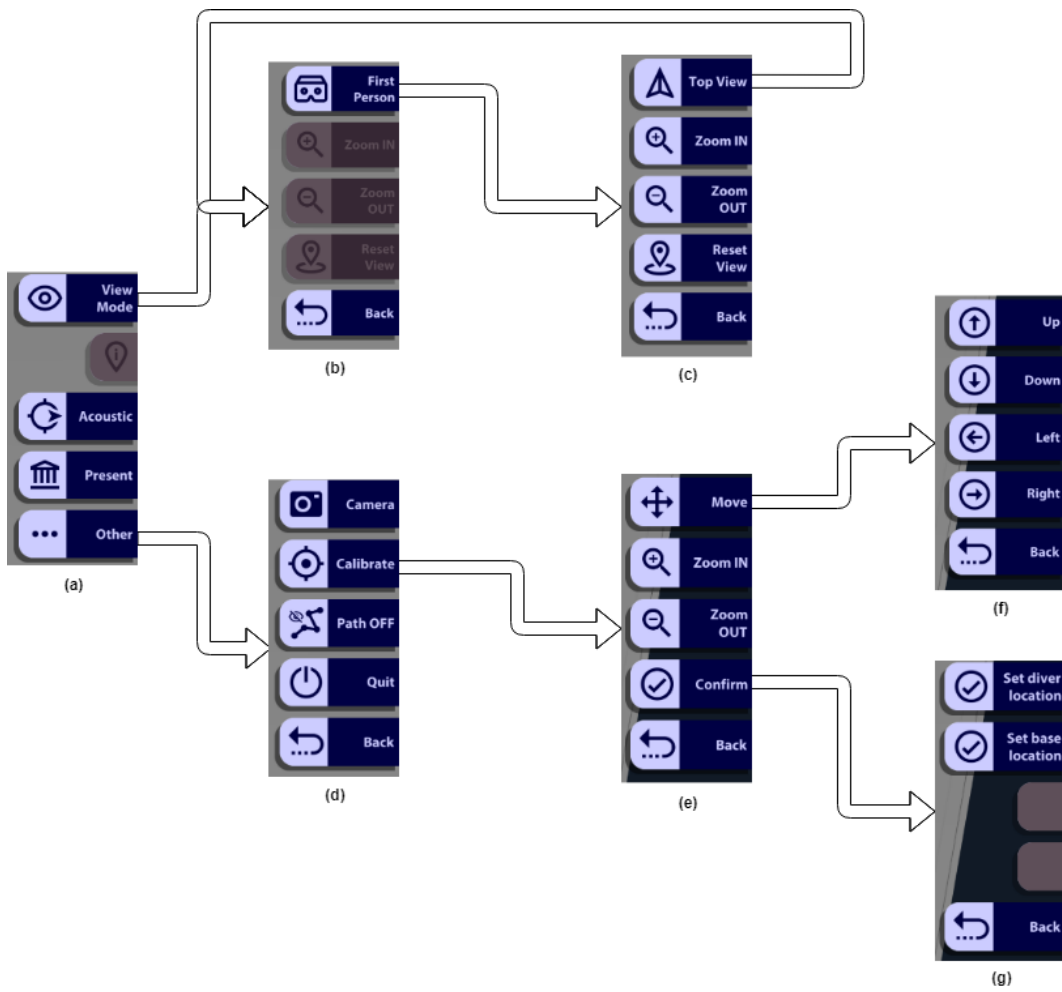


Figure 31. Five Buttons UI menu hierarchy.

The UI is fully customizable and adaptable to different configurations in order to seamlessly switch between a scientific/professional application, with the possibility to acquire geo-localized data, and a touristic application with the opportunity to benefit from the augmented reality feature.

Figure 31 shows a sample configuration of the Five Button UI, that exposes a subset of features. The main menu (a) enables the user to access the major features of the system. The first button permits to switch the view modality between a top view (b) of the underwater site and a first-person view (c). The latter is particularly useful to visualize the hypothetical reconstruction of the structures and artefacts that are superimposed on the present status of an underwater archaeological site. This feature is precisely accessible through the fourth button that enables the user to switch the visualization through the present and the past status. Whenever the visualization is in “top view” modality some additional features are accessible to the user (c), such as the zoom and reset of the viewing. The second button of the main menu (a), which is disabled in Figure 31, is enabled only when there is a POI nearby the diver, and permits to display additional information about this POI. The fifth button opens a menu (d) that enables the user to access additional features such as the camera function that permits to shot geo-localized pictures. In addition, through this menu a calibration feature is accessible (e, f, g), that is mostly a debug feature not intended for the final users.

3.4.2 App navigation flow

The navigation flow of the Divy app should be composed by few screens in order to improve the usability for divers. The implementation of the UI respects this requirement and provides the user with simplified navigation (Figure 32).

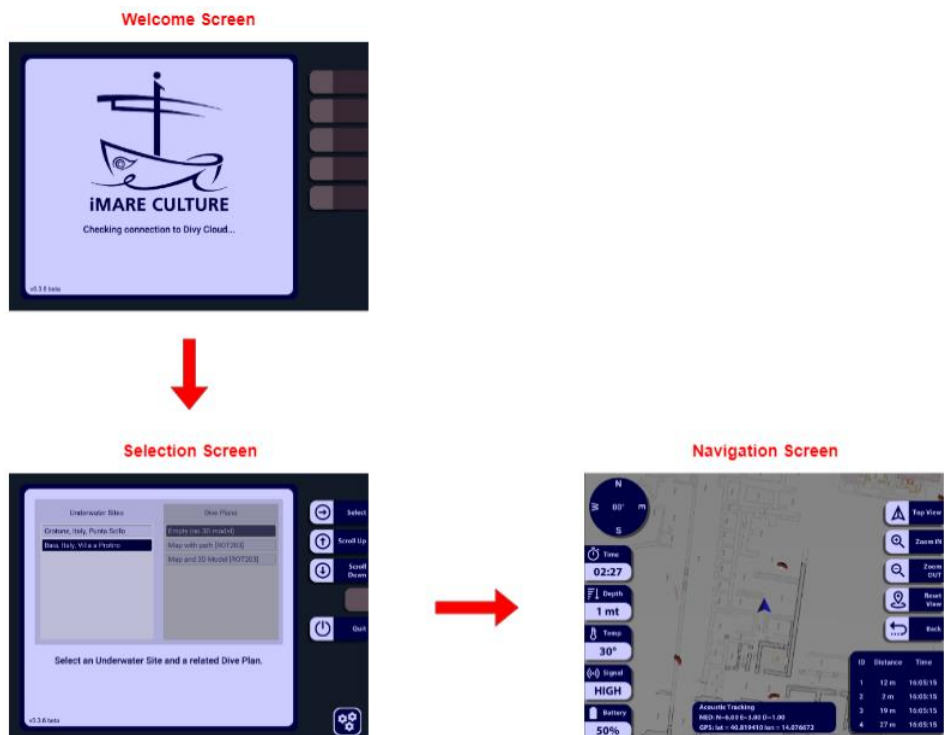


Figure 32. Actual app navigation flow.

The selection screen enables the user to select the underwater site and the related dive plan by the means of the just described five buttons UI. A dive plan is composed of different information such as a list of points of interest, a map and a 3D model of the underwater site. The whole architecture is designed in order to support different underwater sites with multiple dive plans. As showed in Figure 32, the underwater sites are listed in the first panel and the dive plans are listed in the second panel. It is possible to scroll through them using the related “Scroll Down” and “Scroll Up” buttons and to confirm the selection using the “Select” button. Initially, the panel of the underwater sites is enabled and the panel with the dive plan is disabled (Figure 32a). When an underwater site is selected, the related dive plans are listed in the second panel that turns enabled (Figure 32b). At this point, the user can complete the selection by choosing a dive plan or can return to the underwater site selection through the “Back” button (Figure 32). In a first prototype of the UI, the underwater sites were listed as a result of textual search. This required a keyboard to type the name of the underwater site and assumed prior knowledge of the underwater sites stored in the app. In contrast, this simple interaction implemented in the actual UI is more straightforward and do not require any particular knowledge of the system from the final user. Once selected the dive plan, the underwater navigation screen is showed to the user and the dive can be started.

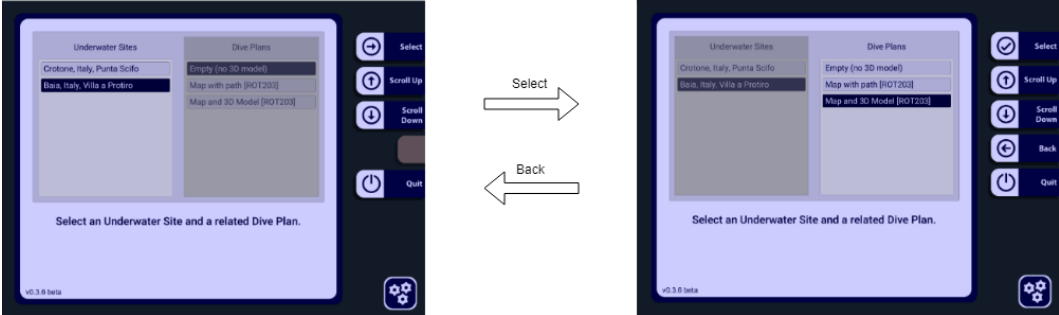


Figure 33. Underwater site and Dive Plan selection.



Figure 34. The user can decide to skip the connection to the computer board.

Another improvement to the app navigation flow and usability is related to the computer board that provides the app with the geo-position data. In the previous prototype, the app was forced to successfully connect to the computer board in order to complete the booting of the app. This unnecessary constraint has been removed and so, if the connection to computer board fails, the user can decide to retry to connect or to skip at all the connection.

3.4.3 Modular UI components

The whole UI architecture of Divy is designed in such a way that each singular UI component can be deactivated or replaced. The “Computer Board UI” is a perfect example of the flexibility of this architecture. In fact, when the user skips the connection to the computer board, all the related UI components are disabled.



Figure 35. Two different setups of the Navigation Screen as an example of the UI modularity.

Figure 35 shows two different setups of the Navigation UI. In one case (Figure 35a), the computer board is connected and the relative UI is showed to the user on the left side of the screen. On the

bottom right corner, it is showed a debug panel that displays some additional information about the acoustic positioning system. On the bottom centre, the position panel is placed which shows the acoustic positioning data received from the computer board. In the other case (Figure 35b), the user decided to skip the connection to the computer board and therefore the relative UI is not shown. The debug panel on the bottom right corner is not shown either. In this case, the position panel is showing the positioning data provided by the visual tracking only, given that no acoustic positioning data are available. In addition, another debug panel is showed on the left top corner displaying information about the status of the visual tracking.

The “Computer Board UI” can be further customized and Figure 36 shows an example of different configurations of this UI. In Figure 36a, the configuration is the same displayed in Figure 35a and the UI is composed by five widgets representing respectively the elapsed time, the depth, the water temperature, the quality of the acoustic signal and the battery status of the computer board. Different widgets can be added or also removed as showed in Figure 36b, where the “Computer Board UI” is composed by only four widgets, two of which has not been modified and the other two represent positioning data in a latitude-longitude format. The UI related to the computer board can be also replaced at all with a more compact layout. Figure 36c shows another layout of the computer board that gives to the user the same information displayed in Figure 36a, but taking up less screen space. The flexibility of this specific UI permits to seamlessly switch between different types of computer board and to consequently interface the underwater tablet to different acoustic positioning systems.

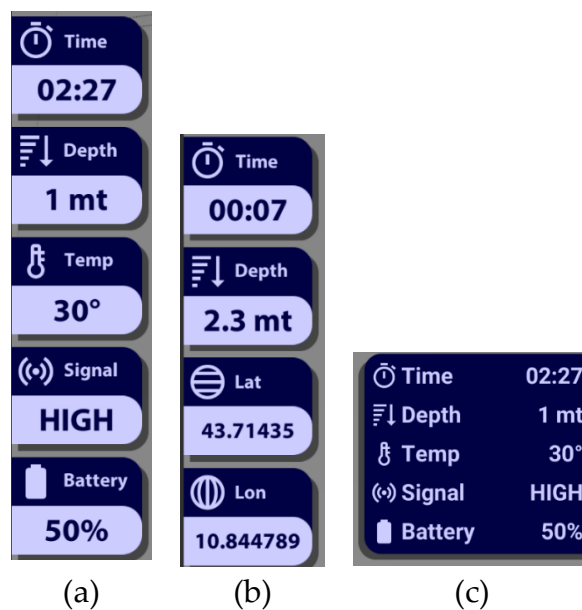


Figure 36. Customizable Computer Board UI.

3.4.4 Configurable Themes

The graphic style adopted for the application is the Flat Design [78]. Most of the major operating systems adopt this design principle, so the user feels familiar with the interfaces designed in this way.

The UI architecture has been designed in order to enable seamless customization of the colours. Different themes can be applied to the whole UI just switching a few configuration parameters. The colour palette of each theme is composed of only two flat colours, one for the foreground and one for the background, in order to enhance the contrasts and consequently the readability. These colours have been checked by using a free colour contrast checker tool [79]. As reported in the description of the tool, it determines if a foreground and a background colour provide enough of contrast “when viewed by someone having colour deficits or when viewed on a black and white screen”, analysing the difference of colour and brightness. A colour pair passes the test only if the colour and the brightness difference exceed the given thresholds (respectively 500 and 125). Table 17 shows the results of the test for the reference colour pair “black and white” (that obviously maximize the contrast), for the selected colour pair and for a dummy colour pair chosen only to illustrate how it is important the right colour combination.

Table 17. Colour contrast test results.

Foreground colour	Background colour	Colour difference (>= 595)	Brightness difference (>= 125)	Test Passed
#FFFFFF	#000000	765	255	YES
#CCCCFF	#000044	595	206	YES
#FF8888	#CC0000	323	110	NO

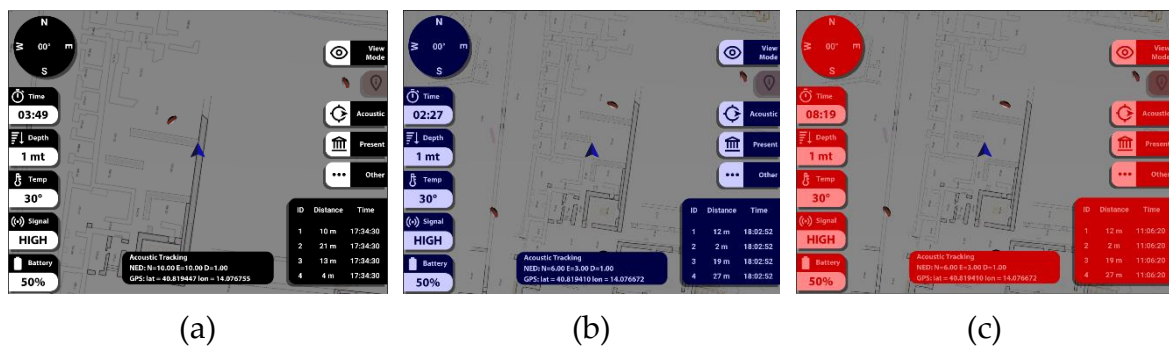


Figure 37. Example of Navigation UI with the colour pairs reported in Table 17.

Figure 37 shows the navigation UI with each colour pairs defined in Table 17. In particular, Figure 37a shows the UI with the colour theme defined in the first row of the table. The readability of the UI is outstanding due to the high contrast provided by the black and white theme. The readability of the UI in Figure 37b is also very good and indeed the concerning colour and brightness difference in the second column are very close to the ones of the black and white theme. So, in the case depicted in Figure 37b the UI maintains a high contrast comparable with the Figure 37a case and

it has more appeal for the final user with respect to the black and white theme. The third row of Table 17 shows as the concerning dummy colour pair has a low colour and brightness difference that prevent this theme from passing the test. The navigation UI in Figure 37c confirms the unsuitability of this theme since the contrast and the readability are very low in this case.

3.4.5 Main navigation screen

The main navigation screen enables the user to visualize all the information concerning the diving state and to access all the features provided by the Divy app (Figure 38). On the background, the map of the underwater site is displayed and the position of the diver within the site is indicated by the related icon at the centre of the screen. Furthermore, the POIs to be visited and the AR zones where the user can activate the UWAR feature are displayed in an overlay over the map. Finally, the control menu, namely the Five Button UI previously described, is placed on the right side, while the information about the dive are placed on the left side.

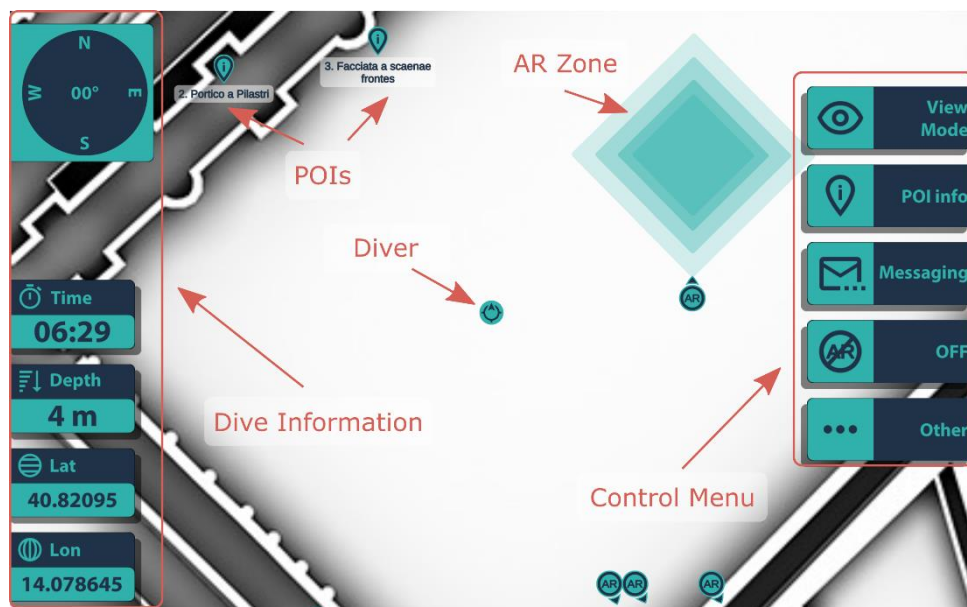


Figure 38. Main navigation screen.

3.4.6 POI information

As depicted in Figure 38, the navigation screen shows the POIs on the map of the underwater site. Each POI can be composed of additional information such as a description or an image, that can be visualized by the diver (Figure 39). When the diver come close to a POI having additional information, this becomes active and turns highlighted in yellow (Figure 40a). Once a POI has been visited, it becomes red (Figure 40b).

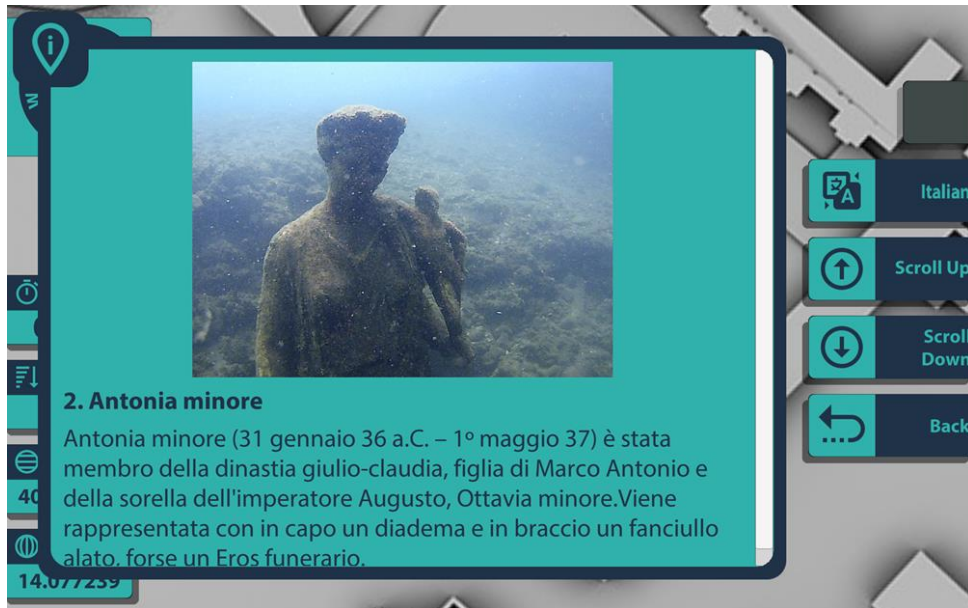
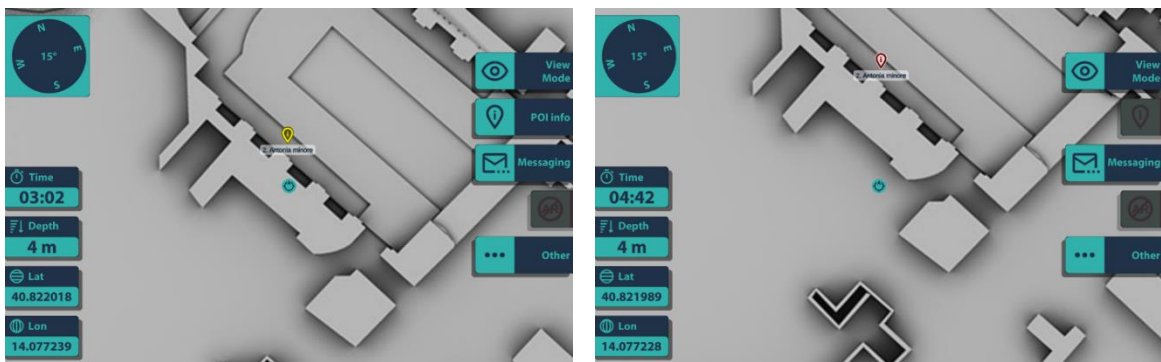


Figure 39. Visualization of additional information regarding the active POI.

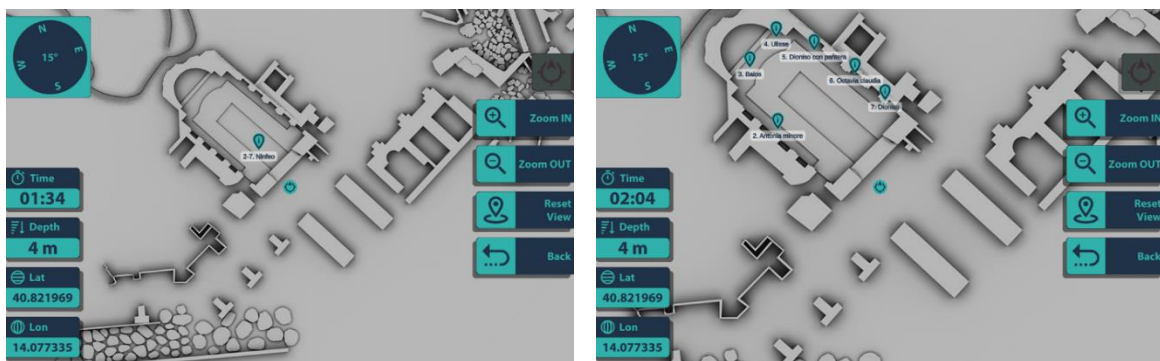


(a)

(b)

Figure 40. An active POI is highlighted in yellow (a). A visited POI is highlighted in red (b).

Furthermore, the user can change the level of zoom of the map and, depending on this, different POI can be visualized on the map. This enables to show more or less detailed information according to the zoom (Figure 47).



(a)

(b)

Figure 41. Different POIs are visualized according to the zoom level. Less zooming (a); more zooming (b).

3.4.7 Acquisition of geo-localized data

The Divy app enables the divers to acquire geo-localized data. In particular, they can acquire photos by the means of the camera embedded in the tablet or an external high-resolution camera (Figure 42a). The navigation software permits also to store textual notes. The waterproof case described in section 3.3.1 does not permit to interact with the touchscreen and consequently with the virtual keyboard, so the user can acquire only a set of predefined notes through this underwater case. When using a different underwater case that enables the use of the touchscreen, the user can type also custom notes as showed in Figure 42b.

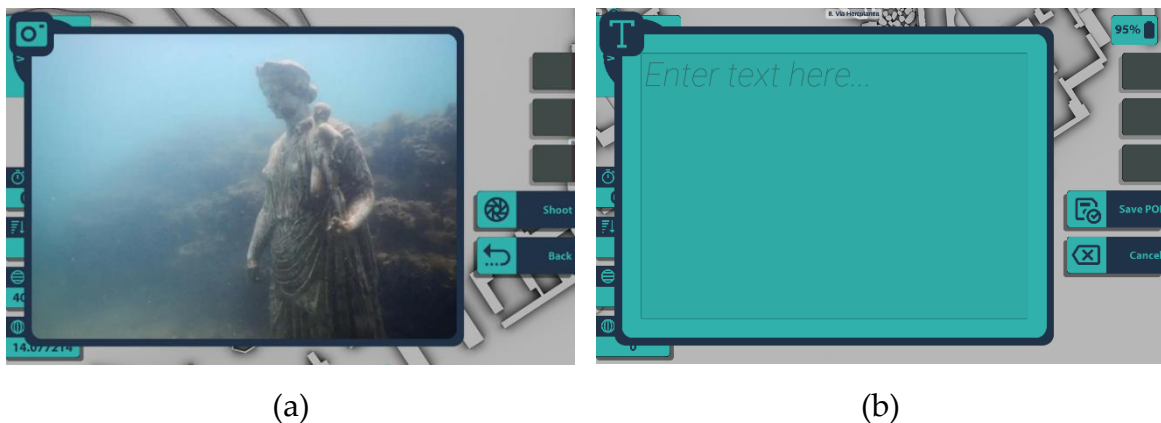


Figure 42. Acquisition of geo-localized photos (a) and textual notes (b) through the underwater tablet.

3.4.8 Messaging

Another feature of the underwater navigation system regards the possibility to exchange messages between the divers in the submerged environment and the surface operators. The messaging data are transmitted through an acoustic channel by the means of the acoustic localization system. This feature enables the diver to choose a predefined message to be sent to the surface (Figure 43a) and to visualize the history of the exchanged messages (Figure 43b).



Figure 43. Messaging feature. Sending a new message (a) and visualize the messaging history (b).

3.5 Conclusions

During this research work, the underwater tablet prototyped during the Visas project has been significantly improved both in terms of hardware and software. The waterproof case has been replaced with a more reliable and functional one, and the software has been redesigned to fit this new configuration. The LBL acoustic localization system has been substituted with two different positioning system based respectively on a USBL and an SBL configuration. These systems have been integrated with the tablet software while ensuring the possibility to employ also other acoustic localization systems with few software modifications.

Indeed, the underwater tablet has been provided with a new and totally redesigned software, namely Divy, that enables the diver to access different features. The UI is fully customizable and adaptable to different configurations in order to seamlessly switch between a scientific/professional application and a touristic application, due to the possibility to activate and deactivate the different features, changing the menus and the UI themes. The underwater tablet has been employed in different research projects and deployed in different underwater sites, due to its software capability to be adapted in each different situation. In some underwater site there is the possibility to activate the UWAR function, while in some projects there is the necessity to take advantage of the messaging function or to acquire textual notes. The acquisition of the geo-localized photos can be configured with the internal camera of the tablet or with an external high-definition camera. In conclusion, the Divy software has the capability to be adapted on the basis of the expertise of the user and the purpose of use.

4 Underwater Augmented Reality (UWAR)

4.1 Introduction

The Mediterranean Sea has a huge cultural and archaeological asset, consisting of ancient shipwrecks and sunken cities, with broad potential for the development of the tourism sector. Furthermore, the latest advances in the field of survey techniques for the exploration of the seabed is exponentially increasing the discovery of underwater cultural heritage (UCH) sites. Nevertheless, many of them are not accessible because of the limitations due to the environmental context, such as depth of the site and sea currents, or to local and international laws and regulations. Furthermore, those that can be visited by diver tourists present some issues related to the marine environmental conditions that do not permit a satisfactory exploitation of the underwater archaeological sites. Simultaneously, the UCH has provoked considerable interest thanks to the work carried out in the recent years by the National Commissions for UNESCO that discourages the adoption of the traditional excavation and recovery methods in favour of on-site examination and in situ preservation and conservation techniques.

To this end, computer graphics techniques like 3D reconstructions, Virtual Reality (VR) and Augmented Reality (AR), have demonstrated to be a highly effective means of communication for facilitating the access and increasing the value and the public awareness about the cultural heritage. In fact, in the last decades, a number of researchers are testing and perfecting reconstruction techniques and developing new technologies for the exploitation of the UCH [48,67,80–82]. Thanks to the advances achieved in the field of photogrammetric reconstruction techniques, it is now possible to make high-resolution and accurate 3D reconstruction of the underwater scene with low-cost technology and in a relatively short time [47,83–85].

Despite these achievements and significant progress made in the last years, VR- and AR-based applications for improving the diving experience in the underwater archaeological sites are still few, with many shortcomings to overcome and huge development potentials to unlock.

A good help for understanding the real extent of these potentials might be the fact that, due to water turbidity and biological colonization, in the submerged archaeological sites the divers often suffer from low visibility conditions and this leads to a less understanding of the underwater environment and a higher probability for them to miss the sense of direction. Unfortunately, GNSS sensors (GPS, GLONASS, and Galileo) are inadequate to this end since their signals are absorbed in water after a few centimetres below the sea level. Furthermore, guided or accompanied archaeological diving tours are carried out with experienced divers, but it is not possible to perform a fluid and direct communication unless they use full-face diving masks or analogous dedicated

equipment. At the moment, there are few attempts to support the divers by facilitating their comprehension of the archaeological context. One of these has been implemented in the underwater archaeological site of Punta Scifo, located in the East coast of Calabria at 10 km far from Crotona, where an underwater trail (Figure 44a), consisting of a guide rope and floating labels fixed at the margins of the archaeological remains, permits divers to know their position, identify artefacts and read the correspondent information printed on plastic slates (Figure 44b).

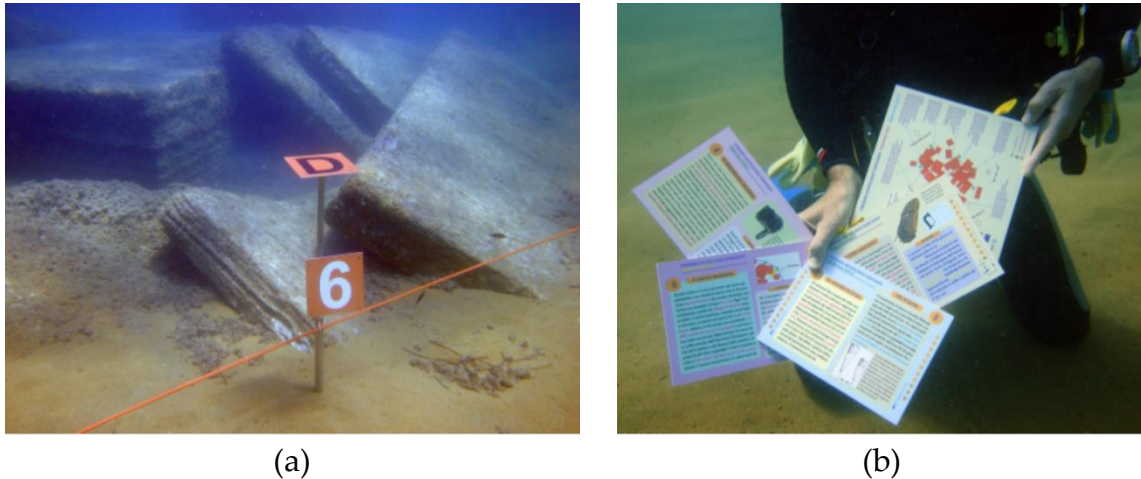


Figure 44. Underwater itinerary in the submerged archaeological site of Punta Scifo. (Images courtesy of the Marine Protected Area of “Capo Rizzuto”).

Another example can be found in Sicily where the Superintendence of the Sea has implemented, in seven underwater archaeological sites, interactive itineraries by identifying the archaeological remains through a small float with a Quick Response (QR) code label that allows divers to get access to the historical and archaeological information employing a handheld waterproof QR code scanner. There are then some fruitful examples, but they are fairly simple and still do not exploit the existing potentials.

On the basis of the abovementioned considerations, AR technologies could be a useful tool to overcome these limitations and could be a valid solution to improve the readability and understandability of the submerged archaeological sites and enhance the overall diving experience by providing interesting information about the ancient remains and artefacts.

In this regard, this chapter investigates the feasibility and potentials offered by the AR technologies for improving the diving experience in the underwater archaeological sites, and provides an overview of the UnderWater Augmented Reality (UWAR) feature, developed as a result of the present research work, in the context of the iMARECulture project. In particular, the Horizon 2020 iMARECulture (Advanced VR, iMmersive Serious Games and Augmented Reality as Tools to Raise Awareness and Access to European Underwater CULTURAL hEritage) project [43,45,48] aims to investigate and develop AR-based solutions for promoting and improving the public awareness about the UCH.

A hybrid tracking technique has been designed, that integrates acoustic localization and visual-inertial odometry, in order to perform an augmented visualization representing the actual conditions of the ancient ruins in the underwater site and a hypothetical 3D reconstruction of the archaeological remains as they appeared in the past of the Roman era by means of the underwater tablet described in the previous chapter.

This chapter is organized as follows. In Section 4.2 the state of the art is presented. The case-study adopted for the field tests is described in Section 4.3. Section 4.4-4.6 details the AR technologies developed and the field tests conducted in the iMARECulture project to improve the divers' experience in the submerged archaeological sites. Finally, Section 4.7 gives the conclusions of the chapter.

4.2 State of the art

AR technology has demonstrated to be a very useful tool for improving the visitor experience in cultural sites since it provides visual information contextualized with the environment and with the user point of view. Through the use of marker or location-based AR applications, tourists can orient themselves inside large areas, receive multimedia contents seamlessly, understand better the cultural value of what they are observing, visualize hypothetical reconstruction of monuments and objects to represent them as these appeared in the past. All these opportunities have been well exploited for the terrestrial cultural heritage while, up to now, the use of AR still remains completely unexplored in the context of the UCH.

In this context, in the last years, various researches are investigating and proposing different frameworks for the reconstruction, collection, and visualization of the UCH but for its exploitation outside of the underwater environment [80,81,86–88].

About Underwater Augmented Reality (UWAR) the first type of application was developed for military purpose in 1999 [89], it consists of an underwater head-mounted display (HMD) for Navy divers that allows augmenting the diver's view with virtual information in military operations, especially under poor visibility conditions. However, this is not an AR application in a strict sense, since the virtual information presented is not registered with the user's 3D perception of the real world.

A more sophisticated system, developed for edutainment purposes, was presented in 2009 [90], it consists of a UWAR system, based on optical square-markers, that provides visual aids to increase divers' capability to detect, perceive, and understand elements in underwater environments. A similar wearable waterproof system, but limited to a swimming pool environment, was developed in the same year by the Fraunhofer Institute for Applied Information Technology [91,92]. Another marker-based AR underwater device, that can be adopted in swimming pools, for aquatic leisure

activities is the Dolphyn system [93]. This system provides AR contents to the user through a tablet, housed in a waterproof case, that has been equipped with GPS and wireless systems. Body movement is restricted because it is necessary to interact with the equipment with both hands.

When compared to visibility conditions in swimming pools, the precision of computer vision algorithms is impaired by bad visibility conditions in the sea. An impact of such conditions on a set of open-source marker detection algorithms was measured in laboratory conditions [94], but fortunately, their performances can increase by using offline image enhancing algorithms [95] and real-time algorithms [96,97]. Registration of objects in images can also be improved for the purpose of underwater photogrammetry [31,98]. These works, however, focus only on specific parts of AR, namely on the detection and recognition of objects. To our knowledge, there is no work that would evaluate a complex underwater AR system in conditions of an open sea.

These efforts demonstrate a strong interest in the research community for the development of the UWAR since this technology could be applied to a large variety of sectors that operate in the marine environment. Nevertheless, as above mentioned, the progress made until now in this area is insufficient and their main limitation is due to the tracking capabilities of the systems adopted for the underwater environment. Indeed, algorithms that face the problem of underwater tracking have mainly been investigated in relation to underwater vehicles and robots [99,100]. Most of these solutions, based on a dead reckoning approach [101], are intended for the use in wide marine environments and are therefore focused on an approximate large distance tracking. Furthermore, these solutions are not able to accurately estimate the user's 6DOF pose and therefore to be used for accomplishing the correct alignment between virtual objects and real underwater world.

4.3 The case-study: the underwater archaeological park of Baiae

The UWAR technology developed in the iMARECulture project has been intended and tested for the Marine Protected Area - Underwater Archaeological Park of Baiae, located in the volcanic area of the Phlegrean Fields, a few kilometres North of Naples (Italy). This is a worldwide known site because it is a typical representative of the phenomenon of bradyseism as the rests of the Roman age are actually at a depth ranged from 0.0 m to 15.00 m from the sea level, and only a few ruins are still on the coastline, inland. The Underwater Park of Baiae (Figure 45) is famous also for its extensive submerged area of 176.600 hectares, and the wide range of different architectural structures, i.e., fisheries and harbour buildings, thermal baths, residential buildings, and villas, with some decorations that are still preserved. In particular, the experimentation has been undertaken in the complex of the "Villa con ingresso a protiro - Villa with Vestibule" dated to the first half of the II century AD.

The use scenario to which the UWAR technology developed in the iMARECulture project is intended consists in providing to the divers the possibility to know their position within the submerged environment and to enable the augmented visualization of the actual conditions of the ancient ruins in the underwater site and a hypothetical reconstruction of the villa, thus easily understanding the luxury and the importance of that building during the Roman era.

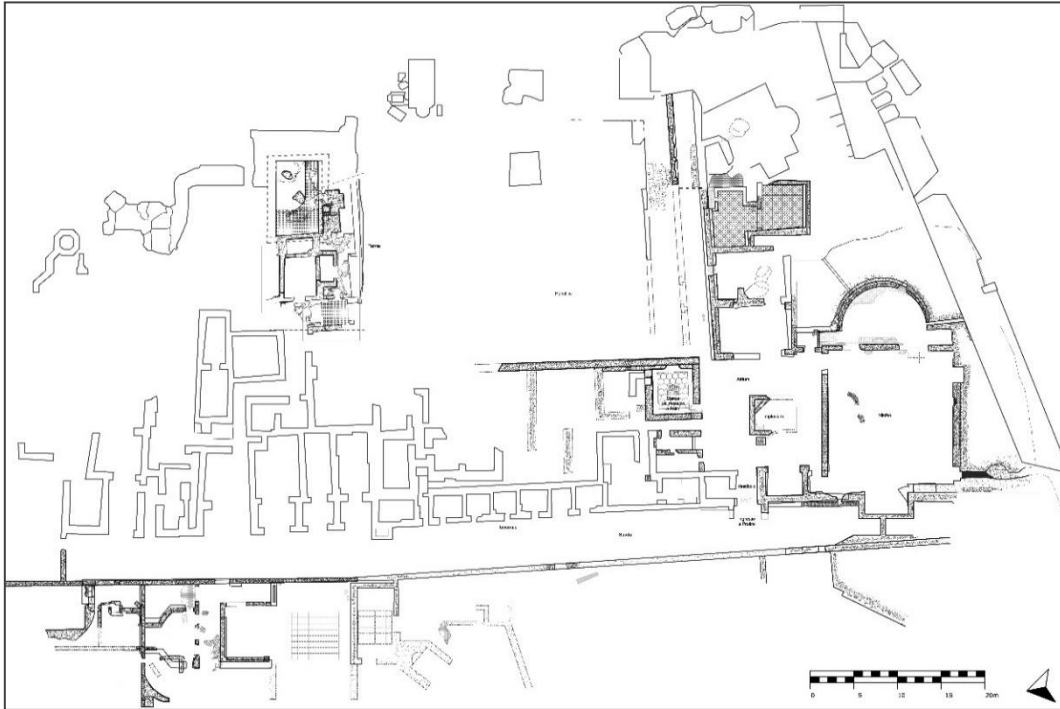


Figure 45. Planimetric archaeological map of “Villa con ingresso a protiro”. (Image courtesy of ISCR).

The starting point for preparing the 3D data and contents that are necessary for the functioning of the proposed UWAR technologies consists of the 3D reconstruction of the abovementioned archaeological area that has been carried out by combining optical and acoustic techniques [2,84]. The 3D reconstruction model is then populated with a number of points of interest (POIs), placed on the seafloor, which provide the position of the distinctive and characteristic elements of the specific underwater site. The POIs can be also represented with different colours depending on the category they belong to, e.g., yellow for the historical and archaeological artefacts and remains and green for biological organisms. Thanks to this data the underwater tablet provides to the user: a map of the underwater scene that allows the diver to know his/her position within the submerged site; archaeological, historical and biological information about the specific archaeological context; and an enhanced diving experience through an on-site augmented visualization representing the actual conditions of the ancient ruins in the underwater site and of a 3D hypothetical reconstruction of the “Villa con ingresso a protiro”.

About the 3D hypothetical reconstruction, this has been achieved by means of a theoretical and multidisciplinary scientific approach [102], under the direction of Barbara Davidde Petriaggi, that

exploits the high-resolution 3D data together with drawings and other historical and archaeological information to build a suggestive and consistent digital reconstruction of the underwater architectures not anymore existing. In particular, the reconstruction process starts with gathering historical documentation, scientific literature and geometric data (archaeological maps, illustrations, photos, Digital Terrain Model, etc.). All the data are then analysed and put in relation by the experts to generate and investigate different interpretation hypotheses that are validated by means of an iterative critical revision. The process, in fact, is based on interleaving a phase of technical reconstruction with a strong critical revision in order to generate a feedback process, iterating the construction /correction loop as much as needed. Finally, to map the evolution of the virtual interpretation, several 3D layers are saved together with the final model, examined and approved by the scientific experts. The following figure depicts the final 3D hypothetical reconstruction, as it appeared in the past, of two different rooms of the complex of “Villa con ingresso a protiro”, and in particular of the *atrium* with *impluvium* (Figure 46a) and the room with pelte mosaic (Figure 46b).

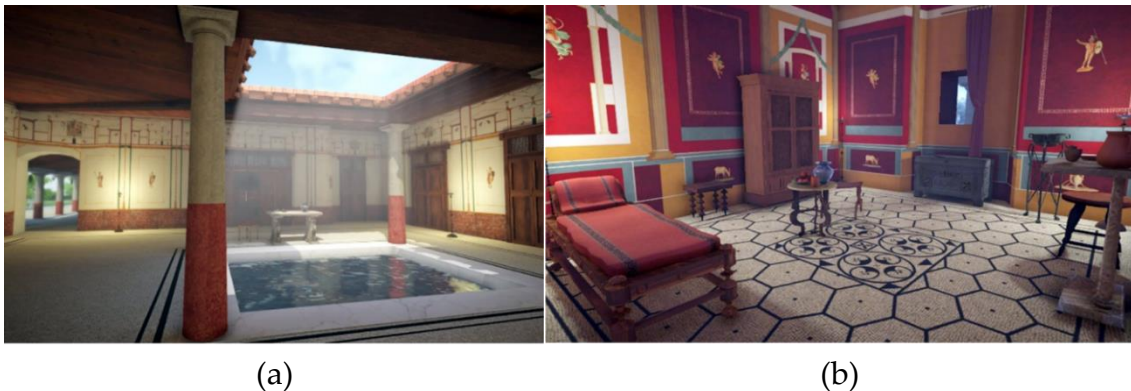


Figure 46. Different portions of the 3D hypothetical reconstruction of the Villa: atrium with impluvium (a), room with pelte mosaic (b).

4.4 UWAR implementation

The UWAR feature is provided to the user through the underwater tablet and navigation software described in Chapter 3. The Augmented Reality (AR) within the underwater navigation is intended to provide the diver with a new and more immersive experience compared to a classic recreational dive. The AR allows the diver to view the hypothetical reconstruction of the structures and artefacts that are superimposed on the present status of the underwater archaeological site. As described in the previous chapter, the Five Buttons UI provides a button (Figure 47) to allow the user to switch between the visualization representing the actual conditions of the ancient ruins in the underwater site (Figure 47) and the hypothetical 3D reconstruction of how the site appeared in the past (Figure 49) during the Roman era. For the sake of clarity, the AR button has been highlighted in Figure 47; the label “Present” suggests to the user that he is visualizing the actual state of the underwater site.

Once the user pushes this button, the concerning label switches its text to “Past” indicating that the user is visualizing the hypothetical reconstruction of how probably the site looked in the past. The diver can choose the type of visualization between the top-view (Figure 48) and the first-person view (Figure 49). The top-view is especially suitable to orientate in the underwater environment whereas the first-person allows to fully enjoy the AR view modality. While in AR modality and first-person view, the user can move around the tablet, rolling and pitching, in order to change the point-of-view of the camera (Figure 49).

It is worth noting that, as depicted in Figure 49, the augmented virtual models are not superimposed on the frames captured by the tablet camera as would be expected in a classical AR. This choice was due to the low picture quality obtainable in the majority of the underwater sites such as the Underwater Archaeological Park of Baiae. In fact, the imagery produced in this kind of environment suffers from a lack of contrast and poor visibility due to the particles suspended in the water.

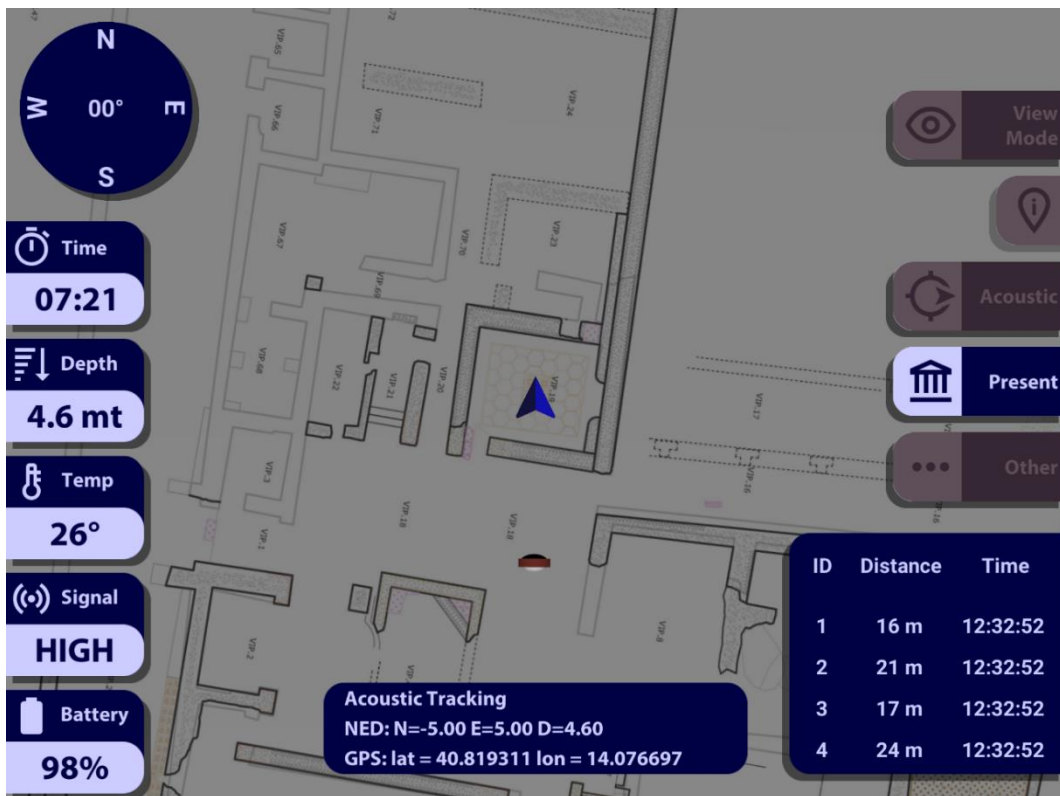


Figure 47. The button to switch the AR status.

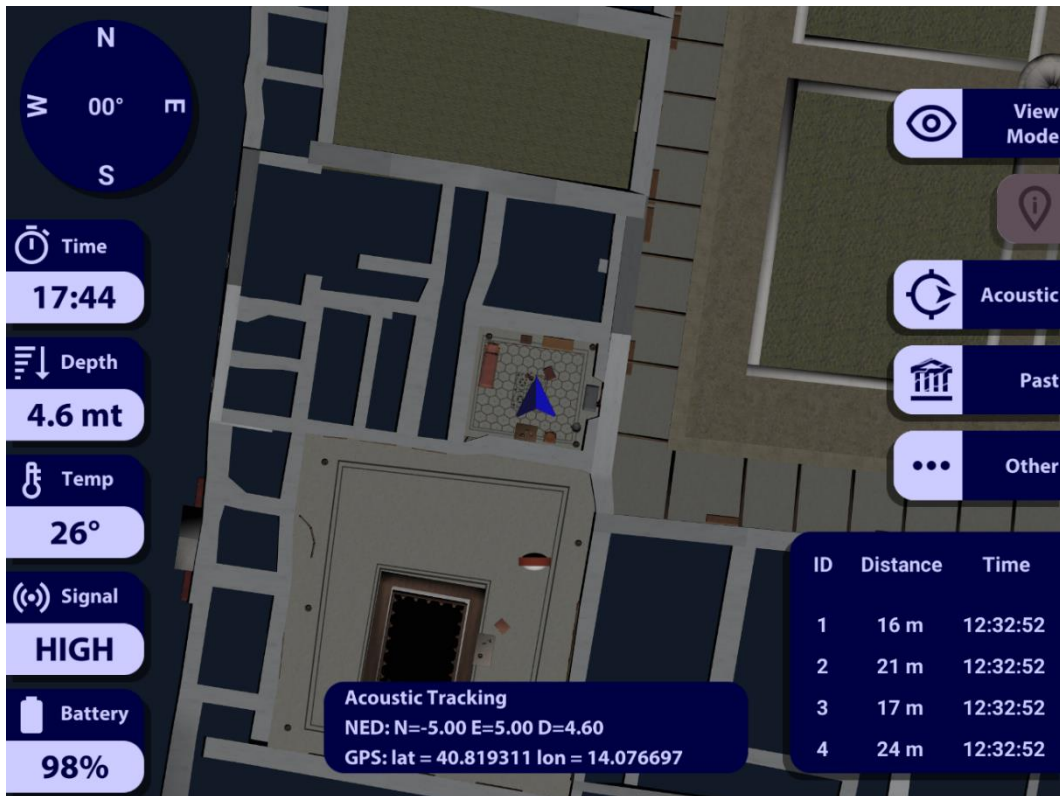


Figure 48. Top View of the hypothetical reconstruction.



Figure 49. First Person View of the hypothetical reconstruction.

4.5 Hybrid Tracking

The information about the diver localization has to be provided to the system with high precision and at a high update rate to deliver a consistent and smooth AR visualization. Unfortunately, the acoustic localization systems suffer from low update rate and low accuracy, and cannot be employed alone for the AR purpose. In fact, the update rate of the acoustic localization system is too low to deliver a seamless AR experience due to the long delay between two subsequent positions provided by this system. Furthermore, whatever acoustic positioning system suffers from packet loss that further compromises the rate and, therefore, the quality of the acoustic positioning. The acoustic communication is also degraded by the presence of the diver that during the immersion can frequently place itself between the acoustic transducer integrated with the tablet and the one on the sea surface. This increments the packet loss issue and decreases the update rate so that even an acoustic positioning system with a formal higher update rate cannot overcome the delay between two subsequent positions.

To overcome these limitations and improve the performance of the proposed UWAR technology, a hybrid tracking system has been specifically developed [103] by integrating acoustic localization and Visual-Inertial Odometry (VIO) to enable a consistently high frame rate and improve the performance of the proposed underwater AR technology. The hybrid tracking system merges positioning data, generated by the acoustic system, with data coming from a commercial VIO framework. In particular, given the low update rate of the acoustic system, a strategy has been implemented aimed to fill the gaps between two consecutive acoustic positioning data.

The developed hybrid tracking system's architecture is shown in Figure 50. As abovementioned, it is composed of two main sub-components: an acoustic positioning system and a VIO framework that is meant to bridge the gap between two consecutive acoustic positions.

As depicted in Figure 50, the acoustic positioning system does not rely only on acoustic measurements, but also on a depth gauge, GPS and IMU sensors in order to compute the absolute position of the diver. Obviously, due to the limitations of GPS, this sensor is placed outside of the underwater environment. At the same time, the VIO framework combines data from the camera and the inertial platform of the tablet to calculate the absolute orientation and relative position with respect to the starting point. In particular, the VIO framework recognizes notable features in the scene, tracks differences in the positions of those features across video frames, and compares that information with motion sensing data. The result is a model of the device's location and motion.

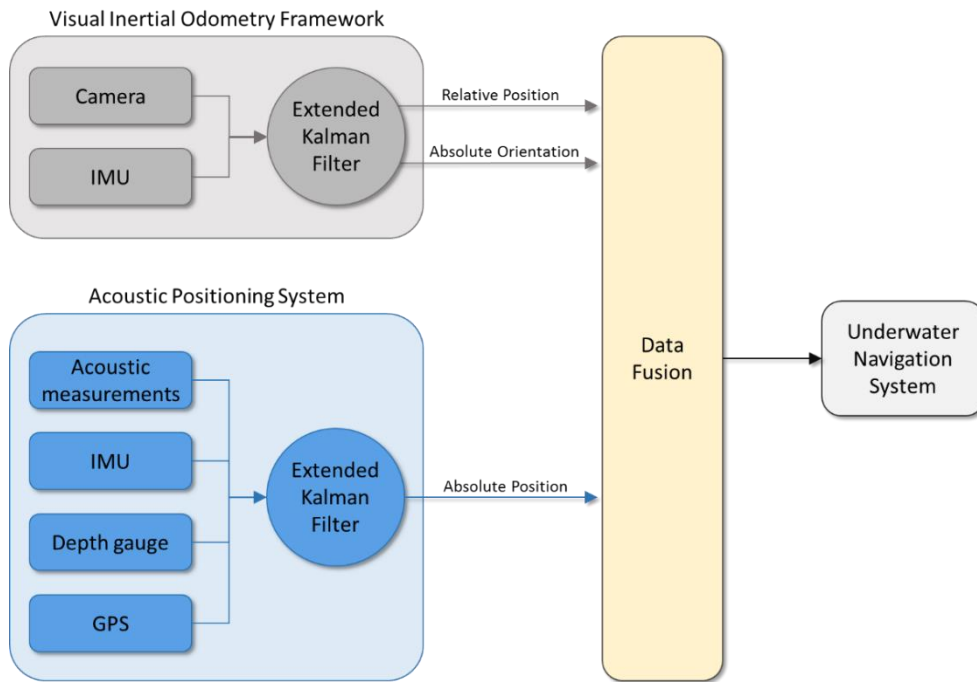


Figure 50. Hybrid tracking system's architecture.

About the fusion of the different typology of data, it has been employed a strategy that consists of using the acoustic positioning data as an initial reference point for the VIO framework that, as previously stated, delivers only local positioning data with respect to a starting point. Whenever a new acoustic positioning data is available, the VIO framework is reset and its reference point is moved to the new acoustic positioning data, while the hybrid tracking system relies only on this acoustic data for the localisation. Until no new acoustic positioning data is available, the hybrid tracking relies on the VIO in order to calculate the actual position. By fusing the data provided by these two positioning systems through the strategy previously described, it is possible to fill the gap between two consecutive acoustic positions.

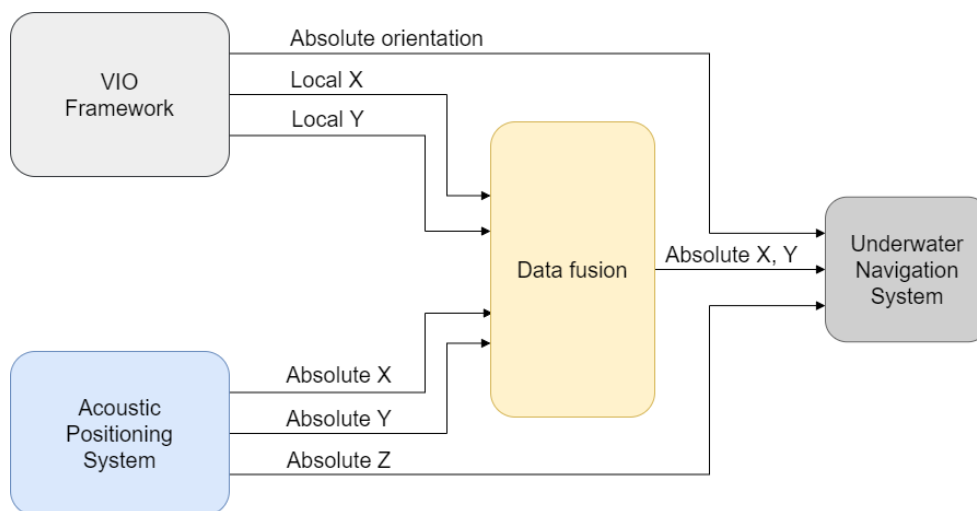


Figure 51. Deepening on the architecture of the hybrid tracking system.

Figure 51 shows in more detail as the different positioning data are fused in the hybrid system. The absolute orientation is provided exclusively by the VIO framework, while the “Z” coordinate, i.e., the depth, is computed by the means of only the pressure sensor integrated with the acoustic system. No acoustic signal is employed to acquire information about the current depth. The “X” and “Y” coordinates are computed by the data fusion of the two positioning systems.

4.5.1 Field test

A field test of the hybrid tracking system, aimed to estimate its performances, has been carried out in the shallow water of the underwater archaeological site of Baiae. The ARKit framework was employed for the visual tracking, while the SeaTrac USBL, manufactured by Blueprint Subsea, was used for the acoustic tracking. The manufacturer declares that this USBL system has an acoustic range of 1km and a range resolution of ± 50 mm. No information about the update-rate and the accuracy of this acoustic system has been released.

This underwater test has been designed to evaluate the capability of the hybrid tracking system to bridge the gap between the calculation of two consecutive acoustic positions. Moving around the underwater site, the estimated position of the framework was compared to a ground-truth (pre-defined know points in a path). The protocol developed for the execution of the test consists of the following six steps:

1. Construction of the underwater ground-truth. It was necessary to compare the collected positioning data with a known path in order to evaluate the performance of the hybrid tracking system. The path is square-shaped (Figure 52a), with edges marked with labelled panels (A, B, C, and D), and sides traced with graduate ropes.
2. Calibration of the acoustic localization system carried-out on the boat.
3. Deployment of the acoustic positioning system in the sea. Usually, the USBL acoustic positioning method involves measuring the range from a vessel, on which the USBL’s transceiver is placed, to a single subsea transponder. Then, the overall positioning error is affected by the positioning error of the ship’s GPS and the positioning error of the transponder relative to the ship’s position. To cancel the effect of the GPS’s error, the local beacon of the USBL system has been placed on the vertex A (Figure 52a) at an approximate distance of 3 meters above the seabed.
4. Measurement of the depth of the local beacon.
5. Annotation of the actual size of the square and its deviations respect to the planned ground-truth. This step is important for having a precise reference for the comparison and evaluation of the data measured during the test.
6. Run the test by starting the navigation software when the diver is on the vertex A. Then the diver performs a complete counterclockwise lap of the squared ground-truth, passing

through the B, C, D vertices, and ending on the starting vertex. The test is carried at a constant depth of about 6 meters deep below sea level.

The navigation software has been modified to automatically save the acoustic, optical and sensor data, measured during the test, into a log file for their next analysis and evaluation.

The real ground-truth built in the underwater site was slightly different from a square-shaped path because of the difficulties encountered in the underwater environment. The actual dimensions reported at the end of its deployment were: $|AB| = 30m$, $|CD| = 30m$, $|AD| = 29.26m$, $|BD| = 43.3m$, and $|AC| = 41m$. Moreover, the AC side was tilted about 11 degrees with respect to the north direction.

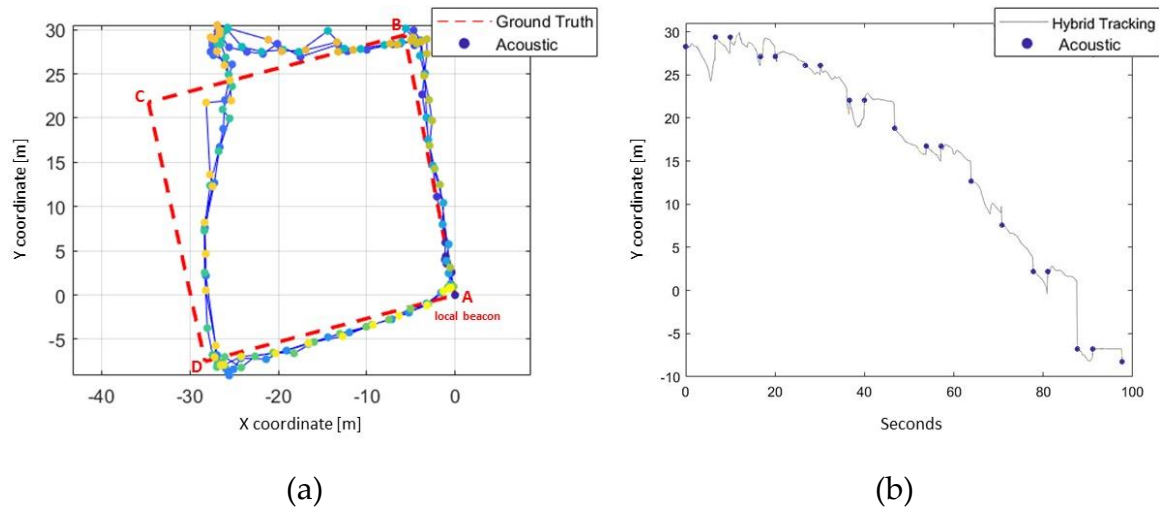


Figure 52. Acoustic data acquired moving along the ground-truth (a), and comparison of acoustic and data tracked according to hybrid approach (b).

Figure 52 shows the result of the test. In particular, Figure 52a depicts the empirical acoustic data acquired during three consecutive counterclockwise laps of the planned ground-truth. The ground-truth is represented with a dotted red line, while the acoustic data are represented in time progression through a scatter colour that goes from violet (start) to yellow (end of the experiment). The blue lines represent the connections between two consecutive acoustic data. The results show that on the upper left edge (edge C in Figure 52a) of the squared ground-truth the error of the acoustic data exceeds 5 meters and this is too much for performing an acceptable augmented reality visualization. Since this error appears in all the three laps it is probably due to multipath propagation which becomes even more evident in the case of shallow waters. As a consequence, this test has pointed out that USBL systems are not adequate to perform the proposed application of UWAR in shallow waters. In fact, as shown in Figure 52a, the USBL works quite well along the planned ground-truth except for some points that make the acoustic positioning system unstable. Nevertheless, an interesting outcome of the hybrid tracking test is depicted in Figure 52b in which the improvement of the tracking becomes evident thanks to the adoption of the VIO. In particular, this figure plots the distance-time graph of

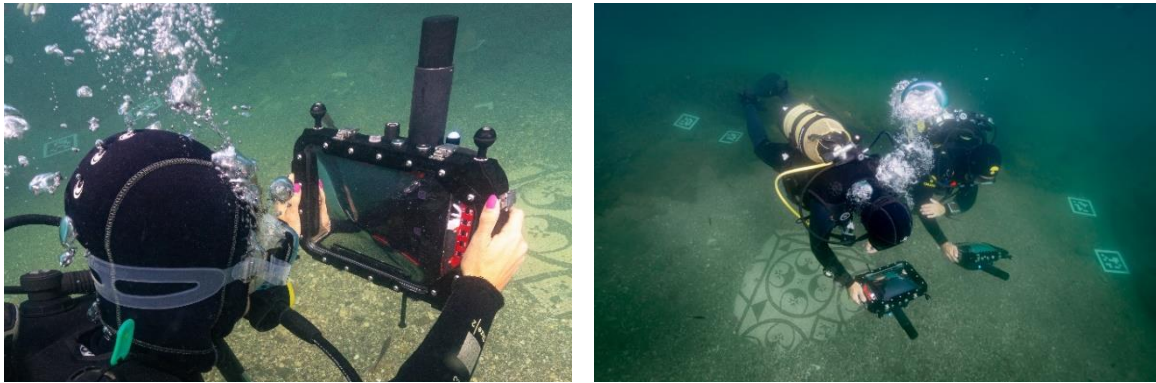
only the “Y” coordinate of the CD segment (Figure 52a) in order to better highlight the impact of the VIO on the tracking of the diver’ position. In particular, the graph shows the acoustic positioning data, acquired by means of the SeaTrac that has a low update rate of approximately 0.2 Hz, and the hybrid tracking data that, thanks to the VIO framework which has an update rate up to 60 Hz, provides a graphical continuity to the path. This continuity is good in some cases (from 28 to 34 seconds, 47-55, 70-77 and 80-88) and not always satisfactory in others (from 37 to 40 seconds, 55-58 and 77-80). However, these results are encouraging and demonstrate that it is then possible to perform a consistent and smooth UWAR visualization by increasing the update rate from the 0.2 Hz of the acoustic positioning system alone up to the 60 Hz of the hybrid tracking system.

4.6 Users evaluation

In order to validate the system, it has been evaluated by ten divers in experiments analysing their perception and remembrance, interests, and user experience (Figure 53). Although past research has been done for virtual scenes on land [104], to our knowledge, this is the first perception study performed in underwater conditions [105]. The system has been deployed on the site of submerged ancient roman *Villa con ingresso a protiro* in Baiae, Italy. The 3D hypothetical reconstruction of this Villa has been achieved under the direction of Barbara Davidde Petriaggi by the 3D Research as described in [102].

After the work presented in [103] and the test described in the previous section, the acoustic localization system has been substituted with a Short Base-Line (SBL) positioning system provided by AppliCon Srl. [77]. This acoustic localization system has been deployed on the underwater site before the test. During the test, three tablets were available to be used simultaneously by three different users. The Divy system has been explained to the users before the dive and each of them had the opportunity to interact with the tablet for a couple of minutes to explore the different features and become familiar with the user interface. Due to the nature of underwater AR application, that was designed to help divers to freely explore the surrounding area getting information on their position and the interesting spots of the site, no precise tasks have been assigned to users. The test has been carried out in this way to evaluate the system in the most common use case: tourist divers exploring an underwater archaeological site. Each of them tested the system freely and without limitations for about fifteen minutes. The only indication they received was to test both the main visualization modalities that the system deliver to the user: the top view visualization of the map that enables the users to locate themselves in the underwater sites quickly and the first-person AR visualization that allows them to observe the hypothetical reconstruction of the Villa. They could focus on the spots that they felt more interesting with the possibility to visualize also additional textual information related to some POIs. This test also enabled us to investigate how comfortable it

is for a diver to bring with him such a big system composed by the tablet and the acoustic modem. The underwater site was perfect for this kind of test because of the low visibility that forced the divers to use the tablet to locate themselves to understand what they were observing. Even with low visibility, the shallow depth of 5 meters and constant observation of the users by the organizers of the tests have guaranteed the maximum safety of the operations.



(a)

(b)

Figure 53. Divers testing the UWAR feature through the underwater tablet.

After the diving sessions, the participants were asked to provide personal feedback and fill two questionnaires about their experience. The first consisted of the following fifteen questions selected from a questionnaire designed by Tcha-Tokey et al. [106]:

1. My interactions with the augmented environment seemed natural.
2. The visual aspects of the augmented environment involved me.
3. I could actively survey the augmented environment using vision.
4. I could examine objects closely.
5. I was involved in the augmented environment experience.
6. I felt stimulated by the augmented environment.
7. I become so involved in the augmented environment that I was not aware of things happening around me.
8. I become so involved in the augmented environment that I lose all track of time.
9. I felt I was experiencing an exciting moment.
10. I enjoyed being in this augmented environment.
11. I felt nervous in the augmented environment.
12. Personally, I would say the augmented environment is practical.
13. Personally, I would say the augmented environment is confusing.
14. I found that this augmented environment is likeable.
15. I suffered from fatigue during my interaction with the augmented environment.

They also filled the NASA TLX questionnaire [107] inquiring the following questions:

1. Mental Demand: How mentally demanding was the task?
2. Physical Demand: How physically demanding was the task?
3. Temporal Demand: How hurried or rushed was the pace of the task?
4. Performance: How successful were you in accomplishing what you were asked to do?
5. Effort: How hard did you have to work to accomplish your level of performance?
6. Frustration: How insecure, discouraged, irritated, stressed, and annoyed were you?

The divers filled these questionnaires once they returned to the diving centre. The results are reported in Figure 54, Table 18 and Table 19.

Table 18 shows the answers to the selected fifteen questions of the Tcha-Tokey questionnaire. The participants found the interaction natural, the visual aspects involved them, they could actively survey the environment and examine the objects closely, they were involved in the experience, felt stimulated, enjoyed being in the environment, and found the environment practical and likeable. The users did not feel nervous, did not find the environment confusing, and did not suffer from fatigue. They did not clearly state that they would become so involved in the environment that they were not aware of things happening around them or lose track of time. This is a positive outcome, since the divers should be only partially involved in the environment because they must be constantly aware of things happening around them. Table 19 shows excellent results in all aspects of the NASA TLX questionnaire. In terms of the qualitative feedback, the divers found the system to be practical, engaging, and a useful tool for diving and archaeology, and they enjoyed the experience. The navigation software was valued for its ability to localize the diver within the underwater site and for the opportunity to switch between viewing modes, but many divers complained about occasional inaccuracies in diver's position. They also criticized the reflections of the sun on the screen of the tablet, which occur mostly in shallow depths of the sea and disappear as the diver descent deeper; this feedback led the producer of the EasyDive waterproof case [76] to modify the screen shape in order to reduce this problem. One user noted that the hardware is not designed well for left-handed people, one found the tablet bulky, but another one mentioned it is easy to use. In general, the divers were especially excited and suggested many more features to add, like a preview of locations, more information about POIs, a sound, a checklist of POIs, an ability to take pictures in the AR environment. The underwater tablet was easy to handle even for divers with the first level diving certificate because its weight in water is almost zero due to buoyancy.

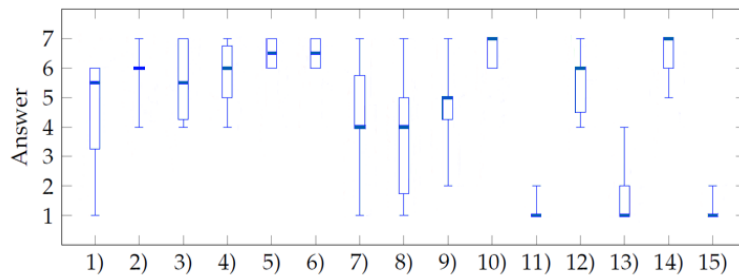
Table 18. Feedback of participants to the user experience; the full text of the questions is reported above.

Question	Average	Standard deviation
My interactions (...)	4.5	1.900
The visual aspects (...)	6.0	0.816
I could actively (...) vision.	5.6	1.350

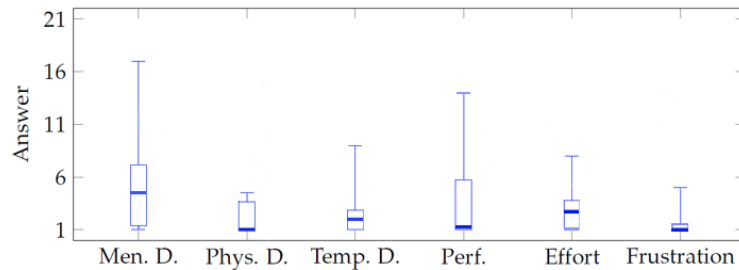
I could examine objects closely.	5.7	1.160
I was involved (...)	6.5	0.527
I felt stimulated (...)	6.5	0.527
(...) things happening around me.	4.3	2.111
(...) I lose all track of time.	3.8	2.150
(...) exciting moment.	4.8	1.317
I enjoyed (...)	6.6	0.516
I felt nervous (...)	1.2	0.422
(...) environment is practical.	5.6	1.174
(...) environment is confusing.	1.6	0.966
(...) environment is likeable.	6.5	0.707
I suffered from fatigue (...)	1.2	0.422

Table 19. Feedback obtained with the NASA TLX questionnaire, lower is better.

Aspect	Average	Standard deviation
Mental Demand	5.5	5.044
Physical Demand	2.1	1.506
Temporal Demand	2.7	2.486
Performance	4.0	4.428
Effort	3.0	2.224
Frustration	1.9	1.647



(a)



(b)

Figure 54. Two graphics about the results of the questionnaires. (a) Tcha-Tokey questionnaire; (b) NASA TLX questionnaire, lower is better.

4.7 Conclusions

A novel UWAR technology has been presented that can improve the divers' experience in submerged archaeological sites. In particular, the proposed technology, developed in the H-2020 funded iMARECulture project, provides to divers, through the interaction with a tablet-based system, their position over the 3D map of the underwater archaeological site, a visualization representing the actual conditions of the ancient ruins in the underwater site and an augmented visualization representing a hypothetical 3D reconstruction of the archaeological remains as they appeared in the past during the Roman era.

A field test has been conducted in the Underwater Archaeological Park of Baiae to assess the feasibility and practical potentials of the proof of concept of the developed UWAR technologies. In particular, the field test made it possible to confirm the proper functioning of the adopted visual tracking techniques in the underwater environment notwithstanding the negative effects of the water turbidity and refraction that occurs at the air-glass-water boundary.

It is worth noticing that since the overall positioning error mainly depends on the underwater acoustic localization system the added value of the developed hybrid approach lies in its capability to interpolate two consecutive acoustic positioning data through VIO tracking techniques in a sufficiently accurate way to perform a consistent and smooth AR visualization.

Finally, the UWAR feature has been successfully evaluated at an underwater cultural heritage site. Ten divers participated in a study that evaluated their perception of virtual objects underwater and user experience. The study showed that divers noticed details about large and more exposed objects and were less aware of details about objects located at the walls of the virtual room. They also enjoyed their time and claimed that the technology had great potential in underwater archaeology and tourism.

5 Underwater Path Planning

The path planning is an aspect of the present research work that has been developed as a part of the MOLUX project. The general purpose of the MOLUX project is the design, development, and testing of an innovative system for supporting divers engaged in environmental monitoring activities, biological or archaeological documentation, bathymetric survey, search and recovery of objects or in judicial police investigations. This system aims to increase the efficiency and safety of underwater operations by allowing the diver to know, at any time, his position within the underwater environment, to acquire geolocated data (such as images, videos, notes, environmental parameters), and to optimize and monitor the path to follow for the execution of the mission.

In this context, a part of the present research work was focused on the development of a novel approach to dive planning based on an original underwater pathfinding algorithm that computes the best 3D path to follow during the dive in order to be able to maximise the number of Points of Interest (POI) visited, while taking into account the safety limitations. This research work has been presented in [108] and proposes, for the first time, to consider the morphology of the 3D space in which the dive takes place to compute the best path, taking into account the decompression limits and avoiding the obstacles through the analysis of a 3D map of the site.

5.1 Introduction

Underwater archaeologists, biologists, and even law enforcement agents are often committed to survey underwater sites for accomplishing a variety of missions that may include the search and recovery of lost items, visual census of benthic species, documentation of cultural assets, etc.

Unfortunately, the underwater environment is unfamiliar and hazardous for humans, so that specific procedures and rules have been defined to ensure the divers' safety. Most of the safety procedures are intended to reduce the risk of drowning, while others aim to reduce the risk of decompression sickness. In some contexts, getting lost is a serious hazard, and specific procedures to minimise this kind of risk have to be followed.

Dive planning is the process of planning the underwater diving operations ahead, aiming to increase the probability that a dive will be safely completed and the goals achieved [109]. The complexity and the details considered in dive planning may vary enormously, but some kind of planning is required for most underwater dives. The purpose of dive planning is to ensure that divers do not exceed their comfort zone and skill level or the safe capacity of their equipment. It includes scuba gas planning to ensure that the amount of breathing gas loaded in the tank is sufficient to complete the diving safely, taking into account any reasonably foreseeable contingencies.

During the ascent, the depressurisation leads the inert gases dissolved in the tissues to come out of the solution, eventually forming bubbles inside the body if the ascent is too fast. This could lead to a condition known as decompression sickness. The risk to contract this disease can be effectively managed through proper decompression procedures, and, therefore, its prevalence has been greatly reduced. Given its potential severity, much research has been dedicated to its prevention, and divers almost universally use dive tables or dive computers to limit their exposure and control their ascent speed.

The activities planned ahead by the diver could require more time than expected. In such a case, a diver could experience difficulties, or at least spend some time, to accurately evaluate during the diving if he/she has enough time to reach all the planned points of interest (POIs). To conduct such an evaluation, he/she should be able to evaluate the distance between all the POIs and the time needed to reach and explore them, taking into account the air still available in the scuba tank and the decompression stops needed at the end of the dive. It would be necessary to employ a system able to calculate the best available path that enables the diver to visit the greatest number of POIs, taking into account all the constraints imposed by the underwater environment. At present, dive computers provide information about the diving and calculate the decompression stops, but they are not capable of performing advanced evaluations as the ones described before.

Many different tools are available for planning a future dive. MultiDeco [110] is a decompression program for PC, Mac, Android, iPad, and iPhone. It uses the varying permeability model (VPM-B) and the Bühlmann model (ZHL-16) for computing the decompression profiles. It provides different settings that allow for customising deep and safety stops, stop times, and air breaks. Subsurface [111] is an open-source dive-log program for recreational, tech, and free divers that runs on Windows, Mac, and Linux Subsurface. It can plan and track single-tank and multi-tank dives using air, Nitrox, or Trimix. It supports a wide range of dive computers and can also import existing dive logs from several sources. Diveroid [112] consists of an underwater case equipped with a small dive computer and an app that turns the phone in an underwater camera, simultaneously showing the information on the dive, like pressure, no-decompression limit, and times. DecoTengu [113] is a Python dive decompression library that allows for various implementations of the Bühlmann decompression model with Erik Baker's gradient factors. The results of the DecoTengu calculations are decompression stops and tissue saturation information that can be used by third-party applications for data analysis or dive planning.

Artificial intelligence has investigated search methods for solving pathfinding and path-planning problems in large domains. Path planning is integral and crucial to various fields, including robotics and videogame design [114,115]. The classic problem of determining the shortest path in a cluttered environment has been one of the main objectives for many research efforts over the years.

Dijkstra [116] proposed an algorithm to address the shortest path problem. Hart [117] used a heuristic function to estimate the cost of the path from a starting point to a given destination. The Dijkstra algorithm is combined with this heuristic function to form a new node-searching strategy known as the A* algorithm. The heuristic function can increase the efficiency of the Dijkstra algorithm by pruning the search space in maps. The A* algorithm uses heuristic knowledge in the form of approximations of the goal distances to focus the search and find the shortest paths for path-planning problems in a potentially faster way with respect to uninformed search methods.

In this research work, the proposed underwater pathfinding algorithm computes the best path, avoiding the obstacles in the site (by analysing a 3D map of the site) and taking into account the limitations of decompression. To the best of our knowledge, approaches similar to ours do not yet exist in the literature.

Currently, there are some works in which algorithms such as A* are applied in the search of paths for autonomous vehicles. For instance, in [118], path planning for unmanned surface vehicles (USVs) and an implementation of path planning in a real map are discussed. In particular, in this paper, satellite thermal images are converted into binary images and are used as the maps for the finite angle A* algorithm (FAA*). To plan a collision-free path, the algorithm considers the dimensions of surface vehicles and their turning ability. In [119], a 3D path planning of an autonomous underwater vehicle (AUV) is proposed by using the hierarchical deep Q network (HDQN) combined with the prioritised experience replay. In [120] and [121], reinforcement learning techniques are proposed in order to allow UAVs to navigate in unknown environments.

In [122], path planning and the resulting control problems of autonomous underwater vehicles (AUV) in three dimensions (3D) are studied. For obstacle avoidance and path optimisation, a path-planning method based on particle swarm optimisation (PSO) and cubic spline interpolation is proposed. The control strategy discussed in this paper is compared with the line-of-sight (LOS) guidance through a simulation experiment.

In [123], a study of the optimal three-dimensional headings of AUVs is presented, with the goal of reaching a given destination in the least amount of time from a known initial position. The authors employ the exact differential equations for time-optimal path planning and develop theoretical and numerical schemes to predict three-dimensional optimal paths for several classes of marine vehicles, taking into account their specific propulsion constraints.

In [124], LPA*, an incremental version of A*, is proposed, combining ideas from the artificial intelligence and the algorithms literature. It repeatedly finds the shortest paths from a given start vertex to a given goal vertex, while the edge costs of a graph change or vertices are added or deleted. Its first search is the same as that of a version of A* that breaks ties in favour of vertices with smaller

g-values, but many of the subsequent searches are potentially faster, because it reuses those parts of the previous search tree that are identical to the new one.

The system described in [125] proposes the use of an omnidirectional ASV with the ability to follow the diver and act as a private satellite in order to increase diver's safety and to enable monitoring from the surface. It is one of the few underwater systems of diving assistance, but it does not offer any kind of path planning to support the diver. The technical contribution of this work consists mainly in the development of a diver-tracking system composed of an autonomous surface marine vehicle and an underwater diver interface used for two-way communication between the diver and the surface vehicle.

The present search work introduces a novel system that can support divers during their underwater surveying activities, computing the optimal path to follow in order to maximise the number of points of interest that can be reached and explored during the dive, while taking into account several safety factors. This work proposes, for the first time, to consider the 3D space in which the survey dive takes place in order to adapt the path planning to the obstacles in the environment. The system is based on a novel underwater pathfinding algorithm that computes the best path while taking into account the decompression limits and avoiding the obstacles by analysing a 3D map of the site.

This original approach can be employed in two different scenarios: before the dive, when estimating a planning of the underwater activities and—an even more challenging scenario—during the dive, when the path needs to be adapted to unexpected situations and the time available for completing the dive. In the latter case, the system enables the diver to know constantly the best path that maximises the number of visited POIs and minimises the cost of the path. The latter, in an underwater environment, can be defined in different ways. This information can be provided to the diver through an underwater tablet, such as the one presented in Chapter 3, housed in a waterproof case and coupled with an acoustic localisation system. This tablet is provided with a dedicated app that enables the diver to access different features, such as the visualisation of a 3D map of the underwater site, the geo-position of the diver, a set of POIs, and a predefined path for the visit. The proposed system allows for extending the functionalities of the underwater tablet to provide an online optimal path planning while taking into account the diving safety conditions.

5.2 Materials and Methods

The proposed pathfinding algorithm is composed of different stages, each addressing a different problem. The first step is a preprocessing stage—namely, the space partitioning, in which the 3D model of the underwater environment is analysed and represented in a way that is simpler to be processed by a search algorithm. Subsequently, the process of searching the best path to visit a set of

points of interest can be divided into two phases. In the first phase, all the best paths between each couple of POIs are generated (links generation). In the second phase, the best sequence to visit the major number of POIs is defined, aiming to minimise the cost of the visit (path optimisation). In both phases, the cost of the underwater movements was assessed with different strategies, where each of them determines the choice of a different best path. In order to take into account the aspects that are inherent to the underwater environment, in this last phase, the search algorithm relies on an external API (application programming interface)—namely, the DecoAPI, which records the history of the dive and evaluates the actual state of the diver parameters related to the dive. This API was developed separately from the pathfinding algorithm, and it implements the Bühlmann model ZH-16LC [126,127] extended with a gradient factor [128] to track and compute the decompression profile of the diver.

All stages of the pathfinding algorithm are represented in Figure 55 and described in more detail in the following sections.

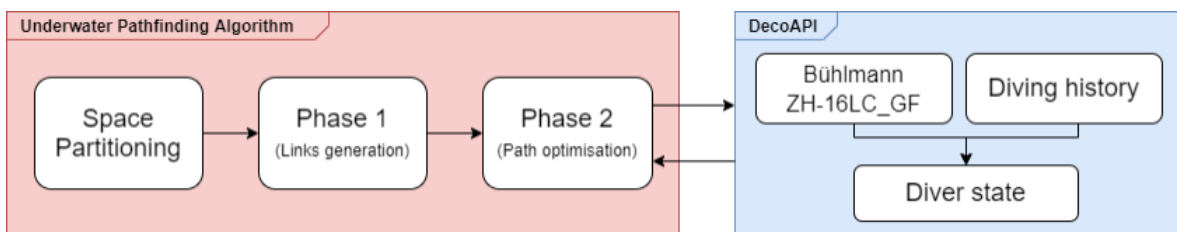


Figure 55. The stages of the pathfinding algorithm and communication with DecoAPI.

5.2.1 Space Partitioning

The space partitioning is the process of dividing a space into nonoverlapping regions so that any point in the space can be associated with a single specific region. Representing a geometrical space in such a way can simplify different kinds of geometry queries, e.g., determining whether a ray intersects an object. Space partitioning is often used in 2D/3D path planning. In this case, the adjacent regions are connected to each other by modelling a graph, so the process of searching for the shortest path can be performed by the means of algorithms that operate in a graph.

For this purpose, it is very useful to divide the space into regions and to label the ones that correspond to the “water” and the ones matching the “terrain”, with the aim of discerning between the areas of the underwater site that the diver can pass through and the obstacles he/she has to avoid. In particular, the space is partitioned into voxels with shapes of equal size cubes (namely, one metre), forming a 3D grid. The exact dimension of the voxel was chosen in relation to the approximate dimension of a diver. Indeed, a voxel not bigger than the diver is enough to represent the underwater environment with sufficient accuracy. Even though it can produce a better approximation of the 3D map, a too-small voxel could be counterproductive. In fact, an undersized voxel could lead to paths

that go through narrow passages where the diver should not and could not dive through. Moreover, it is worth noting that the size of the voxel directly affects the algorithm performance, because the smaller the voxel, the larger the total number of voxels that composes the 3D grid, and the computational cost of the search algorithm employed in phase 1 depends on the number of voxels involved in the search.

5.2.2 Phase 1 (Links Generation): Calculating Optimal Links between Pairs of POIs

In phase one, a graph was defined, where each node represents a “water” voxel of the 3D grid, i.e., a region that is accessible to the diver. Each voxel is connected to its neighbours, which are the adjacent voxels. The weight of the edges, connecting each node of the graph with its neighbours, depends on the strategy by which the cost of the underwater movements is defined. Given this graph, the problem that needs to be solved is the generation of the best paths between each couple of POIs. These best paths are referred to as “links”, because they represent the links of a second different graph that will be defined and used in phase 2. The best path between two given POIs is the one that minimises the defined cost, i.e., the shortest path. In graph theory, the shortest path problem requires to find a path between two nodes in a graph, so that the sum of the weight of the edges that belong to the path is minimised. In the literature, an algorithm that is widely used to solve this kind of a problem is A*, which is often used in many fields of computer science due to its completeness, optimality, and optimal efficiency [129]. A* is an informed search algorithm that uses a heuristic function to estimate the cost of the cheapest path from a given node to the goal node. The algorithm uses this information to focus its search toward a direction that most likely will lead to the optimal solution. The heuristic function is problem-specific, so it needs to be defined according to the context. If the heuristic function is admissible, meaning that it never overestimates the actual cost to reach the goal node, A* will always return a least-cost path from the starting node to the goal node.

As regards the weight of the edges of the graph, i.e., the cost of the underwater movements, three possible strategies were considered to define it: one based on the distance covered by the path, one on the air consumption, and the last on the decompression cost. Since the heuristic function is problem-specific, it is defined in a specific way for each strategy. These strategies are described in detail in the following subsections.

5.2.2.1 Distance

The simpler strategy is to consider the cost of an underwater path as the mere distance covered by the path. In the 3D grid, the allowable movements are restricted by the nature of the grid itself. Basically, three different types of movements are allowed in a 3D grid, and each of them has a different cost:

- Mov1D: It is the movement along only one axis. Given a voxel diameter of one meter, the cost of this kind of movement is defined as $c = 1$ (Figure 56, yellow line).
- Mov2D: It is the movement along two axes. Its cost is defined as the diagonal of a square of a side equal to one: $c = \sqrt{2} \cong 1.4$ (Figure 56, blue line).
- Mov3D: It is the movement along three axes. Its cost is defined as $c = \sqrt{1^2 + 1.4^2} \cong 1.7$ (Figure 56, green line).

In this case, given two nodes, the heuristic function (1) is computed as the distance between the two nodes evaluated as movements in the 3D grid. Since the heuristic should not overestimate the distance, it is considered the best case, i.e., the minimum number of movements of a different kind that permits to reach one node from the other:

$$h = 1.7 \times Mov3D + 1.4 \times Mov2D + 1 \times Mov1D \quad (1)$$

where $MovXD$ is the number of movements for each type of movement.

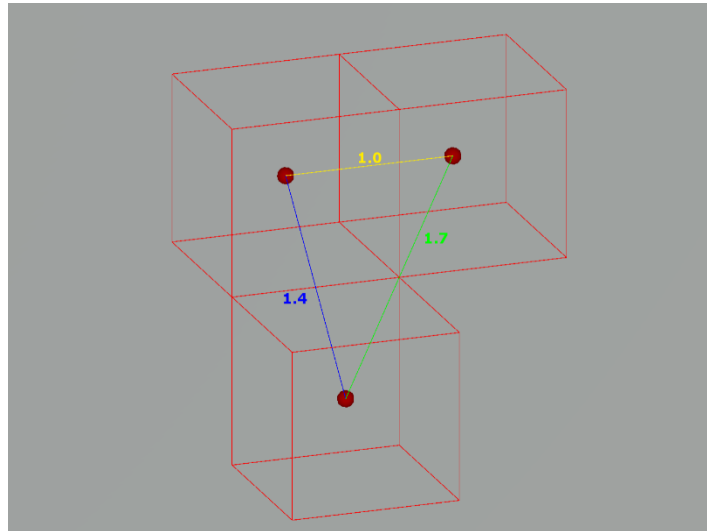


Figure 56. A representation of the three different types of movements allowed in a 3D grid with the related distance costs.

5.2.2.2 Air Consumption

In an underwater environment, the covered distance is not the only factor to take into account while evaluating the cost of a path. Indeed, the diving depth is a factor that affects different aspects of the dive, such as the air consumption, the quantity of nitrogen absorbed, and, consequently, the need and the duration of the decompression stops at the end of diving. The air consumption depends both on the distance covered and the diving depth. Therefore, it could be a valid parameter to consider as a cost to be minimised.

To compute the air consumption, the respiratory minute volume (RMV) has to be considered as the air consumption rate [109]. The RMV is the total volume of air moved in and out of the lungs in

one minute, and it is directly related to different exertion levels among divers. The air consumed at a given depth can be computed calculating the consumption rate at the depth with Equation (2):

$$C_d = RMV \times P_a \quad (2)$$

where C_d is expressed in scfm (standard cubic feet per minute), and P_a is the absolute pressure (ata) at the given depth. Then, the air consumed (3) can be calculated by multiplying the C_d by the travel time (min).

$$C_{air} = C_d \times Mov_{time} \quad (3)$$

Given the distance of each type of movement, as described in the previous section, the travel time (4) can be defined as

$$Mov_{time} = \frac{Mov_{distance}}{v} \quad (4)$$

where v is the traveling speed that can be considered as a constant. Therefore, the cost (5) can be defined as

$$C_{air} = \frac{RMV}{v} \times P_a \times Mov_{distance} \quad (5)$$

As $\frac{RMV}{v}$ is constant, i.e., it remains the same in the cost computation of whatever path, the cost function (5) can be simplified as follows (6):

$$C_{air} = P_a \times Mov_{distance} \quad (6)$$

On this basis, the heuristic function (7) can be defined, and it considers the best case of a path with the minimum distance, as computed in the previous section, and the minimum air consumption that matches the one evaluated on the surface ($P_a = 1$).

$$h = Mov3D_{distance} \times Mov3D + Mov2D_{distance} \times Mov2D + Mov1D_{distance} \times Mov1D \quad (7)$$

where $MovXD$ is the number of movements for each type of movement, and the movement distances are the ones described in the previous section.

5.2.2.3 Decompression cost

On the basis of the theory of the dissolved gas model of Bühlmann [127], it is possible to evaluate the partial pressure of inert gas dissolved in the tissue compartments of the diver. This pressure is an important parameter in the computation of decompression stops. In fact, the greater the pressure, the longer the time that will be eventually needed to complete safely the decompression.

Hence, the formulation of a “decompression cost” that is based on the inert gas pressure in the tissues and is computed by means of the Schreiner equation (8) [130]:

$$P_t = P_{alv0} + R \left(t - \frac{1}{k} \right) - \left(P_{alv0} - P_{t0} - \frac{R}{k} \right) e^{-kt} \quad (8)$$

- P_t , compartment inert gas pressure (bar).
- P_{t0} , initial compartment inert gas pressure (bar).
- P_{alv0} , initial inspired alveolar inert gas pressure (bar). $P_{alv0} = (P_{amb} - P_{wv})Q$, where P_{amb} is the initial ambient pressure, P_{wv} is the water vapour pressure at 37 degrees Celsius, i.e., 0.0627 bar, and Q is the fraction of inert gas.
- k , half-time constant related to the compartment (min^{-1}), $k = \frac{\ln 2}{\text{half-time}}$.
- t , time of exposure (min).
- R , rate of change in inspired inert gas pressure with change in the ambient pressure (bar/min). $R = QR_{amb}$, where R_{amb} is the rate of change in the ambient pressure, and Q is the fraction of inert gas.

In short, this equation evaluates the tissue inert gas pressure according to its initial state P_{t0} to the ambient pressure P_{amb} and to the ascent/descent rate. The idea is to define P_t as the decompression cost, but in order to solve the concerning equation, some assumptions were necessary. It is assumed that the breathing mixture is atmospheric air, and therefore, the only inert gas considered is nitrogen. Typically, on the basis of the Bühlmann model, the equation is calculated for all 16 tissue compartments, but in this case, for the sake of simplicity, only the first compartment was considered, i.e., the one with the highest diffusion rate. This compartment has a half-time equal to 4 [126]. Furthermore, the time of exposure t and the rate of change in inspired gas pressure R are calculated assuming a speed of the diver equal to 10m/min. In addition, for the evaluation of R , a fixed value $Q = 0.79$ stands for the fraction of nitrogen in the air. Finally, it was necessary to define the value of P_{t0} that is related to the diver initial state. Since the diver state is not known at this stage, it is assumed as a constant P_{t0} equal to the one computed on the surface before starting the dive. On the surface, the amount of nitrogen in the body is constant, so, in this case, the partial pressure of nitrogen (9) corresponds to the alveolar partial pressure:

$$P_{t0} = P_{alv0} = (P_{amb} - P_{wv})Q = (1.0132\text{bar} - 0.0627\text{bar}) \times 0.79 = 0.7509\text{ bar} \quad (9)$$

On these bases, a table of the decompression costs was created. For each depth, three cases were considered: remaining at the same depth, ascending, and descending. For each of these cases, the cost of the three different movements allowed in the 3D grid were computed, as described previously. In Table 20, as a sample, only a part of the decompression cost table is reported.

Table 20. A part of the decompression cost table.

Depth	Direction	Mov1D	Mov2D	Mov3D	P_alv0
0	Same	0.752156728	0.753014201	0.753655358	1
0	Down	0.752493664	0.753485367	0.754226993	1
1	Up	0.752682484	0.753748715	0.754545865	1.1
1	Same	0.753019419	0.754219881	0.755117501	1.1
1	Down	0.753356355	0.754691047	0.755689137	1.1
2	Up	0.753545175	0.754954395	0.756008008	1.2
2	Same	0.753882111	0.755425561	0.756579644	1.2
2	Down	0.754219046	0.755896727	0.75715128	1.2
3	Up	0.754407866	0.756160076	0.757470151	1.3
3	Same	0.754744802	0.756631242	0.758041787	1.3
3	Down	0.755081737	0.757102408	0.758613423	1.3
4	Up	0.755270558	0.757365756	0.758932294	1.4
4	Same	0.755607493	0.757836922	0.75950393	1.4
4	Down	0.755944429	0.758308088	0.760075566	1.4
5	Up	0.756133249	0.758571436	0.760394438	1.5
5	Same	0.756470184	0.759042602	0.760966073	1.5
5	Down	0.75680712	0.759513768	0.761537709	1.5

As regards the heuristic function (10), similar to the other strategies, a path with the minimum distance and the minimum decompression cost that corresponds with the one evaluated on the surface was considered:

$$h = Mov3D_{surface_cost} \times Mov3D + Mov2D_{surface_cost} \times Mov2 + Mov1D_{surface_cost} \times Mov1D \quad (10)$$

5.2.3 Phase 2 (Path Optimisation): Calculating Optimal Path to Visit all POIs

Once phase 1 is completed, all the best links through each couple of POIs have been computed. In phase two, a new graph with a node for each POI can be considered. This is a complete graph for which the links were computed in phase 1. Given this graph, the problem is to find the path that visits the highest possible number of POIs with the minimum cost. It is worth noting that it could be not possible to safely visit all the POIs. This is due to the constraint related to the diving safety procedures that take into account the remaining air in the tank and the absorption of nitrogen in the tissues that should not go beyond the limits. Taking into account all of these aspects, the search algorithm in this phase relies on the DecoAPI introduced before.

Therefore, the algorithm of phase 2 searches for the path that visits the highest possible number of POIs with the minimum cost and that is safe and feasible for the diver, given his/her actual state.

The cost of the path depends on the strategy employed in phase 1. In the case of strategies based on the distance and on the air consumption, the cost considered in phase 2 is the same as the one evaluated in phase 1, so each link of the new graph has a cost that matches the one computed for the related best link found in phase 1. In the other case of the strategy based on the decompression cost, the cost considered in phase 2 is based on a parameter evaluated by DecoAPI, i.e., the ascent pressure

limit. It was decided to consider this cost during this phase, because it is directly related to the inert gas dissolved in the tissues on which the decompression cost of phase 1 is based as well. In particular, the ascent pressure limit stands for the minimum ambient pressure to which the diver can ascend without exceeding the critical supersaturation limit. Furthermore, the ascent pressure limit computed by DecoAPI can rely on the knowledge of the complete decompression profile of the diver, and, therefore, it is more realistic than the decompression cost computed in phase 1, which is based on some strong assumptions that could not correspond to the real case.

The space of the solutions can be represented as a tree (Figure 57). The root of the tree is represented by the diver, and the first level of the tree is composed of all the POIs. The child nodes of each branch node are all the POIs except the ones that are just present in the branch. The tree has a number of leaves that is $N!$, where N is the number of POIs. The number of the leaves corresponds to all possible paths that visit all the POIs. The total number of nodes of the tree (11) is given by the following formula:

$$\sum_{k=0}^N \frac{N!}{(N - k)!} \quad (11)$$

that represents all the possible partial paths, i.e., the paths that visit only a subset of the given POIs.

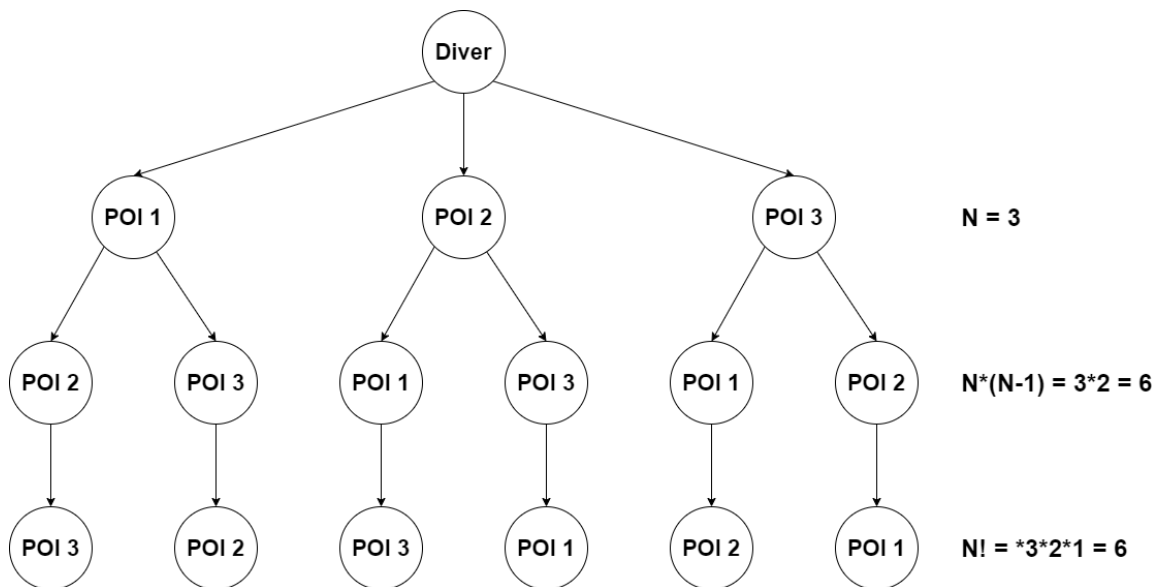


Figure 57. The search tree in the sample case of three points of interest (POIs).

A depth-first search algorithm for traversing the tree was implemented. As soon as it finds a path with a cost lower than the actual best path (if any), this is recorded as the best path. In addition, also, the best partial path is recorded, i.e., the path that visits the greater number of POIs with the lowest cost. If there is not a path that can visit all the existing POIs, this partial path will be returned as the best path. This is due to the fact that, apart from different strategies employed in phase 1, in phase 2, each eligible path is processed by DecoAPI and should result safe to be considered as a

possible solution. A path is considered safe if the diver does not exceed the decompression limits and if he/she has enough time to fulfil the deco stops, thus concluding the dive in complete safety. DecoAPI performs this evaluation on the basis of the actual state of the diver. In fact, it records the dive profile of the diver in order to perform the estimation of the nitrogen absorbed by the tissues of the diver. When the tree is generated, the initial state of the diver corresponding to the root of the tree is recorded. At each branch node, the state of the diver is computed according to the actual path of the related branch and is propagated in the lowest level of the tree. This step avoids the repetition of expensive calculations that were previously done. Furthermore, a pruning of the search tree is implemented, i.e., a technique for the optimisation of the tree through the removal of the branches that are redundant in order to find the optimal solution. In particular, when a partial path has a cost that is greater than the cost of the actual minimal path, the related branch is deleted from the tree, and the search proceeds on to the next branch.

5.3 Results

The behaviour of the pathfinding algorithm was tested on each underwater site for each of the three strategies previously described. For each 3D model of the underwater sites, space partitioning was performed in order to produce a 3D grid on which the algorithm could perform the search of the best path.

5.3.1 Case Studies

Three cases of study were considered to evaluate the behaviour and the performance of the pathfinding algorithm. Each of them consisted of a 3D model that represented an underwater site with different environmental features. Five POIs were placed in each site, and they represented the spots that the diver needed to visit. The different environments are described in the following subsections.

5.3.1.1 Shipwreck

This underwater site is a typical sample of an artificial obstacle in an underwater environment that could restrict the freedom of movement of the diver, and it has to be taken into account while computing a diving plan. In particular, in this case study, the obstacle is also the focus of the mission and is represented by a modern shipwreck that is 85 meters long and approximately 13 meters wide (Figure 58). The shipwreck lays on the seabed in an upright position at a depth of around 35 meters. The deck of the ship is at a depth of around 30 meters.

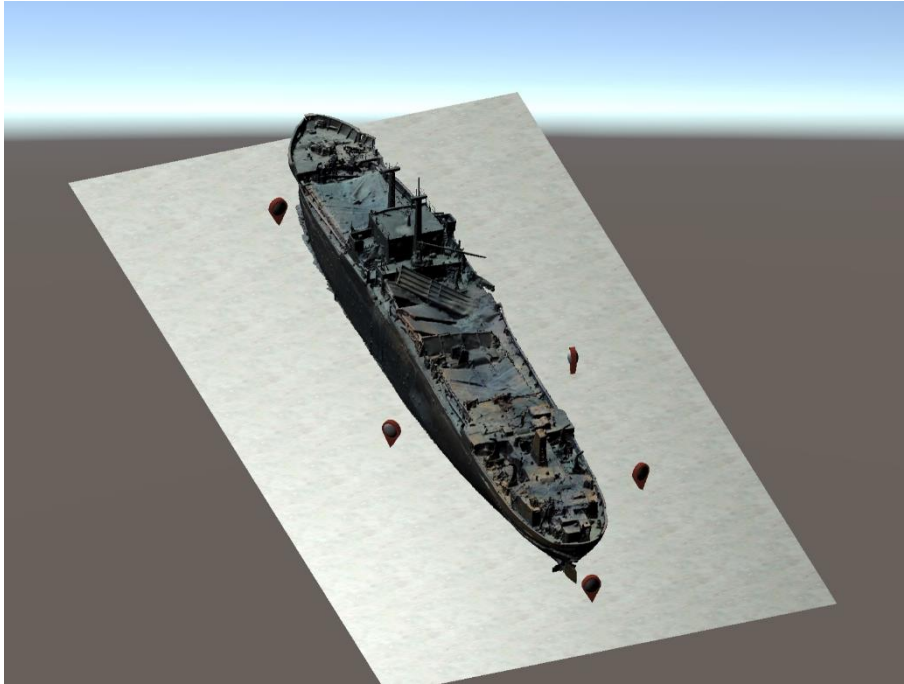


Figure 58. A modern shipwreck.

5.3.1.2 Seamount

This case study represents a sample of a natural obstacle in the underwater environment, such as a seamount (Figure 59). It is not a real environment but a 3D-modelled one. The depth at the seabed level is around 30 meters, and the top of the seamount is 10 meters deep.

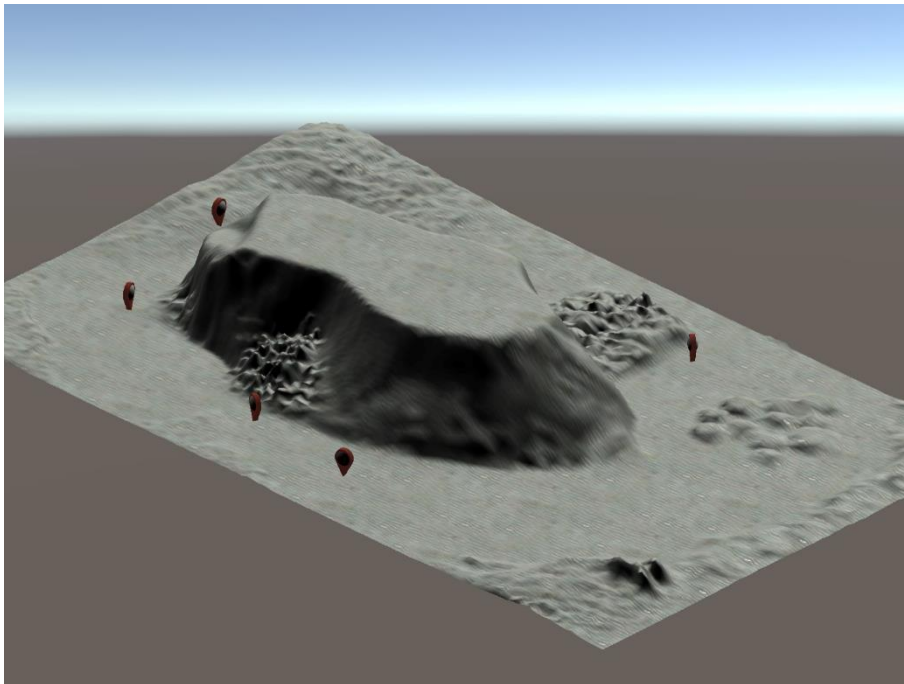


Figure 59. A sample of a seamount.

5.3.1.3 Landslide

A typical natural underwater formation is the landslide, i.e., an underwater slope where the depth increases gradually (Figure 60). In this case, the environment was modelled as well. The top region is around 7 to 8 meters deep, and the bottom of the seabed is at a depth of around 27 meters.

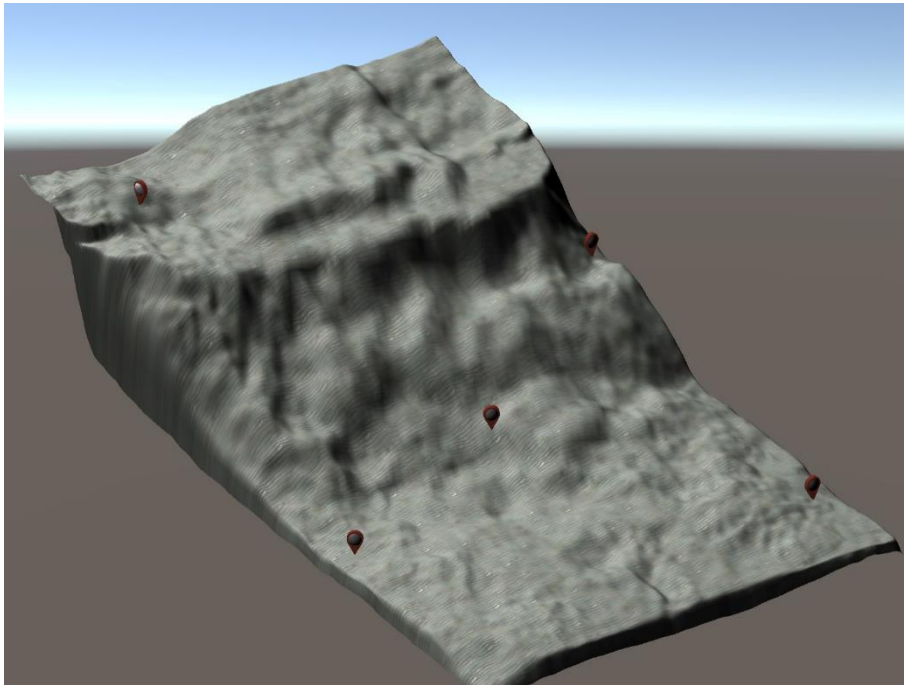


Figure 60. A sample of a landslide.

5.3.2 Space Partitioning: 3D Grids

Figure 61 represents the 3D grids for each case study. More precisely, the figure shows the voxels of the grids that represent the “terrain”, i.e., the regions of the underwater site that cannot be traversed by the diver, as described in the related section. The whole grid covers the entire underwater sites from the seabed to the surface. In the figure, the bounds of the grids are represented by the white lines.

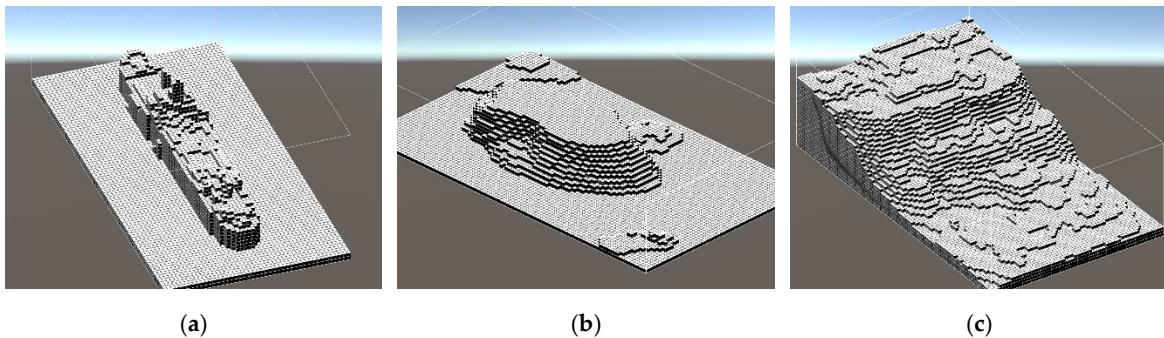
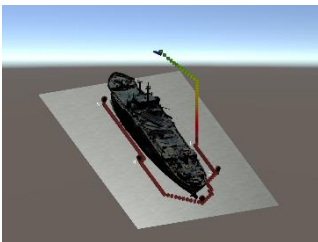
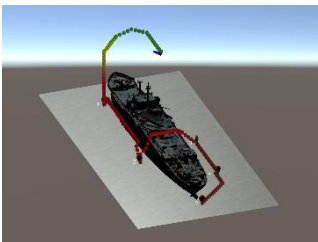
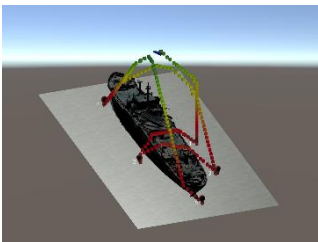
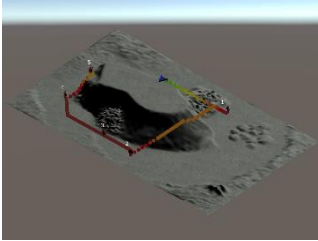
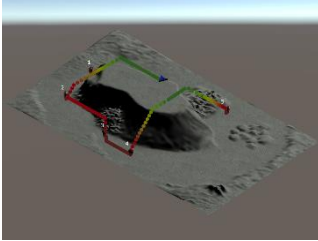
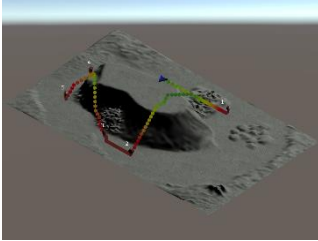
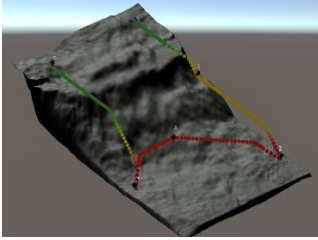
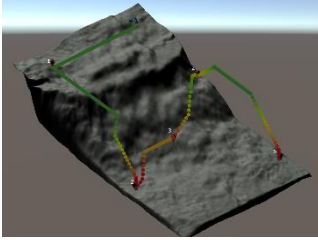
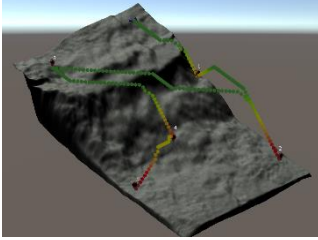


Figure 61. The 3D grids of each underwater site: (a) the shipwreck, (b) the seamount, and (c) the landslide.

5.3.3 Generated Paths

In Table 21, all generated paths are reported for each case. The rows represent the underwater sites, and the columns represent the strategy adopted to compute the related path. The position of the diver is set always on the surface, and the generated paths visit all the POIs in each case. The generated path is represented by the voxels of the grid that are part of the path. A gradient colour is used to better identify the depth of the path. The gradient ranges from the green colour on the surface to the red colour on the seabed. A numbered label near each POI indicates the order of visit.

Table 21. The paths generated with three different strategies for three different case studies.

Underwater Site	Strategy		
	Distance	Air Consumption	Decompression
Shipwreck			
Seamount			
Landslide			

For each path generated with a specific strategy, the costs of the other two strategies are also computed for the path. These costs are reported in Table 22, where each column represents the paths generated by the related strategy divided by the underwater site. Consequently, each row represents a specific type of cost. Within the row, the value highlighted in grey represents the minimum cost, and the value in bold represents the cost closest to the minimum.

Table 22. The costs computed for each path with the tree strategies.

Underwater Site	Cost	Strategy		
		Distance	Air Consumption	Decompression
Shipwreck	Distance	167	172.2	301.7
	Air Consumption	13.5292	13.4948	20.6618
	Decompression	2.277739	2.14631	0.8656095

Seamount	Distance	139.2	143.5	175.6
	Air Consumption	8.3121	8.2405	9.3926
	Decompression	0.5507061	0.548093	0.5466153
Landslide	Distance	223.7	227.4	292.4
	Air Consumption	12.1802	11.7076	13.9602
	Decompression	0.5526806	0.548951	0.5451685

Over time, the paths determined by the pathfinding algorithm could change. In fact, the history of dives is recorded by DecoAPI, which evaluates the diving profile of the diver and establishes if a certain path is safe or not for the diver. Figure 62 and Table 23 depict two different moments of the same dive. In the first moment, the diver is diving at a depth of 18 meters, and the related dive data are reported in the first column of Table 23, labelled as “Case a”. In this situation, the algorithm succeeds in finding a safe path to visit all the five POIs (Figure 8a). After fifteen minutes at the same depth of 18 meters, the situation changes, as reported in the second column of Table 23, labelled as “Case b”. In fact, the ascent pressure limit, which meaning was defined before, increases from 0.97 to 1.64 bar. The air available in the tank goes down to 66 bar, and the time to surface (TTS) goes up to six minutes. In particular, the TTS is a typical diving concept that represents the time estimated for the diver to complete the eventual decompression stops and ascend safely to the surface. In this new situation, the pathfinding algorithm evaluates that it is no longer safe for the diver to visit all the five POIs. Therefore, it suggests an optimal partial path, i.e., a path that visits four POIs with the minimum cost and in complete safety.

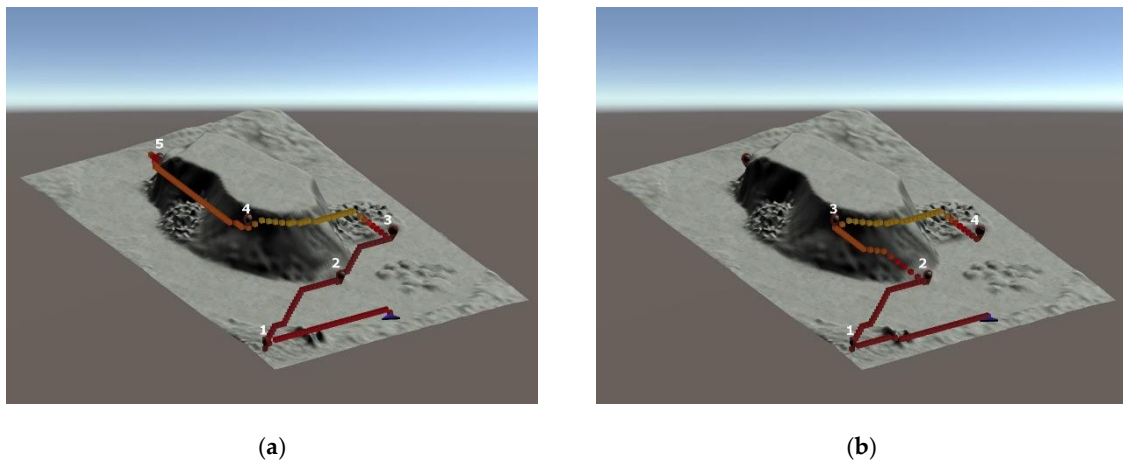


Figure 62. The path suggested by the algorithm changes over time.

Table 23. The dive data associated with the two cases presented in Figure 62.

Dive data	Initial state	
	Case “a”	Case “b”
Time (min)	39	54
Diving depth (meter)	18	18
Ascent pressure limit (bar)	0.97	1.64
Tank (bar)	95	66
Time to Surface (min)	2	6

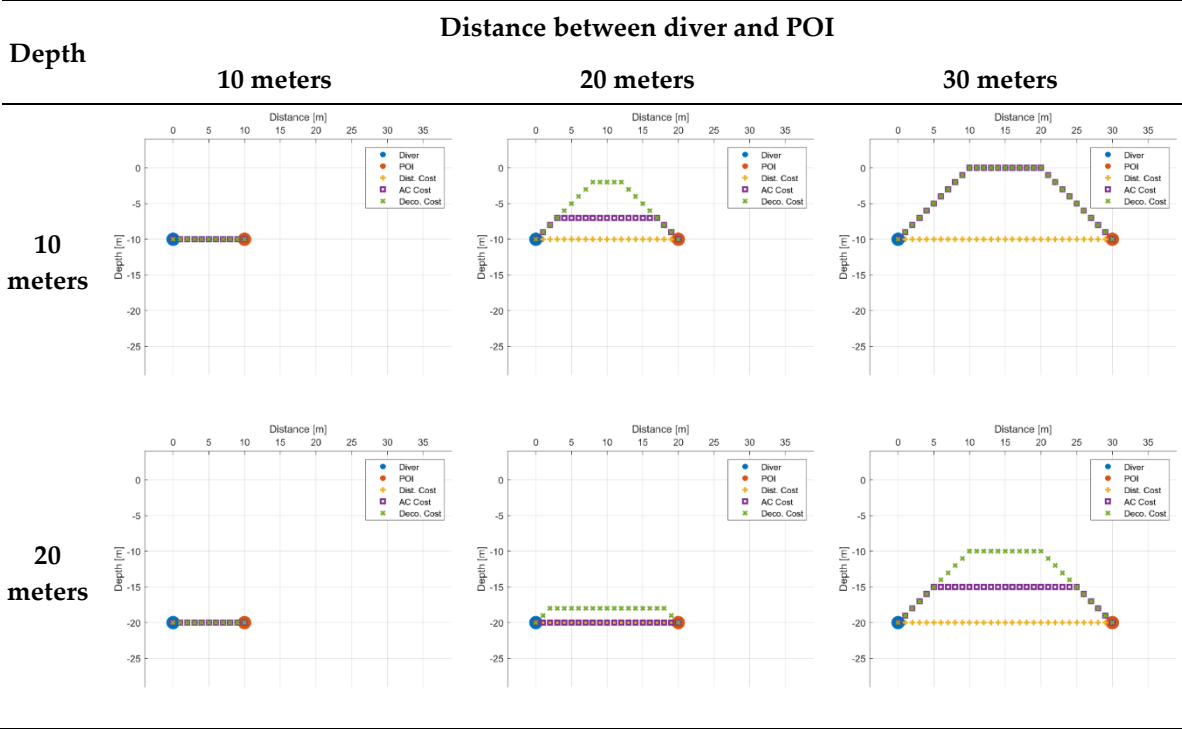
5.4 Discussion

The results reported in Table 21 show that the algorithm behaves in a different way according to the adopted strategy. In particular, the strategy based on the distance produces a straightforward path that obviously takes into account only the distance covered by the path whilst ignoring the depth. On the contrary, the strategy that relies on the air consumption cost considers both the distance and the depth of the generated path. As a result, this strategy produces paths that suggest ascending a little in some cases, in order to dive at a lower depth and consume less air without impacting too much on the distance covered by the path. Finally, the strategy based on the decompression cost generates paths that suggest ascending more and more frequently with respect to the air consumption strategy. In addition, the strategy based on the decompression cost suggests visiting the POIs in an order that does not seem to be convenient or logical. This is due to the fact that this strategy does not take into account the distance covered by the path and suggests diving at lower depths as much as possible in order to minimise the ascent pressure limit. In fact, the ascent pressure limit is not an increasing function during the dive, but it can decrease while ascending. The costs reported in Table 22 allow for better addressing the differences between the results obtained by the alternative strategies. Obviously, each strategy obtains the best values (highlighted in grey) as regards the cost related to the strategy itself. The strategy based on the distance obtains an air consumption cost that is the closest to the minimum. The strategy based on air consumption seems to suggest paths that minimise the consumption of air, but, in addition, it obtains a distance cost and ascent pressure limit that are the closest to the minimum. On the contrary, the strategy based on the decompression cost seems successful only in optimising the ascent pressure limit while suggesting paths that have a distance and air consumption cost that are considerably higher with respect to the other two strategies.

Each strategy may consider or not the diving depth and, eventually, can suggest paths with an ascent of a variable entity before moving towards the target. In this respect, Table 24 reports some figures that address the different behaviours of strategies in suggesting the entity of the ascent. Each figure shows the paths suggested by each strategy that goes from the diver to a POI placed at a given distance and depth. At a depth of 10 meters and a distance of 10 meters, all the three strategies suggest moving straightforward, maintaining the depth. Increasing the distance to 20 meters, the air consumption (AC) strategy suggests ascending a few meters, and the decompression strategy suggests ascending even more. With a distance of 30 meters, both strategies suggest ascending up to the surface. Obviously, the strategy based on the distance does not ever suggest ascending, because it does not consider depth as a cost. Going deeper, to 20 meters, with the POI placed at a distance of 10 meters, the three strategies continue to suggest remaining the same depth. At a distance of 20

meters, the only strategy that suggests ascending a few meters is the one based on the decompression cost. A further increasing of the distance of the POI up to 30 meters leads the AC strategy to suggest ascending about five meters, while the strategy based on the decompression cost suggests ascending about 10 meters. It is worth noting that, basically, the AC strategy suggests ascending less with respect to the decompression strategy, placing itself in the middle between the other two strategies.

Table 24. Different behaviours of the strategies in suggesting the ascent by varying the depth and the distance between the diver and point of interest (POI).



In addition, it could be noted that both the AC and decompression strategies suggest ascending less with the increase of the depth. This could be explained by observing the graphs in Figure 63. In both graphs, each line represents the evolution of the different types of movements with the increase of the depth. It could be noticed that the slope of each line is different. Consequently, as the depth increases, the gap between different types of movement increases as well. This shows that it is less affordable to extend the path ascending with diagonal movements.

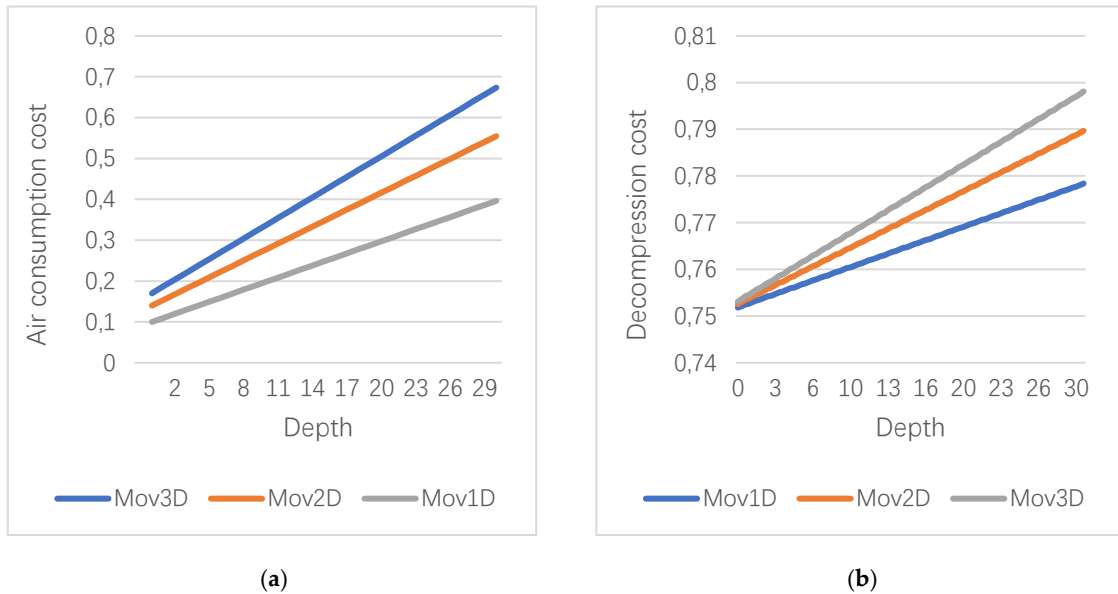


Figure 63. The evolution of the air consumption cost (a) and the decompression cost (b) with the increasing of the depth.

Finally, it has to be noted that, in the results reported, the strategies could also decide to ascend up to the surface without any constraint in order to evaluate the pure behaviour of the strategy. In a real case, it is convenient to introduce an ascent limit that can prevent the strategies from ascending too much. Indeed, the possibility to enable this limit was introduced in the pathfinding algorithm, and it was set at the depth of the safety decompression stop, which, usually, is at five meters and has to be completed at the end of every dive.

5.5 Conclusions

In this chapter, a novel system was presented that enabled computing an underwater path that visits the highest possible number of POIs with the minimum cost and in total safety. This was achieved by designing an original pathfinding algorithm that took into account several factors strictly inherent to scuba diving. In fact, the algorithm considered the decompression limits and the remaining air in the scuba tank. Furthermore, for the first time in the field of path planning aimed to support divers, the proposed system took into account the topography of the underwater environment to produce a path that considered and avoided obstacles.

The pathfinding algorithm computes the path with the minimal cost. In order to define the cost of the underwater movements, three possible strategies are considered: the first one based on the distance covered by the path, the second on the air consumption, and the last one on the decompression cost.

The analysis of the results suggests that the best strategy is the one based on the optimisation of the air consumption. The decompression cost is based on the ascent pressure limit that takes into account only nitrogen absorbed in the tissues. For this reason, the strategy based on this cost tends to

suggest paths that ascend too much towards the surface, without taking into consideration the additional distance of the path. Conversely, the strategy based only on the distance cost does not consider the depth of the path and optimises only the length of the path. In the middle, between these two strategies, the strategy based on air consumption takes into account both the distance and the depth, minimising the diving at great depths without affecting too much the path's length. Furthermore, since the AC strategy tends to ascend less than the strategy based on the decompression cost, it suggests paths that are more plausible and relevant to the standard scuba diving practices. An ascent limit that can prevent the strategies from ascending too much was designed as well.

In the future, it will be necessary to evaluate additional strategies or to combine the existing ones in a different fashion. Indeed, it could be possible to adopt different strategies for the evaluation of the costs in the two different phases of the algorithm. Some field tests will be conducted with real users that could give important feedback to evaluate which strategy could perform better in a real case scenario. In addition, since divers often return to known locations at the end of the dive (i.e., the boat), a fixed final node in the computation of the best path could be introduced. This will strongly change the generated paths and may ensure a better suiting of real diving demands. Finally, a further extension could also take into account the sea currents that may affect considerably the cost of a specific path.

6 Conclusions and Future Work

This chapter closes this thesis by presenting the main conclusions in Section 6.1 and proposing some research lines for future work in Section 6.2.

6.1 Conclusions

The aim of this research was to design and develop innovative solutions to support the diver through a novel system for the underwater navigation and exploration. The research focused on three main aspects: a study about the techniques for enhancing the underwater imagery has been conducted since underwater photography is the documentation method most used by divers; the development of a system that provides the divers with underwater assisted navigation and an enhanced diving experience through an on-site augmented visualization representing a 3D hypothetical reconstruction of the ancient ruins present in the underwater site; the conceiving of an innovative approach to dive planning based on an original underwater pathfinding algorithm.

As regards the underwater image enhancement, five well-known state-of-the-art methods have been selected for the enhancement of images taken on various underwater sites with five different environmental and illumination conditions. A benchmark for these methods has been produced based on three different evaluation techniques:

- an objective evaluation based on metrics selected among those already adopted in the field of underwater image enhancement;
- a subjective evaluation based on a survey conducted with a panel of experts in the field of underwater imagery;
- an evaluation based on the improvement that these methods may bring to 3D reconstructions.

The purpose was twofold. First of all, it has been tried to establish which methods perform better than the others and whether or not there existed an image enhancement method, among the selected ones, that could be employed seamlessly in different environmental conditions in order to accomplish different tasks such as visual enhancement, colour correction and 3D reconstruction improvement.

The second aspect was the comparison of the three above mentioned evaluation techniques in order to understand if they provide consistent results. Starting from the second aspect, it can be stated that the 3D reconstructions are not significantly improved by discussed methods, probably the minor improvement obtainable with the LAB could not justify the effort to pre-process hundreds or thousands of images required for larger models. On the other hand, the subjective metrics and the expert panel appear to be quietly consistent and, in particular, the \bar{E} identifies the same best methods of the expert panel on all the datasets. Consequently, an important conclusion that can be drawn from

this analysis is that \bar{E} should be adopted in order to have an objective evaluation that provides results consistent with the judgement of qualitative evaluations performed by experts in image enhancement. This is an interesting point, because it is not so easy to organize an expert panel for such kind of benchmark.

Moreover, thanks to the tool described in 2.3, the community working in underwater imaging would be able to quickly generate a dataset of enhanced images processed with five state of the art methods and use them in their works or to compare new methods. For instance, in case of an underwater 3D reconstruction, the tool can be employed to try different combinations of methods and quickly verify if the reconstruction process can be improved somehow. A possible strategy could be to pre-process the images with the LAB method trying to produce a more accurate 3D model and, afterwards, to enhance the original images with another method such as ACE to achieve a textured model more faithful to the reality. Employing the tool for the enhancement of the underwater images ensures to minimize the pre-processing effort and enables the underwater community to quickly verify the performance of the different methods on their own datasets.

Furthermore, as far as the evaluation of other methods that have not debated here is concerned, our guideline is to evaluate them with the \bar{E} metric, as pursuant to our results, it is the metric that is closest to the expert panel evaluation.

Another purpose of the present research work was the development of a system able to provide the divers with underwater assisted navigation and an enhanced diving experience. In this regard, the underwater tablet prototyped during the Visas project has been significantly improved both in terms of hardware and software. The waterproof case has been replaced with a more reliable and functional one, and the software has been redesigned to fit this new configuration. The LBL acoustic localization system has been substituted with two different positioning system based respectively on a USBL and an SBL configuration. These systems have been integrated with the tablet software while ensuring the possibility to employ also other acoustic localization systems with few software modifications.

Indeed, the underwater tablet has been provided with a new and totally redesigned software, namely Divy, that enables the diver to access different features. The UI is fully customizable and adaptable to different configurations in order to seamlessly switch between a scientific/professional application and a touristic application, due to the possibility to activate and deactivate the different features, changing the menu and the UI themes. The underwater tablet has been employed in different research projects and deployed in different underwater sites, due to its software capability to be adapted in each different situation. In some underwater site there is the possibility to activate the UWAR function, while in some projects there is the necessity to take advantage of the messaging function or to acquire textual notes. The acquisition of the geo-localized photos can be configured

with the internal camera of the tablet or with an external high-definition camera. In conclusion, the Divy software has the capability to be adapted on the basis of the expertise of the user and the purpose of use.

In the fourth chapter, a novel UWAR technology has been presented that can improve the divers' experience in submerged archaeological sites. In particular, the proposed technology provides the divers with their position over the 3D map of the underwater archaeological site, a visualization representing the actual conditions of the ancient ruins in the underwater site and an augmented visualization representing a hypothetical 3D reconstruction of the archaeological remains as they appeared in the past during the Roman era. A field test has been conducted in the Underwater Archaeological Park of Baiae to assess the feasibility and practical potentials of the proof of concept of the developed UWAR technologies. In particular, the field test made it possible to confirm the proper functioning of the adopted visual tracking techniques in the underwater environment notwithstanding the negative effects of the water turbidity and refraction that occurs at the air-glass-water boundary. It is worth noticing that since the overall positioning error mainly depends on the underwater acoustic localization system the added value of the developed hybrid approach lies in its capability to interpolate two consecutive acoustic positioning data through VIO tracking techniques in a sufficiently accurate way to perform a consistent and smooth AR visualization.

Furthermore, the UWAR feature has been successfully evaluated at an underwater cultural heritage site. Ten divers participated in a study that evaluated their perception of virtual objects underwater and user experience. The participants found the interaction natural, the visual aspects involved them, they stated that could actively survey the environment and examine the objects closely. They also enjoyed their time and claimed that the technology had great potential in underwater archaeology and tourism. The users did not clearly state that they would become so involved in the environment that they were not aware of things happening around them or lose track of time. This is a positive outcome, since the divers should be only partially involved in the environment because they must be constantly aware of things happening around them. In terms of the qualitative feedback, the divers found the system to be practical, engaging, and a useful tool for diving and archaeology, and they enjoyed the experience. The Divy navigation software was valued for its ability to localize the diver within the underwater site and for the opportunity to switch between viewing modes, but many divers complained about occasional inaccuracies in diver's position. In general, the divers were especially excited and suggested many more features to add, like a preview of locations, more information about POIs, and an ability to take pictures in the AR environment. The underwater tablet resulted easy to handle even for divers with the first level diving certificate because its weight in water is almost zero due to buoyancy.

In the last chapter, a novel system was presented that enabled computing an underwater path that visits the highest possible number of POIs with the minimum cost and in total safety. This was achieved by designing an original pathfinding algorithm that took into account several factors strictly inherent to scuba diving. In fact, the algorithm considered the decompression limits and the remaining air in the scuba tank. Furthermore, for the first time in the field of path planning aimed to support divers, the proposed system took into account the topography of the underwater environment to produce a path that considered and avoided obstacles. The pathfinding algorithm computes the path with the minimal cost. In order to define the cost of the underwater movements, three possible strategies are considered: the first one based on the distance covered by the path, the second on the air consumption, and the last one on the decompression cost. The analysis of the results suggests that the best strategy is the one based on the optimisation of the air consumption. The decompression cost is based on the ascent pressure limit that takes into account only nitrogen absorbed in the tissues. For this reason, the strategy based on this cost tends to suggest paths that ascend too much towards the surface, without taking into consideration the additional distance of the path. Conversely, the strategy based only on the distance cost does not consider the depth of the path and optimises only the length of the path. In the middle, between these two strategies, the strategy based on air consumption takes into account both the distance and the depth, minimising the diving at great depths without affecting too much the path's length. Furthermore, since the AC strategy tends to ascend less than the strategy based on the decompression cost, it suggests paths that are more plausible and relevant to the standard scuba diving practices. An ascent limit that can prevent the strategies from ascending too much was designed as well.

6.2 Future work

The underwater navigation system will be further improved and integrated with new functionalities, particularly in the context of other ongoing research projects. For example, in the DiveSafe project [131], the aim is to integrate the system with an underwater scooter and sensors for monitoring the health and the safety of the diver. In particular, we are introducing three health sensors, that are intended to measure the breath rate, the heartbeat and the glycemia of the diver. When a health parameter results to be outside the safety range, Divy will send a visual notification to the diver and an alert message to the surface operators. Moreover, the hardware setup is going to be improved, leaving the solution based on a commercial tablet and going towards a custom underwater device composed of an embedded board, a dedicated display and a tailored waterproof case. This solution will enable us to reduce the dimensions and enhance the performances of the underwater tablet.

In the context of the Musas project [132], the Underwater Navigation and Exploration system has been also deployed and released to the public in the Underwater Archaeological Parks of Baiae and of Egnazia. Within these two submerged sites, the system will be used by final users starting from summer 2021, taking also advantage of the UWAR to visualize how the ancient ruins present in the sites appeared during the Roman era.

The reliability of the UWAR feature mainly depends on the accuracy of the localization provided by the hybrid tracking system. Therefore, further solutions for the hybrid tracking will be investigated in the future, defining new data fusion strategies, and enhancing the VIO capabilities of the system. In this regard, new hardware solutions should also be investigated. Newer commercial mobile devices incorporate depth sensors which could help the VIO framework to reduce the time of initialization and to improve the visual tracking. It is worth noting that the performance of this kind of devices in an underwater environment is unknown and should be further investigated.

As regards the pathfinding algorithm, additional strategies will be evaluated for the definition of the cost of an underwater path. In the presented work, the same fixed strategy is used for the two different phases of the pathfinding algorithm. Another solution could be to adopt different strategies for the evaluation of the costs in the two different phases. Some field tests will be conducted with real users that could give important feedback to evaluate which strategy could perform better in a real case scenario. Additional features and constraints can be added to the pathfinding algorithm. Since divers often return to known locations at the end of the dive (i.e., the boat), a fixed final node in the computation of the best path could be introduced. This will strongly change the generated paths and may ensure a better suiting of real diving demands. The sea currents may affect considerably the cost of a specific path and this will be also considered in a further extension of the pathfinding algorithm.

References

1. Mangeruga, M.; Cozza, M.; Bruno, F. Evaluation of Underwater Image Enhancement Algorithms under Different Environmental Conditions. *Journal of Marine Science and Engineering* **2018**, *6*, 10, doi:10.3390/jmse6010010.
2. Mangeruga, M.; Bruno, F.; Cozza, M.; Agrafiotis, P.; Skarlatos, D. Guidelines for Underwater Image Enhancement Based on Benchmarking of Different Methods. *Remote Sensing* **2018**, *10*, 1652, doi:10.3390/rs10101652.
3. He, K.; Sun, J.; Tang, X. Single Image Haze Removal Using Dark Channel Prior. *IEEE Transactions on Pattern Analysis and Machine Intelligence* **2011**, *33*, 2341–2353, doi:10.1109/TPAMI.2010.168.
4. Drews, P.; Nascimento, E.; Moraes, F.; Botelho, S.; Campos, M. Transmission Estimation in Underwater Single Images.; **2013**; pp. 825–830.
5. Fattal, R. Single Image Dehazing. *ACM transactions on graphics (TOG)* **2008**, *27*, 72.
6. Fattal, R. Dehazing Using Color-Lines. *ACM transactions on graphics (TOG)* **2014**, *34*, 13.
7. Berman, D.; Avidan, S. Non-Local Image Dehazing. In Proceedings of the Proceedings of the IEEE conference on computer vision and pattern recognition; **2016**; pp. 1674–1682.
8. Berman, D.; Treibitz, T.; Avidan, S. Air-Light Estimation Using Haze-Lines. In Proceedings of the 2017 IEEE International Conference on Computational Photography (ICCP); May **2017**; pp. 1–9.
9. Sankpal, S.S.; Deshpande, S.S. Nonuniform Illumination Correction Algorithm for Underwater Images Using Maximum Likelihood Estimation Method. *Journal of Engineering* **2016**, *2016*.
10. Morel, J.-M.; Petro, A.-B.; Sbert, C. Screened Poisson Equation for Image Contrast Enhancement. *Image Processing On Line* **2014**, *4*, 16–29, doi:10.5201/ipol.2014.84.
11. Carlevaris-Bianco, N.; Mohan, A.; Eustice, R.M. Initial Results in Underwater Single Image Dehazing. In Proceedings of the OCEANS 2010; IEEE, 2010; pp. 1–8.
12. Bianco, G.; Muzzupappa, M.; Bruno, F.; Garcia, R.; Neumann, L. A New Color Correction Method for Underwater Imaging. *The International Archives of Photogrammetry, Remote Sensing and Spatial Information Sciences* **2015**, *40*, 25.
13. Bianco, G.; Neumann, L. A Fast Enhancing Method for Non-Uniformly Illuminated Underwater Images. In Proceedings of the OCEANS 2017 - Anchorage; September **2017**; pp. 1–6.
14. Gatta, C.; Rizzi, A.; Marini, D. Ace: An Automatic Color Equalization Algorithm. In Proceedings of the Conference on Colour in Graphics, Imaging, and Vision; Society for Imaging Science and Technology, **2002**; Vol. 2002, pp. 316–320.
15. Getreuer, P. Automatic Color Enhancement (ACE) and Its Fast Implementation. *Image Processing On Line* **2012**, *2*, 266–277, doi:10.5201/ipol.2012.g-ace.
16. Pizer, S.M.; Amburn, E.P.; Austin, J.D.; Cromartie, R.; Geselowitz, A.; Greer, T.; ter Haar Romeny, B.; Zimmerman, J.B.; Zuiderveld, K. Adaptive Histogram Equalization and Its Variations. *Computer vision, graphics, and image processing* **1987**, *39*, 355–368.
17. Zuiderveld, K. Contrast Limited Adaptive Histogram Equalization. In Proceedings of the Graphics gems IV; Academic Press Professional, Inc., **1994**; pp. 474–485.
18. Singh, R.; Biswas, M. Contrast and Color Improvement Based Haze Removal of Underwater Images Using Fusion Technique. In Proceedings of the 2017 4th International Conference on Signal Processing, Computing and Control (ISPCC); September **2017**; pp. 138–143.
19. Ancuti, C.O.; Ancuti, C.; Vleeschouwer, C.D.; Neumann, L.; Garcia, R. Color Transfer for Underwater Dehazing and Depth Estimation. In Proceedings of the 2017 IEEE International Conference on Image Processing (ICIP); September **2017**; pp. 695–699.

20. Galdran, A.; Pardo, D.; Picón, A.; Alvarez-Gila, A. Automatic Red-Channel Underwater Image Restoration. *Journal of Visual Communication and Image Representation* **2015**, *26*, 132–145, doi:10.1016/j.jvcir.2014.11.006.
21. Łuczynski, T.; Birk, A. Underwater Image Haze Removal and Color Correction with an Underwater-Ready Dark Channel Prior. *arXiv:1807.04169 [cs]* **2018**.
22. Lu, J.; Li, N.; Zhang, S.; Yu, Z.; Zheng, H.; Zheng, B. Multi-Scale Adversarial Network for Underwater Image Restoration. *Optics & Laser Technology* **2018**, doi:10.1016/j.optlastec.2018.05.048.
23. Li, C.Y.; Cavallaro, A. Background Light Estimation for Depth-Dependent Underwater Image Restoration. In Proceedings of the 2018 25th IEEE International Conference on Image Processing (ICIP); October **2018**; pp. 1528–1532.
24. Anwar, S.; Li, C.; Porikli, F. Deep Underwater Image Enhancement. *arXiv:1807.03528 [cs]* **2018**.
25. Nomura, K.; Sugimura, D.; Hamamoto, T. Underwater Image Color Correction Using Exposure-Bracketing Imaging. *IEEE Signal Processing Letters* **2018**, *25*, 893–897, doi:10.1109/LSP.2018.2831630.
26. Chang, H.; Cheng, C.; Sung, C. Single Underwater Image Restoration Based on Depth Estimation and Transmission Compensation. *IEEE Journal of Oceanic Engineering* **2018**, 1–20, doi:10.1109/JOE.2018.2865045.
27. Akkaynak, D.; Treibitz, T. Sea-Thru: A Method for Removing Water From Underwater Images.; **2019**; pp. 1682–1691.
28. Ancuti, C.; Ancuti, C.O.; Haber, T.; Bekaert, P. Enhancing Underwater Images and Videos by Fusion. In Proceedings of the 2012 IEEE Conference on Computer Vision and Pattern Recognition; June **2012**; pp. 81–88.
29. Ancuti, C.O.; Ancuti, C.; Vleeschouwer, C.D.; Bekaert, P. Color Balance and Fusion for Underwater Image Enhancement. *IEEE Transactions on Image Processing* **2018**, *27*, 379–393, doi:10.1109/TIP.2017.2759252.
30. Lowe, D.G. Object Recognition from Local Scale-Invariant Features. In Proceedings of the Computer vision, 1999. The proceedings of the seventh IEEE international conference on; Ieee, **1999**; Vol. 2, pp. 1150–1157.
31. Agrafiotis, P.; Drakonakis, G.I.; Georgopoulos, A.; Skarlatos, D. The Effect of Underwater Imagery Radiometry on 3d Reconstruction and Orthoimagery. *ISPRS-International Archives of the Photogrammetry, Remote Sensing and Spatial Information Sciences* **2017**, 25–31.
32. Agrafiotis, P.; Drakonakis, G.I.; Skarlatos, D.; Georgopoulos, A. Underwater Image Enhancement before Three-Dimensional (3D) Reconstruction and Orthoimage Production Steps: Is It Worth? In; MDPI, **2018** ISBN 978-3-03842-685-1.
33. Agrafiotis, P.; Skarlatos, D.; Forbes, T.; Poullis, C.; Skamantzari, M.; Georgopoulos, A. Underwater Photogrammetry in Very Shallow Waters: Main Challenges and Caustics Effect Removal. *International Archives of the Photogrammetry, Remote Sensing & Spatial Information Sciences vol. 42, no. 2*, **2018**.
34. Forbes, T.; Goldsmith, M.; Mudur, S.; Poullis, C. DeepCaustics: Classification and Removal of Caustics From Underwater Imagery. *IEEE Journal of Oceanic Engineering* **2018**, 1–11, doi:10.1109/JOE.2018.2838939.
35. Agisoft, L.L.C. Agisoft PhotoScan User Manual: Professional Edition. **2017**.
36. Bay, H.; Tuytelaars, T.; Van Gool, L. SURF: Speeded Up Robust Features. In Proceedings of the Computer Vision – ECCV 2006; Leonardis, A., Bischof, H., Pinz, A., Eds.; Springer Berlin Heidelberg, 2006; pp. 404–417.
37. Fischler, M.A.; Bolles, R.C. Random Sample Consensus: A Paradigm for Model Fitting with Applications to Image Analysis and Automated Cartography. *Commun. ACM* **1981**, *24*, 381–395, doi:10.1145/358669.358692.
38. OpenCV Library Available online: <https://opencv.org/> (accessed on 4 December 2017).
39. Eigen Available online: <http://eigen.tuxfamily.org/index.php> (accessed on 4 December 2017).

40. FLANN - Fast Library for Approximate Nearest Neighbors: FLANN - FLANN Browse Available online: <https://www.cs.ubc.ca/research/flann/> (accessed on 4 December 2017).
41. Limare, N.; Lisani, J.-L.; Morel, J.-M.; Petro, A.B.; Sbert, C. Simplest Color Balance. *Image Processing On Line* **2011**, *1*, 297–315, doi:10.5201/ipol.2011.llmps-scb.
42. FFTW Home Page Available online: <http://www.fftw.org/> (accessed on 4 December 2017).
43. I-MareCulture Available online: <http://www.imareculture.eu/> (accessed on 8 January 2018).
44. Bruno, F.; Lagudi, A.; Ritacco, G.; Čejka, J.; Kouřil, P.; Liarokapis, F.; Agrafiotis, P.; Skarlatos, D.; Philpin-Briscoe, O.; Poullis, C. Development and Integration of Digital Technologies Addressed to Raise Awareness and Access to European Underwater Cultural Heritage. An Overview of the H2020 i-MARECULTURE Project.
45. Skarlatos, D.; Agrafiotis, P.; Balogh, T.; Bruno, F.; Castro, F.; Petriaggi, B.D.; Demesticha, S.; Doulamis, A.; Drap, P.; Georgopoulos, A.; et al. Project IMARECULTURE: Advanced VR, IMmersive Serious Games and Augmented REality as Tools to Raise Awareness and Access to European Underwater CULTURAl Heritage. In *Proceedings of the Digital Heritage. Progress in Cultural Heritage: Documentation, Preservation, and Protection*; Ioannides, M., Fink, E., Moropoulou, A., Hagedorn-Saupe, M., Fresa, A., Liestøl, G., Rajcic, V., Grussenmeyer, P., Eds.; Springer International Publishing, **2016**; pp. 805–813.
46. Bruno, F.; Lagudi, A.; Gallo, A.; Muzzupappa, M.; Davidde Petriaggi, B.; Passaro, S. 3d Documentation of Archeological Remains in the Underwater Park of Baiae. *International Archives of the Photogrammetry, Remote Sensing & Spatial Information Sciences* **2015**.
47. Skarlatos, D.; Demesticha, S.; Kiparissi, S. An ‘Open’ Method for 3D Modelling and Mapping in Underwater Archaeological Sites. *International Journal of Heritage in the digital era* **2012**, *1*, 1–24.
48. Bruno, F.; Barbieri, L.; Lagudi, A.; Cozza, M.; Cozza, A.; Peluso, R.; Muzzupappa, M. Virtual Dives into the Underwater Archaeological Treasures of South Italy. *Virtual Reality* 1–12.
49. Bruno, F.; Barbieri, L.; Lagudi, A.; Medaglia, S.; Miriello, D.; Muzzupappa, M.; Taliano Grasso, A. Survey and Documentation of the “Cala Cicala” Shipwreck.; Lecce, Italy, October 23 **2017**.
50. Qing, C.; Yu, F.; Xu, X.; Huang, W.; Jin, J. Underwater Video Dehazing Based on Spatial–Temporal Information Fusion. *Multidim Syst Sign Process* **2016**, *27*, 909–924, doi:10.1007/s11045-016-0407-2.
51. Xie, Z.-X.; Wang, Z.-F. Color Image Quality Assessment Based on Image Quality Parameters Perceived by Human Vision System. In *Proceedings of the Multimedia Technology (ICMT), 2010 International Conference on*; IEEE, **2010**; pp. 1–4.
52. Menna, F.; Agrafiotis, P.; Georgopoulos, A. State of the Art and Applications in Archaeological Underwater 3D Recording and Mapping. *Journal of Cultural Heritage* **2018**, *33*, 231–248, doi:10.1016/j.culher.2018.02.017.
53. Han, M.; Lyu, Z.; Qiu, T.; Xu, M. A Review on Intelligence Dehazing and Color Restoration for Underwater Images. *IEEE Transactions on Systems, Man, and Cybernetics: Systems* **2018**, 1–13, doi:10.1109/TSMC.2017.2788902.
54. von Lukas, U.F. Underwater Visual Computing: The Grand Challenge Just around the Corner. *IEEE computer graphics and applications* **2016**, *36*, 10–15.
55. Mahiddine, A.; Seinturier, J.; Boi, D.P.J.; Drap, P.; Merad, D.; Long, L. Underwater Image Preprocessing for Automated Photogrammetry in High Turbidity Water: An Application on the Arles-Rhone XIII Roman Wreck in the Rhodano River, France. In *Proceedings of the 2012 18th International Conference on Virtual Systems and Multimedia*; September **2012**; pp. 189–194.
56. *CloudCompare (Version 2.8.1) [GPL Software]., 2016 Retrieved from <Http://Www.Cloudcompare.Org/>*;
57. Demesticha, S. The 4th-Century-BC Mazotos Shipwreck, Cyprus: A Preliminary Report. *International Journal of Nautical Archaeology* **2011**, *40*, 39–59, doi:10.1111/j.1095-9270.2010.00269.x.

58. Remondino, F.; Nocerino, E.; Toschi, I.; Menna, F. A Critical Review of Automated Photogrammetric Processing of Large Datasets. *International Archives of the Photogrammetry, Remote Sensing & Spatial Information Sciences* **2017**, *42*.
59. Tefera, Y.; Poiesi, F.; Morabito, D.; Remondino, F.; Nocerino, E.; Chippendale, P. 3D NOW: Image-Based 3D Reconstruction and Modeling via WEB. *International Archives of the Photogrammetry, Remote Sensing and Spatial Information Sciences-ISPRS Archives* **2018**, *42*, 1097–1103.
60. Skarlatos, D.; Agrafiotis, P.; Menna, F.; Nocerino, E.; Remondino, F. Ground Control Networks for Underwater Photogrammetry in Archaeological Excavations. In Proceedings of the Proceedings of the 3rd IMEKO International Conference on Metrology for Archaeology and Cultural Heritage, MetroArcheo; **2017**; pp. 23–25.
61. Steimle, E.T.; Hall, M.L. Unmanned Surface Vehicles as Environmental Monitoring and Assessment Tools. In Proceedings of the OCEANS 2006; September **2006**; pp. 1–5.
62. Dunbabin, M.; Grinham, A.; Udy, J. An Autonomous Surface Vehicle for Water Quality Monitoring. **2009**, *6*.
63. Scaradozzi, D.; Sorbi, L.; Zoppini, F.; Conte, G.; Ramirez, P.A.Z.; Cerrano, C. Innovative Strategy and Process for Underwater Data Gathering and Results Elaboration. In Proceedings of the 22nd Mediterranean Conference on Control and Automation; June **2014**; pp. 652–657.
64. Vasilijević, A.; Nađ, Đ.; Mandić, F.; Mišković, N.; Vukić, Z. Coordinated Navigation of Surface and Underwater Marine Robotic Vehicles for Ocean Sampling and Environmental Monitoring. *IEEE/ASME Transactions on Mechatronics* **2017**, *22*, 1174–1184, doi:10.1109/TMECH.2017.2684423.
65. DocuScooter: A Novel Robotics Platform for Marine Citizen Science. - OnePetro Available online: <https://www.onepetro.org/conference-paper/ISOPE-I-17-503> (accessed on 30 December 2020).
66. Jorge, V.A.M.; Granada, R.; Maidana, R.G.; Jurak, D.A.; Heck, G.; Negreiros, A.P.F.; dos Santos, D.H.; Gonçalves, L.M.G.; Amory, A.M. A Survey on Unmanned Surface Vehicles for Disaster Robotics: Main Challenges and Directions. *Sensors* **2019**, *19*, 702, doi:10.3390/s19030702.
67. Bruno, F.; Lagudi, A.; Muzzupappa, M.; Lupia, M.; Cario, G.; Barbieri, L.; Passaro, S.; Saggiomo, R. Project VISAS: Virtual and Augmented Exploitation of Submerged Archaeological Sites-Overview and First Results. *Marine Technology Society Journal* **2016**, *50*, 119–129, doi:10.4031/MTSJ.50.4.4.
68. Bruno, F.; Lagudi, A.; Barbieri, L.; Muzzupappa, M.; Mangeruga, M.; Pupo, F.; Cozza, M.; Cozza, A.; Ritacco, G.; Peluso, R.; et al. Virtual Diving in the Underwater Archaeological Site of Cala Minnola. In Proceedings of the ISPRS - International Archives of the Photogrammetry, Remote Sensing and Spatial Information Sciences; Copernicus GmbH, February 23 **2017**; Vol. XLII-2-W3, pp. 121–126.
69. Bruno, F.; Barbieri, L.; Muzzupappa, M.; Tusa, S.; Fresina, A.; Oliveri, F.; Lagudi, A.; Cozza, A.; Peluso, R. Enhancing Learning and Access to Underwater Cultural Heritage through Digital Technologies: The Case Study of the “Cala Minnola” Shipwreck Site. *Digital Applications in Archaeology and Cultural Heritage* **2019**, *13*, e00103, doi:10.1016/j.daach.2019.e00103.
70. Zingaretti, S.; Scaradozzi, D.; Ciuccoli, N.; Costa, D.; Palmieri, G.; Bruno, F.; Ritacco, G.; Cozza, M.; Raxis, P.; Tzifopanosopoulos, T.; et al. A Complete IoT Infrastructure to Ensure Responsible, Effective and Efficient Execution of Field Survey, Documentation and Preservation of Archaeological Sites. In Proceedings of the 2018 IEEE 4th International Forum on Research and Technology for Society and Industry (RTSI); September **2018**; pp. 1–6.
71. A Cooperative Monitoring System for Diver Global Localization and Operation Support | Request PDF Available online: https://www.researchgate.net/publication/335941947_A_Cooperative_Monitoring_System_for_Diver_Global_Localization_and_Operation_Support (accessed on 29 September 2020).

72. Kenautics Available online: <http://kenautics.com/> (accessed on 26 April 2021).
73. Mistral Inc Available online: <http://www.mistralinc.com/Technologies/Underwater-Communications-and-Navi> (accessed on 26 April 2021).
74. ArtemisDVL System. Available online: <https://www.blueprintsubsea.com/pages/product.php?PN=BP00979> (accessed on 26 April 2021).
75. Mišković, N.; Bibuli, M.; Birk, A.; Caccia, M.; Egi, M.; Grammer, K.; Marroni, A.; Neasham, J.; Pascoal, A.; Vasiljević, A.; et al. "CADDY – Cognitive Autonomous Diving Buddy." In Proceedings of the OCEANS 2015 - Genova; May 2015; pp. 1–5.
76. Easydive | the Universal Housing Available online: <https://www.easydive.it/en> (accessed on 30 December 2020).
77. Cario, G.; Casavola, A.; Gagliardi, G.; Lupia, M.; Severino, U.; Bruno, F. Analysis of Error Sources in Underwater Localization Systems. In Proceedings of the OCEANS 2019 - Marseille; June 2019; pp. 1–6.
78. Burmistrov, I.; Zlokazova, T.; Izmalkova, A.; Leonova, A. Flat Design vs Traditional Design: Comparative Experimental Study. In Proceedings of the Human-Computer Interaction – INTERACT 2015; Abascal, J., Barbosa, S., Fetter, M., Gross, T., Palanque, P., Winckler, M., Eds.; Springer International Publishing: Cham, 2015; pp. 106–114.
79. Colour Contrast Check - Snook.Ca Available online: https://snook.ca/technical/colour_contrast/colour.html#fg=33FF33,bg=333333 (accessed on 30 December 2020).
80. Haydar, M.; Mairi, M.; Roussel, D.; Mallem, M.; Drap, P.; Bale, K.; Chapman, P. Virtual Exploration of Underwater Archaeological Sites: Visualization and Interaction in Mixed Reality Environments. In Proceedings of the Proceedings of the 9th International conference on Virtual Reality, Archaeology and Cultural Heritage; Eurographics Association: Goslar, DEU, December 2 2008; pp. 141–148.
81. Haydar, M.; Roussel, D.; Mairi, M.; Otmame, S.; Mallem, M. Virtual and Augmented Reality for Cultural Computing and Heritage: A Case Study of Virtual Exploration of Underwater Archaeological Sites (Preprint). *Virtual Reality* 2011, 15, 311–327, doi:10.1007/s10055-010-0176-4.
82. Bruno, F.; Lagudi, A.; Barbieri, L.; Muzzupappa, M.; Ritacco, G.; Cozza, A.; Cozza, M.; Peluso, R.; Lupia, M.; Cario, G. Virtual and Augmented Reality Tools to Improve the Exploitation of Underwater Archaeological Sites by Diver and Non-Diver Tourists. In Proceedings of the Digital Heritage. Progress in Cultural Heritage: Documentation, Preservation, and Protection; Ioannides, M., Fink, E., Moropoulou, A., Hagedorn-Saupe, M., Fresa, A., Liestøl, G., Rajcic, V., Grussenmeyer, P., Eds.; Springer International Publishing: Cham, 2016; pp. 269–280.
83. Cebrián-Robles, D.; Ortega-Casanova, J. Low Cost 3D Underwater Surface Reconstruction Technique by Image Processing. *Ocean Engineering* 2016, 113, 24–33, doi:10.1016/j.oceaneng.2015.12.029.
84. Lagudi, A.; Bianco, G.; Muzzupappa, M.; Bruno, F. An Alignment Method for the Integration of Underwater 3D Data Captured by a Stereovision System and an Acoustic Camera. *Sensors* 2016, 16, 536, doi:10.3390/s16040536.
85. Łuczyński, T.; Pfingsthorn, M.; Birk, A. The Pinax-Model for Accurate and Efficient Refraction Correction of Underwater Cameras in Flat-Pane Housings. *Ocean Engineering* 2017, 133, 9–22, doi:10.1016/j.oceaneng.2017.01.029.
86. Gallo, A.; Angilica, A.; Bianco, G.; Filippo, F.D.; Muzzupappa, M.; Davidde, B.; Bruno, F. 3D Reconstruction and Virtual Exploration of Submerged Structures: A Case Study in the Underwater Archaeological Site of Baia (Italy). 8.
87. Katsouri, I.; Tzanavari, A.; Herakleous, K.; Poullis, C. Visualizing and Assessing Hypotheses for Marine Archaeology in a VR CAVE Environment. *J. Comput. Cult. Herit.* 2015, 8, 10:1-10:18, doi:10.1145/2665072.

88. Varinlioglu, G. Data Collection for a Virtual Museum on the Underwater Survey at Kaş, Turkey. *International Journal of Nautical Archaeology* **2011**, *40*, 182–189, doi:10.1111/j.1095-9270.2010.00304.x.
89. Gallagher, D.G. Development of Miniature, Head-Mounted, Virtual Image Displays for Navy Divers. In Proceedings of the Oceans '99. MTS/IEEE. Riding the Crest into the 21st Century. Conference and Exhibition. Conference Proceedings (IEEE Cat. No.99CH37008); September **1999**; Vol. 3, pp. 1098–1104 vol.3.
90. Morales, R.; Keitler, P.; Maier, P.; Klinker, G. An Underwater Augmented Reality System for Commercial Diving Operations. In Proceedings of the OCEANS 2009; October **2009**; pp. 1–8.
91. Blum, L.; Broll, W.; Müller, S. Augmented Reality under Water. In Proceedings of the SIGGRAPH '09: Posters; Association for Computing Machinery: New York, NY, USA, August 3 **2009**; p. 1.
92. Oppermann, L.; Blum, L.; Shekow, M. Playing on AREEF: Evaluation of an Underwater Augmented Reality Game for Kids. In Proceedings of the Proceedings of the 18th International Conference on Human-Computer Interaction with Mobile Devices and Services; Association for Computing Machinery: New York, NY, USA, September 6 **2016**; pp. 330–340.
93. Bellarbi, A.; Domingues, C.; Otmame, S.; Benbelkacem, S.; Dinis, A. Augmented Reality for Underwater Activities with the Use of the DOLPHYN. In Proceedings of the 2013 10th IEEE INTERNATIONAL CONFERENCE ON NETWORKING, SENSING AND CONTROL (ICNSC); April **2013**; pp. 409–412.
94. Cesar, D.B. dos S.; Gaudig, C.; Fritsche, M.; Reis, M.A. dos; Kirchner, F. An Evaluation of Artificial Fiducial Markers in Underwater Environments. In Proceedings of the OCEANS 2015 - Genova; May **2015**; pp. 1–6.
95. Frontiers | Impact of Dehazing on Underwater Marker Detection for Augmented Reality | Robotics and AI Available online: <https://www.frontiersin.org/articles/10.3389/frobt.2018.00092/full> (accessed on 30 December 2020).
96. Čejka, J.; Bruno, F.; Skarlatos, D.; Liarokapis, F. Detecting Square Markers in Underwater Environments. *Remote Sensing* **2019**, *11*, 459, doi:10.3390/rs11040459.
97. Čejka, J.; Agrafiotis, P.; Bruno, F.; Skarlatos, D.; Liarokapis, F. *Improving Marker-Based Tracking for Augmented Reality in Underwater Environments*; The Eurographics Association, **2018**; ISBN 978-3-03868-057-4.
98. Sarakinou, I.; Papadimitriou, K.; Olga, G.; Patias, P. UNDERWATER 3D MODELING: IMAGE ENHANCEMENT AND POINT CLOUD FILTERING. *ISPRS - International Archives of the Photogrammetry, Remote Sensing and Spatial Information Sciences* **2016**, *XLI-B2*, 441–447, doi:10.5194/isprs-archives-XLI-B2-441-2016.
99. Tan, H.-P.; Diamant, R.; Seah, W.K.G.; Waldmeyer, M. A Survey of Techniques and Challenges in Underwater Localization. *Ocean Engineering* **2011**, *38*, 1663–1676, doi:10.1016/j.oceaneng.2011.07.017.
100. Costanzi, R.; Monnini, N.; Ridolfi, A.; Allotta, B.; Caiti, A. On Field Experience on Underwater Acoustic Localization through USBL Modems. In Proceedings of the OCEANS 2017 - Aberdeen; June **2017**; pp. 1–5.
101. Allotta, B.; Caiti, A.; Costanzi, R.; Fanelli, F.; Fenucci, D.; Meli, E.; Ridolfi, A. A New AUV Navigation System Exploiting Unscented Kalman Filter. *Ocean Engineering* **2016**, *113*, 121–132, doi:10.1016/j.oceaneng.2015.12.058.
102. Petriaggi, B.D.; Petriaggi, R.; Bruno, F.; Lagudi, A.; Peluso, R.; Passaro, S. A Digital Reconstruction of the Sunken “Villa Con Ingresso a Protiro” in the Underwater Archaeological Site of Baiae. *IOP Conf. Ser.: Mater. Sci. Eng.* **2018**, *364*, 012013, doi:10.1088/1757-899X/364/1/012013.
103. Bruno, F.; Barbieri, L.; Mangeruga, M.; Cozza, M.; Lagudi, A.; Čejka, J.; Liarokapis, F.; Skarlatos, D. Underwater Augmented Reality for Improving the Diving Experience in

- Submerged Archaeological Sites. *Ocean Engineering* **2019**, *190*, 106487, doi:10.1016/j.oceaneng.2019.106487.
104. Mania, K.; Chalmers, A. The Effects of Levels of Immersion on Memory and Presence in Virtual Environments: A Reality Centered Approach. *Cyberpsychol Behav* **2001**, *4*, 247–264, doi:10.1089/109493101300117938.
 105. Čejka, J.; Mangeruga, M.; Bruno, F.; Skarlatos, D.; Liarokapis, F. Evaluating the Potential of Augmented Reality Interfaces for Exploring Underwater Historical Sites. *IEEE Access* **2021**, *9*, 45017–45031, doi:10.1109/ACCESS.2021.3059978.
 106. Tcha-Tokey, K.; Christmann, O.; Loup-Escande, E.; Richir, S. Proposition and Validation of a Questionnaire to Measure the User Experience in Immersive Virtual Environments. *International Journal of Virtual Reality* **2016**, *16*, 33–48, doi:10.20870/IJVR.2016.16.1.2880.
 107. Hart, S.G.; Staveland, L.E. Development of NASA-TLX (Task Load Index): Results of Empirical and Theoretical Research. In *Advances in Psychology*; Hancock, P.A., Meshkati, N., Eds.; Human Mental Workload; North-Holland, **1988**; Vol. 52, pp. 139–183.
 108. Mangeruga, M.; Casavola, A.; Pupo, F.; Bruno, F. An Underwater Pathfinding Algorithm for Optimised Planning of Survey Dives. *Remote Sensing* **2020**, *12*, 3974, doi:10.3390/rs12233974.
 109. Joiner, J.T. *NOAA Diving Manual: Diving for Science and Technology*; 4th ed.; Best Publishing Company: Flagstaff, AZ, USA, **2001**; ISBN 978-0-941332-70-5.
 110. MultiDeco VPM & VPM-B & VPM-B/E & ZHL GF Dive Decompression Software for Technical Divers Available online: <http://www.hhssoftware.com/multideco/> (accessed on 31 August 2020).
 111. Subsurface | An Open Source DiveLog Available online: <https://subsurface-diveLog.org/it/> (accessed on 31 August 2020).
 112. DIVEROID Available online: <https://app.diveroid.com/en/main> (accessed on 31 August 2020).
 113. Wroblewski, A. Decotengu: DecoTengu - Dive Decompression Library Available online: <https://wrobell.dcmo.org/decotengu/> (accessed on 31 August 2020).
 114. Choset, H.M.; Hutchinson, S.; Lynch, K.M.; Kantor, G.; Burgard, W.; Kavraki, L.E.; Thrun, S.; Arkin, R.C. *Principles of Robot Motion: Theory, Algorithms, and Implementation*; MIT Press, **2005**; ISBN 978-0-262-03327-5.
 115. Murphy, R.R. Introduction to AI Robotics. *Industrial Robot: An International Journal* **2001**, *28*, 266–267, doi:10.1108/ir.2001.28.3.266.1.
 116. Dijkstra, E.W. A Note on Two Problems in Connexion with Graphs. *Numerische mathematik* **1959**, *1*, 269–271.
 117. Hart, P.E.; Nilsson, N.J.; Raphael, B. A Formal Basis for the Heuristic Determination of Minimum Cost Paths. *IEEE transactions on Systems Science and Cybernetics* **1968**, *4*, 100–107.
 118. Yang, J.-M.; Tseng, C.-M.; Tseng, P.S. Path Planning on Satellite Images for Unmanned Surface Vehicles. *International Journal of Naval Architecture and Ocean Engineering* **2015**, *7*, 87–99.
 119. Sun, Y.; Ran, X.; Zhang, G.; Xu, H.; Wang, X. AUV 3D Path Planning Based on the Improved Hierarchical Deep Q Network. *Journal of Marine Science and Engineering* **2020**, *8*, 145.
 120. Pham, H.X.; La, H.M.; Feil-Seifer, D.; Nguyen, L.V. Autonomous Uav Navigation Using Reinforcement Learning. *arXiv preprint arXiv:1801.05086* **2018**.
 121. Wang, C.; Wang, J.; Wang, J.; Zhang, X. Deep Reinforcement Learning-Based Autonomous UAV Navigation with Sparse Rewards. *IEEE Internet of Things Journal* **2020**.
 122. Wang, X.; Yao, X.; Zhang, L. Path Planning under Constraints and Path Following Control of Autonomous Underwater Vehicle with Dynamical Uncertainties and Wave Disturbances. *Journal of Intelligent & Robotic Systems* **2020**, 1–18.
 123. Kulkarni, C.S.; Lermusiaux, P.F.J. Three-Dimensional Time-Optimal Path Planning in the Ocean. *Ocean Modelling* **2020**, *152*, 101644, doi:10.1016/j.ocemod.2020.101644.
 124. Koenig, S.; Likhachev, M.; Furcy, D. Lifelong Planning A*. *Artificial Intelligence* **2004**, *155*, 93–146.
 125. Miskovic, N.; Nad, D.; Rendulic, I. Tracking Divers: An Autonomous Marine Surface Vehicle to Increase Diver Safety. *IEEE Robotics & Automation Magazine* **2015**, *22*, 72–84.

126. Bühlmann, A.A.; Völm, E.B.; Nussberger, P. *Tauchmedizin: Barotrauma Gasembolie · Dekompression Dekompressionskrankheit Dekompressionscomputer*; Springer-Verlag, **2013**; ISBN 978-3-642-55939-6.
127. Bühlmann, A.A. *Decompression — Decompression Sickness*; Springer Science & Business Media, 2013; ISBN 978-3-662-02409-6.
128. Baker, E.C. Understanding M-Values. *Immersed* **1998**, 3, 23–27.
129. Brewka, G. Artificial Intelligence—a Modern Approach by Stuart Russell and Peter Norvig, Prentice Hall. Series in Artificial Intelligence, Englewood Cliffs, NJ. *The Knowledge Engineering Review* **1996**, 11, 78–79, doi:10.1017/S0269888900007724.
130. Schreiner, H.R.; Kelley, P.L. A PRAGMATIC VIEW OF DECOMPRESSION. In *Underwater Physiology*; Lambertsen, C.J., Ed.; Academic Press, **1971**; pp. 205–219 ISBN 978-0-12-434750-2.
131. DiveSafe Available online: <https://divesafe.eu/> (accessed on 4 January 2021).
132. Progetto Musas – Musei di archeologia subacquea. Available online: <https://www.progettomusas.eu/> (accessed on 5 May 2021)